KAUNAS UNIVERSITY OF TECHNOLOGY

DONATA ZUBAUSKIENĖ

UPHOLSTERY MATERIALS BEHAVIOR EVALUATION METHOD

Doctoral dissertation
Technological Sciences, Materials Engineering (08 T)

2017, Kaunas

This doctoral dissertation was prepared at Kaunas University of Technology, Faculty of Mechanical Engineering and Design, Department of Materials Engineering during the period of 2011–2017. The studies were supported by the Research Council of Lithuania.

Scientific Supervisor:

Prof. dr. Eugenija STRAZDIENĖ (Kaunas University of Technology, Technological Sciences, Materials Engineering, 08T).

Scientific Advisor:

Assoc. prof. dr. Virginijus URBELIS (Kaunas University of Technology, Technological Sciences, Materials Engineering, 08T).

This doctoral dissertation has been published at:
http://ktu.edu

Editor:

Armandas Rumšas (Publishing Office “Technologija”)

ISBN 978-609-02-1393-3

The bibliographic information about the publication is available in the National Bibliographic Data Bank (NBDB) of Martynas Mažvydas National Library of Lithuania

KAUNO TECHNOLOGIJOS UNIVERSITETAS

DONATA ZUBAUSKIENĖ

TEKSTILINIŲ BALDINIŲ MEDŽIAGŲ ELGSENOS VERTINIMO METODAS

Daktaro disertacija
Technologijos mokslai, medžiagų inžinerija (08 T)

2017, Kaunas

Disertacija rengta 2011-2017 metais Kauno technologijos universiteto Mechanikos inžinerijos ir dizaino fakultete Medžiagų inžinerijos katedroje. Mokslinius tyrimus rėmė Lietuvos mokslo taryba.

Mokslinis vadovas:

Prof. dr. Eugenija STRAZDIENĖ (Kauno technologijos universitetas, technologijos mokslai, medžiagų inžinerija, 08T).

Mokslinis konsultantas:

Doc. dr. Virginijus URBELIS (Kauno technologijos universitetas, technologijos mokslai, medžiagų inžinerija, 08T).

Interneto svetainės, kurioje skelbiama disertacija, adresas:
http://ktu.edu

Redagavo:

Armandas Rumšas (leidykla “Technologija”)

ISBN 978-609-02-1393-3

Leidinio bibliografinė informacija pateikiama Lietuvos nacionalinės Martyno Mažvydo bibliotekos Nacionalinės bibliografijos duomenų banke (NBDB)

CONTENTS

LIST OF MAIN ABBREVIATIONS

2HB	bending hysteresis in KES-F system, Nm/m
2HG	shear hysteresis in KES-F system, N/m
2HG5	shear hysteresis at 5° angle in KES-F system, N/m
a	ratio between the area of polar diagram which was outlined by tested samples punching heights H_{max} at each pre-tension level, mm
B	bending rigidity in KES-F system, Nm^2/m
B_P	bending rigidity determined by F.T. Pierce's method, μNm
b	ratio between the area of the polar diagram which was outlined by punching height H_{max} values of non-tensioned samples, mm
b_0	specimen width, cm
b_i	i-th element time coefficient of relaxation duration
c	area of any pre-tension level except for 0.0%
c_a	anisotropy coefficient
c_{amax}	anisotropy coefficient calculated at maximal breakage
c_{a100}	anisotropy coefficient calculated at 100 N force
c_{a25}	anisotropy coefficient calculated at 25 N force
d	area determined by tested systems deformability without pre-tension
D	density stitches, dm^{-1}
D_L	linear density, tex
E	long-term elasticity modulus after loading, N/cm
E'	long-term elasticity modulus after unloading, N/cm
E_m	rigidity modulus, N/cm
E_{mmax}	rigidity modulus calculated at maximal breakage, N/cm
E_{m100}	rigidity modulus calculated at 100 N force, N/cm
E_{m25}	rigidity modulus calculated at 25 N force, N/cm
EMT	deformation under the maximum load in KES-F system, %
F	uniaxial tension force, N
F_D	dynamic force of friction, N
F_{max}	uniaxial tension maximal force, N
F_S	static force of friction, N
f	specific tensile strength, N/tex
G	shear stiffness in KES-F system, N/m°
g	variables
H	instantaneous rigidity modulus of model when the specimen is loaded at constant load, N/cm
H'	instantaneous rigidity modulus of model when the specimen is unloaded, N/cm
H_{max}	maximal punching height, mm
I_β	confidence interval
j	variables
k	variables
LT	linearity of the load-extension in KES-F system

L_0	application without lubricant
L_A	pure water
L_B	commercial leather cleaner *Smash* treatment *Arexons*
L_C	silicone CRC Industrial
L_D	commercial leather cleaner and conditioner *Turtle Wax Professional*
l	path, mm
m	the quantity of the duration coefficients of relaxation
MIU	coefficient of friction in KES-F system
n	radius of the tearing zone, mm
P_m	maximum pressure in the compression test of KES-F system, N/m^2
P_{max}	breaking force in the biaxial punching process, N
R	radius of the specimen work zone, mm
R^2	determination coefficient
RC	compression resilience in KES-F system, %
RT	tensile resilience in KES-F system, %
R_{WA}	the number of warp yarns in the report of fabric weave
R_{WE}	the number of weft yarns in the report of fabric weave
r	radius of punch, mm
r_c	correlation coefficient
S	complex criterion
S_n	area of the tearing zone, mm^2
S_R	area of the specimen work zone, mm^2
S_1	total deformability criterion which was defined on the basis of the changes of punching height H_{max}
S_2	total strength criterion which was defined on the basis of the changes of punching force P_{max}
SMD	roughness in KES-F system, µm
T	material thickness, mm
T_0	thickness of uncompressed sample in KES-F system, mm
T_m	thickness after compression in KES-F system, mm
WT	energy consumption during the loading cycle in KES-F system, Nm/m^2
δ	relative error, %
ε_c	creep deformation, mm
ε_{cal}	theoretical (calculated) values of deformation, mm
ε_e	elastic deformation, mm
ε_{exp}	experimental values of deformation, mm
ε_G	general deformation, mm
ε_{max}	uniaxial tension strain, mm or %
ε_R	reversible deformation, mm
ε_r	residual deformation, mm
ε_s	sudden deformation, mm
ε_v	viscoelastic deformation, mm
ε_{100}	uniaxial tension strain determined at 100 N force, mm
ε_{25}	uniaxial tension strain determined at 25 N force, mm

η	dynamic viscosity
Δ	absolute random error
μ_S	static coefficient of friction
μ_{SA}	averaged static coefficient of friction
μ_D	dynamic coefficient of friction
μ_{DA}	averaged dynamic coefficient of friction
v	coefficient of variation, %
ρ	surface density, g/m^2
σ	standard deviation
σ^2	variance
τ	relaxation duration for relaxation deformation process, s
φ	shear angle, °
$\bar{\chi}$	arithmetic mean

Introduction

The Problem of the Research

Textiles being an inseparable part of everyday human life leads to continual improvements of their quality, aesthetic and wear properties, expanding assortment, focusing on and integrating up-to-date technologies so that to keep pace with the modern times and contemporary technology, current challenges and demand trends. The range of the application of textiles extends from fashion to furniture, to construction and even to medical appliances. This study focuses on upholstery materials applications which have specific requirements for wear, stress/strain concentrations during manufacturing processes, contact with human body, care and support of the product for extended lifetime, etc.

The quality of both fashion and furniture textiles is evaluated by their physical and mechanical parameters which are determined by standard research methods applied until the complete disintegration of the subject. However, better wear and strength properties are required for upholstery textiles, this being the main distinction in opposition to the clothing textiles. The load and wear processes are significantly more prominent in the furniture applications, upholstering products, manufacturing and exploitation. Tensile properties are the key factor in projecting the fabric deformational behavior which are manifested in the manufacture and use processes. The furniture cover is always under biaxial deformation on the inside, where constant friction is present between the fabric and other components of the furnishing (foam, the metal or wooden frame and other materials). The outside of the fabric is affected by friction and deformation when the piece of furniture is in use, the main requirement here being durability and resistance to wear. This is why the upholstery textiles, compared to the clothing, must be adequately thick and stiff, must feature the best stability, strength and durability properties. Clothing pieces are more often replaced if compared to upholstery, not only because of wear off, but also due to the dynamic fashion trends. Thus furniture upholsteries are usually used for many years until complete wear off (fabric disintegration). It is crucial that the fabrics carry not only the best tensile properties, but are also investigated for the deformation properties, both inside and outside, by considering friction and loads appearing in the process of upholstery. Therefore, making the development and manufacturing predictable and less time consuming is a major objective of our times.

The textile industry is rapidly expanding. This is a result of the introduction of new technologies, robotic components and automation. Production time is getting reduced while the quality and quantity of the products increase. Up-to-date software shortens the design process, and optimizes the whole manufacturing process line: from the design to the final product. 3D model simulation requires specific parameters of the fabrics used for the product. Software package *Design Concept* by *Lectra Company* is a common measure which uses the KES-F and FAST system parameters. Therefore, any investigation of the textile deformation behavior

indispensably involves the proper use of the design software (e.g. *DesignConcept*) and successful product manufacturing.

The Relevance of the Research

Different fiber structure, flexible and anisotropic fabrics are used for upholstery materials. Naturally, the deformation-relaxation behavior is widely spread. When a new fabric is introduced into furniture manufacturing, the ease allowances of previous materials may not be applied for the new material due to different mechanical properties. Ease allowances must allow the cover to be upholstered on the piece of furniture and perfectly mould to the shape. The shape must be retained while the furniture is in use – this is where the exploitation loads and the relaxation caused by them need to be investigated considering the relaxation behavior, that is, creep and deformation relaxation. Furniture manufacturers aim to satisfy their client's needs – to achieve proper long-lasting quality and aesthetic properties of the produced furniture. Therefore, fabrics must be chosen considering the tensile properties and the deformational behavior at low-stress loading taking into account their non-linearity and anisotropy.

The Aim of the Work

The investigation and evaluation of upholstery materials performance properties under uniaxial and biaxial deformations in respect to low-stress and breaking loading.

Scientific Tasks of the Work:

1. to perform experimental analysis of upholstery materials uniaxial low-stress properties defined by the KES-F testing system;
2. to define the effect of the properties of upholstery materials determined by the KES-F testing system upon creep deformation processes;
3. to analyze creep and relaxation processes of upholstery materials in respect to the anisotropy level under uniaxial loadings;
4. to define the effect of fused upholstery system structure upon the variations of its spatial shape under biaxial punching;
5. to evaluate the effect of uniaxial pre-tension level upon biaxial punching deformation of fused upholstery systems;
6. to determine the effect of friction in the contact zone between the punch and upholstery material surface during biaxial deformation process.

The Novelty of the Work and Its Importance

Rapid prototyping is the key feature of innovative production, and it is closely associated with the digitization of product development processes. Virtual prototyping is inextricably linked with the properties of the materials to be applied in new products. The novelty of this research is that it has proven that low-stress

KES-F parameters of upholstery materials can be applied in virtual simulation of furniture cover behavior during wear. The results were validated by further developing the method of pull-on ease level measurement directly on the furniture (pouffe) earlier developed by the author of this dissertation thesis.

There is no specific equipment that covers the whole set of actual properties regarding the investigation of furniture textile deformational and exploitational behavior. Upholstery textile research was carried out by using a variety of research methods. It enables to investigate the textile behavior under deformation, to detect mechanical properties and to conduct surface experiments according to KES-F measuring system thus expanding the variety of the subjects that can be investigated. This study is integrated with and contributes to the long term scientific database and analysis of other researches performed in the field of investigation of flexible multilayer textile and polymer materials deformational behavior considering exclusive attention to friction. There are fewer scholarly studies analyzing the influence of friction between upholstery materials.

This study has tackled a highly topical problem of furniture manufacturers. Creep and deformation relaxation experiments were performed on the specific materials used in the production in real life thus enabling to determine the deformation properties of the textiles which develop in the process of upholstering and under application of the relevant force (100 N load). A specific method was developed in order to solve the production issue – it registers the initial tensile load, determines its influence upon biaxial deformation as these parameters are crucial for the fluent upholstering process.

1. Literature Review

1.1. Textile Fabrics for Upholstery

The variety of materials used in upholstery production is extremely large. It is not easy to select the proper upholstery material suitable to interior design or environment, yet the main factor characterizing upholstery is the quality, low exploitation rate, durability, stability, the strength, the ergonomics and comfort. In terms of raw materials, upholstery fabrics are classified into natural fiber, man-made fiber and synthetic fiber textiles (Jabbar & Shaker, 2016), (Ahmad, Choi, & Park, 2015), (Preston, 2016), (Costa, Aguiar, Luz, Pessoa, & Costa, 2015).

Natural textiles are made from linen, cotton, wool, natural leather and silk (Guide to upholstery fabrics, 2017). ***Linen*** is an extremely strong natural textile fiber but not very resilient, and it wrinkles easily (Abbas, 2017). ***Cotton*** is strong, versatile and breathable, but not very resistant to wrinkling and stretching (Abbas, 2017). ***Wool*** is wrinkle-resistant, soil resistant, and can stand up to abrasion, mildew and sunlight (Abbas, 2017). ***Silk*** dupioni, silk shantung and silk linen are most commonly used in upholstery (Silk Fabrics for Upholstery, 2014). Silk is backed with cotton to add weight, durability and long-lasting (Understanding Upholstery: From Fabric to Frame, 2017). ***Natural leather*** is the most durable upholstered material which is difficult to scratch (Leather Classics, 2016).

Synthetic textiles are made of acetate, acrylic, nylon, olefin, polyester, microfiber, rayon and vinyl. ***Acetate*** looks like silk, is resistant to mildew, pilling, shrinkage, wrinkling, but does not resist against soil, sun or abrasion (Guide to upholstery fabrics, 2017), (Abbas, 2017). ***Acrylic*** fibers were developed by imitating wool, they are resistant to wearing, sunlight, fading, soiling, wrinkling, mildew and insects, but they are not flame-retardant (Upholstery Cover Fabrics and Leathers, 2017). ***Nylon*** is usually blended with other fibers to become one of the strongest and durable upholstery fabrics (Understanding Upholstery: From Fabric to Frame, 2017). ***Olefin*** is made from melting down plastic pellets, during which any color is added, and for this purpose olefin is resistant to chemicals, moisture, mildew and abrasion (Upholstery Cover Fabrics and Leathers, 2017). ***Polyester*** is usually blended with natural fibers (cotton, wool) to avoid wrinkling, fading, to decrease pilling in the case of wool blends, to provide strength and resistance against abrasion. Polyester automotive upholstery woven fabrics were investigated by (Akgun, Becerir, Alpay, Karaaslan, & Eke, 2010) in order to determine the changes in color and percentage reflectance values at different abrasion levels. It was established that surface color coordinates changed with the changes of the yarn float length of the different weave patterns and that color differences increase with the increase of the yarn float length. ***Microfiber*** is a blend of polyester and polyamide, it is very resistant against soiling and wrinkling. ***Rayon*** is a cellulose-based material developed to mimic such fabrics as silk, cotton and linen; unfortunately it wrinkles (Guide to upholstery fabrics, 2017). Vinyl is similar to leather in appearance, possesses lots of great properties such as water, UV and fade resistances, durability, excellent abrasion resistance, great strength and stretch (Nikki, 2014).

1.1.1. Structure of upholstery textiles

In terms of the manufacturing technique, upholstery fabrics are classified into woven, non-woven, and knitted materials. Woven fabrics are woven with a loom machine which is made of two systems of threads (the warp and the weft) perpendicular to each other, and braided in a certain order. The types of woven upholstery fabrics are presented in Figure 1.1.

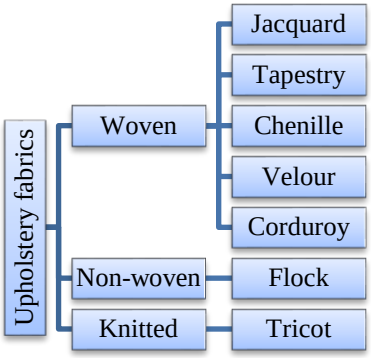

Figure 1.1. Types of upholstery fabrics

Non-woven upholstery fabrics are similar to fabric in appearance but are made from lengthy fibers which are bonded (not weaved) to each other by chemical, mechanical, heat or solvent treatment (Shanthi & Iswariya, 2013). Non-woven fabrics can be formed in the following ways (Stanys, Adomavičiūtė, & Jonaitienė, 2012), (Shanthi & Iswariya, 2013): dry forming of a fiber layer; wet forming of a fiber layer; directly from polymer; mechanical interlocking method. After weaving, the fabrics are taken off the weaving machine, and such fabrics are termed as heavy fabrics which are applied with different finishing processes, such as dyeing, printing, bleaching, mercerizing (applied only to cottons and linens by using soda for luster effect and strengthening), shearing (it is a cutting process used to trim pile fabrics), flameproofing (Baldiniai audiniai ir jų klasifikavimas, 2011), (James, 2001).

Jacquard materials are described as complex patterned fabrics with floats and luster (Kadole, Gotipamul, Dhanabalan, & Saloni, 2013). These fabrics are stable, strong and stretchy compared to the ones of basic weaves. Jacquard fabrics are divided into flat-jacquard (the patterns have the equal number of loops in each wale of the pattern knitting) and blister fabrics. Jacquard fabric is sub-divided into 14 types of jacquard: brocade fabric, brocatelle, damask fabric, French jacquard, poly x catonic jacquard, jacquard nets, velour jacquard fabric, blackout fabrics, matelasse fabric, pile jacquard, jacquard tapes, multi-layer jacquard one-piece-woven fabric for airbags, polymeric optical fiber jacquard, 3D weaving (Kadole, Gotipamul, Dhanabalan, & Saloni, 2013).

Tapestry is weft-faced weaving, different from cloth weaving, where all warp threads are hidden in the finished product, weft yarns of tapestry are discountinuous and of different colors (Mallett, 2000). Usually, in tapestry weaving, linen or cotton

warp thread is used while weft threads are made of wool or cotton, in some cases including silk, gold, silver (McKoy, 2015).

Other fabrics with jacquard weaving are named **chenilles**; they have one or two chenille yarns. Unlike the jacquard fabrics, the chenille yarn is manufactured by putting short lengths of yarn, which is called the 'pile', between two 'core yarns' and twisting the yarn together (Chenille fabric, 2017). The pile can be on one side or on both sides. In the case when the pile is on one side, the yarn must be folded before it is woven, otherwise it will be on both sides (Technical manual chapter 2: Yarns - Chenille , 2013). Chenille fabric is usually made of cotton fiber, including acrylic, olefin and rayon fibers as well (Manea, Scarlet, Amariei, Nechita, & Sandu, 2015), (Calin, et al., 2013), (Manea, Stanescu, Nechita, & Agop, 2015). Different chenille yarns of 100% wool and 50% wool-50% polyester blend yarns produced from sirospun and a two-folded ring were analyzed by (Ceven & Ozdemir, 2006). Strong linear relationships between the mass loss values obtained in abrasion tests and the abrasion coefficients of the chenille yarns were determined.

The pile length of chenille yarn influences the abrasion resistance of upholstery fabrics (Ulku, Ortek, & Omeroglu, 2003). Longer fibers which are inserted into the twists of chenille yarns are not easily removable compared to the shorter fibers (Ulku, Ortek, & Omeroglu, 2003), (Ozdemir & Ceven, 2004). The tendency of decreasing pile loss readings increases the pile length; in the case when the rubbing cycle increases when all the fibers of chenille have the same linear density, this tendency is not valid (Ulku, Ortek, & Omeroglu, 2003). Chenille yarns with high pile density are abraded less compared to the yarns with low pile density (Ceven & Ozdemir, 2006).

Other researchers (Pasayev, Korkmaz, & Baspinar, 2011) determined that it is possible to decrease the seam slippage by driving the energy of the applied mechanical forces to a seam.

Velour is an upholstery fabric with a thick, soft nap (McMahon, 2017). Velvet is often confused with velour – although the materials are similar, they are still different in their properties and application. Velour is a knit combined with cotton fabric mostly used for curtains, drapes, furniture (couches, car seats) and blankets; meanwhile, velvet is a woven fabric with a silk pile on top most used for clothing (What is the difference between velvet and velour, 2017), (McMahon, 2017). Velour is more stretchy and resistant to hard wear, easier to care for (What is the difference between velvet and velour, 2017), (Madkaikar, 2012). Velour fabric can be made of a flame-resistant thread or can be treated with flame-resistant compounds (McMahon, 2017). Interior fabrics designed for automotive seats demand higher requirements compared to clothing fabrics, such as mechanical, application and light resistance properties, as well as durability. (Siyuan, Yonggang, & Aiying, 2013) analyzed the design and development of warp-knitted velour concerning the fiber choice, fabric structure, dyeing, sanding and brushing.

Corduroy is a ribbed pile fabric with soft hand touch feel and a high luster (Madkaikar, 2012) mostly made from cotton or mixed with lycra as well in order to make the fabric easier to wear or keep in shape (Thomas & Thomas, 2006).

Corduroy fabric has the extra set of filling yarns which floats over the ground threads (Madkaikar, 2012), (Fancy weaves, 2012). These floats are cut and brushed after the weaving, forming a pile in parallel lines or cords (called wales) along the length of the warp/fabric (Fancy weaves, 2012), (Madkaikar, 2012), (Thomas & Thomas, 2006). There are two types of corduroy fabric: the V-shaped and the W-shaped pile structure (Pai, 2009). Corduroy fabric is characterized by the number of wales per inch, and it can vary from 1.5 to 21 wales per inch (Fancy weaves, 2012), (Arnald, 2014). The fabrics with the higher number of wales are used in clothing garments (jeans, jackets, shirts, caps, skirts, suits, children's cloths, dresses) and are usually called corded velveteen, pin cord, elephant cord, Manchester cloth, whereas the fabric with a wide wale is mostly used for upholstery and trousers (Thomas & Thomas, 2006), (Fancy weaves, 2012), (Madkaikar, 2012), (Arnald, 2014). The types of corduroy fabric are determined by the width of the wales – the wide wale, the pinwale (it is the finest wale), the standard wale (11 wales/inch) and the featherwale (Fancy weaves, 2012), (Arnald, 2014). Corduroy fabric is described as a warm, durable, thick and stable fabric which absorbs and releases moisture (Madkaikar, 2012).

The acoustical properties of corduroy fabrics in relation to air permeability and airflow resistance were investigated by (Tang, Zhang, Zhuang, Zhang, & Yan, 2017). For the experiments, five specimens with similar surface density and different wale width were used. It was revealed that corduroy fabrics with the thicker wale width showed higher air permeability and lower airflow resistance.

Flocked yarns for upholstery and car seat fabrics are produced by running adhesive-coated filament yarns through the flock cloud chamber and a curing oven (Kim, 2011). Flocked yarn does not shed as chenille yarn because pile fibers create a dense coverage (Kim, 2011). Usually, weave structures are plain, twill, sateen as well as drills made of rayon or a polyester/cotton blend; unfortunately, flocked fabrics are weak enough (Kim, 2011). Fabrics are flocked when seeking to increase the value of aesthetics, the tactile sensation, the color and appearance, and also to boost insulation, slip-or-grip friction, low reflectivity (Flocking (texture), 2017).

The flocked fabrics of low flock fiber density and high flock fiber length are more resistant to abrasion compared to the ones with high flock fiber density and short flock fiber length (Bilisik & Yolacan, 2009). Also, it was determined that rubbing resistance depends on the wet or dry flocked fabrics, i.e. the wet rubbing resistance was lower than the dry resistance because of the low wet properties of the adhesive (Bilisik & Yolacan, 2009).

(Slot, Weerd, Roos, Baiker, Stoel, & Zuidberg, 2017) in their investigation tried to achieve the optimal use of flock fibers as tracers, i.e. they sought to be able to select a fit-for-purpose flock fiber, in order to be able to predict the amount of flock fibers to be recovered from crime-related items, and to be able to use these numbers so that to exclude accidental uptake. The length of flock fiber, car upholstery and trousers fabric were studied. It was concluded that flock fibers can serve as invisible evidence to reconstruct a series of events.

Tricot is a knitted fabric bending the yarns in loops which interlace with each other in longitudinal and transverse directions. Tricot is specific in terms of its softness, stability, lower wrinkling, and fitting to the surface, which makes it more popular when choosing upholstery fabrics for modern furniture. Upholstery fabrics warp knitting is commonly used: most tricot machines used for upholstery, wall partition, office panel fabrics are at least four-bar warp knits (Kadolph, 2009), raschel machines produce high pile upholstery fabrics (Kumar, 2014).

1.1.2. Structure of upholstery synthetic leathers

Among the variety of upholstery materials, there are different leathers (natural, synthetic, perforated) which are applied for cars, boats, aircraft seats, etc. Many scientists have studied physical, mechanical and thermal properties of natural (Sureshkumar, Thanikaivelan, Phebe, Kaliappa, Jagadeeswaran, & Chandrasekaran, 2012), (Tsaknaki, Fernaeus, & Schaub, 2014), (Turk, Ehrmann, & Mahltig, 2014) and artificial leathers (Turk, Ehrmann, & Mahltig, 2014), (Schwarz, Kovacevic, & Kos, 2015), (Ujevic, Kovacevic, Wadsworth, Schwarz, & Sajatovic, 2009).

Synthetic leather is called in many different ways: faux leather, vegan leather, artificial leather, vinyl or leatherette. It is a manmade fabric which is made by using PVC or PU that is treated and dyed to resemble real leather and is used in upholstery, clothing, fabrics and other uses where a leather-like finish is required (Kinge, Landage, & Wasif, 2013), (Schaefferr, 2003).

Vinyl is a synthetic man-made plastic material (Jezek, 2015) made from ethylene and chlorine. When processed, both substances are combined to form the Polyvinyl Chloride (PVC) resin, or – as it is commonly referred to – Vinyl. Vinyl is defined as a very strong and durable plastic material. The advantages of this plastic is the resistance against moisture and humidity; also, the production of this material is not expensive, and it can be manufactured in a variety of colors (Jezek, 2015). Vinyl fabrics are classified into groups or ‘grades’ according to their uses (Nikki, 2014), (Different Grades of Vinyl Upholstery Fabric, 2016): *Marine Grade Vinyls*, *Automotive Grade Vinyls*, *Decorative Vinyls*, *PVC Coated Vinyls*.

Perforated leather features small equally spaced holes, which delivers the advantage of using it for heated leather seats (Popely, 2012), (Are Perforated Leather Seats Better, 2014). Usually, perforated leather is used not only in furniture upholstery, but also in automotive, especially sports cars (also named SUV), interior, where not only luxury seats are coated, but so is the internal panel, the console, and the steering wheel (Are Perforated Leather Seats Better, 2014). Perforated leather is usually related with adjustable temperature controlled seats. The biggest advantage of perforated seats is revealed in summer due to the breathable nature of this material: through the holes of perforated leather, the airflow offers the seat comfort for hot weather when the holes provide a natural cooling of the seat. Perforated leather is thicker than non-perforated leather; therefore, it is more comfortable (Leather Seats and Trims, Are Perforated Leather Seats Better, 2014), (Popely, 2012).

Some investigations of normal sound absorption, airflow permeability, mass, thickness and perforation density were analyzed for perforated leathers. It was established that perforated leathers exhibit good absorption but are still out-performed by most cloth seat fabrics (McMullan & Mealman, 2001).

Artificial (or natural) leather may be perforated with eight standard patterns (Fig. 1.2) that play with geometry and repetition (Spinneybeck, 2016). For all the patterns, the perforation diameter is 1.32 mm except for pattern 6 with its 2.16 mm diameter. The density is very different for the patterns, and it is shown in Fig. 1.2.

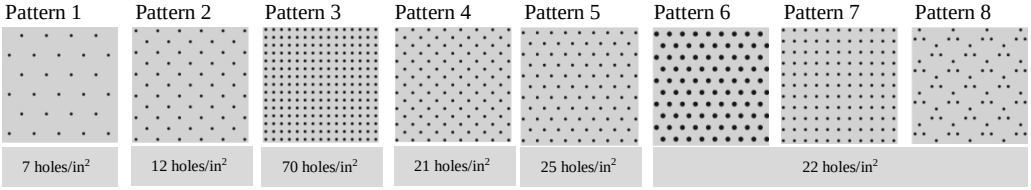

Figure 1.2. Standard patterns of artificial leather (Spinneybeck, 2016)

(Daukantiene & Gutauskas, 2001) in their research established that the character of punch deformation curve *P-H*, as well as the level of the resistance parameters, depend on the size of perforation (defect).

Automotive upholstery materials are usually classified into two categories (Automotive Interior, 2010-2016) – 'Fabric' and 'Non-fabric' materials, which are available in various types according to their compatibility with the car interior cabin and the formability to the seat shape. The category of fabric materials for automotive upholstery is divided into woven (moquette and plain weave fabric), circular knitted fabric (jersey and sinker pile fabric) and warp knitted fabric (tricot and double raschel fabric). Moquette is a type of woven pile fabric in which cut or uncut threads form a short dense cut or a loop pile (Moquette, 2017). Generally, moquette fabrics are made from a wool nylon face with interwoven cotton backing (Moquette, 2017). Circular knitted jersey fabrics have excellent elongation, which is generally applicable to moulded automotive seats. Sinker pile knitted fabric also has excellent elongation values thus providing good form ability regarding the seat shape or configuration.

Tricot is commonly applicable as the most standard material (like woven fabrics of plain weave) in automotive upholstery, as well as in furniture upholstery. The warp knitted double raschel fabric is more resistant against abrasion than flat woven, circular knitted flat and warp knit flat fabrics (Pamuk & Ceken, 2008).

The category of non-fabric materials for automotive upholstery are divided into woven natural leather (Luxnova), synthetic leather (neosofeel, neosofeel Quole, neosofeel mythos), artificial leather (Lux suede and Grand luxe) and PVC leather (Automotive Interior, 2010-2016). Luxnova is a new material based on natural leather using its natural characteristics and improving its weaknesses. Synthetic leathers are not only as durable as natural leathers, but also are light enough and are thus being increasingly used in automotive upholstery. Synthetic leathers neosofeel are manufactured so that to achieve balance between appearance and durability,

herewith remaining environmentally friendly. Neosofeel Quole leather is very durable and functional due to possessing high appearance quality. Neosofeel mythos leather was designed to feature new colors and luster. Artificial leathers are characterized by smooth hand feel and high quality thus finding applications in the high grade automotive upholstery. Two types of artificial leather are used in automotive upholstery – lux suede (durable and smooth hand feel) and grand luxe (great elongation properties). The last of the non-fabrics is PVC leather which is a low-priced material characterized by its durability, and it is generally used in upholstery for commercial vehicles.

There are lots of requirements for seat upholstery textiles such as mechanical, thermal, chemical, ultraviolet and infrared resistances including comfort and aesthetics (Hada & Garg, 2015).

One of the most important criteria about ergonomically designed car seats is to make the passenger feel no bodily fatigue due to the sitting discomfort (Fung, 2000). In this case, the upholstery is also very significant, which is responsible for the pleasant contact between the passenger's body and the seat.

The main uses of non-woven material in the interior of the seat are lining solid metal, wooden and plastic car components. Upholstery fabric must be strong enough and must be denoted by good aesthetics, rigidity and abrasion resistance during the car exploitation period. The advantage of artificial leather is that additional properties may be constructed into the fabric (Fung & Hardcastle, 2000).

Other researches describe automotive textile as an integral aspect of technical textile (Gupta, Maheshwari, & Kumari, 2016). Gupta *et al*. in their study define the significant role of monofilament yarn at fabric and seat trim levels in automotive seating application, due to the influence of monofilament in fabric which provides aesthetics and strength to the seat trim. Fabrics with monofilaments must be evaluated during the stitching process. The authors conclude that the main parameters are the importance of the monofilament yarn, its evaluation criteria and its performance at fabric and seat trim levels.

(Koc, Mecit, Boyaci, Ornek, & Hockenberger, 2016) investigated the effects of the filament cross section on the performance of automotive upholstery fabrics. They prepared thirty-six yarns by changing the cross section of poly(ethylene terephthalate) fibers (round, octolobal and W-channel) and the air-jet texturing parameters (overfeed and the number of core and effect yarns). First of all, the yarns were heated and dyed, and then woven into fabrics and laminated. When analyzing the test results of air-jet textured yarns and fabrics, it was observed that the air-jet textured yarn structure depends on the W-channel which gives the most prominent difference. It forms a massive, irregular yarn structure with lots of open loops. The results of recovery from strain behaviors of the air-jet textured yarns were observed to be insignificant. With the looped structure's increase, the higher regular elongation values were observed for all the cross-section types. All the filament cross sections provided adequate light fastness and the abrasion resistance test results for fabrics. The researchers found that the most important effect on air permeability was detected for filament cross section changing. The lowest air

permeability was obtained from the W-channel; on the contrary, the highest value was obtained for octolobal.

1.1.3. Coating and laminating processes for upholstery textiles

Generally speaking, upholstery fabric is a textile material of complex weave or a compound textile material whose stability is improved when fusing with woven, non-woven or knitted fabrics, the same as laminating artificial leather with the woven or knitted back side (Fung, 2002).

Coating and lamination are the main processes used to complete the finishing of a textile material. Such polymers as PVC, PU, acrylic, PTFE are usually used in textile coating with the aim to waterproof fabrics, protect fabrics, implant electrical installation, laminate blackout curtains, etc. (Singha, 2012).

Laminating is obtained by thermal joining, which is performed by coating a thin adhesive film and using a high temperature bonding so that to join the surfaces together (Fung, 2002). Laminated upholstery fabrics are denoted by higher strength and reduced elasticity compared to the basic upholstery fabrics (Technical textile laminates and interlinings for upholstery, 2014). Upholstery fabrics can be made of two-layer, three-layer or multi-layer laminates. There are two main categories of post-finishing fabric (Nielsen, 2007):

- laminating a fabric of another material (vinyl, knit, paper);
- the adhesion of a liquid used on the back of the fabric, including foam flame-retardant finishes, acrylic latex, and silicone.

Vinyl lamination is usually used for seat cushions, headboards, table covers, shower curtains and upholstery (Nielsen, 2007). High-quality vinyl lamination will meet most upholstery flammability standards and should contain an ultraviolet (UV) inhibitor to deter fabric fading and deterioration from sunlight and other light sources. **Moisture-barrier** (interlining) **backing** is a vinyl barrier laminated to the back of upholstery fabrics (Nielsen, 2007). Such laminated fabrics are used to protect from fluids (spills, urine) and feature antibacterial and antifungal properties as well. **Water-repellent finish** is irreplaceable in outdoor fabrics and marine upholstery (Nielsen, 2007). **Stain protection** or **siliconizing** does not require laminating. The fabric is protected from oil, water stains, dust and soil. **Moth** and **mildew resistance** gives a protection against mould, mildew, and fungus growth, which can be applied at the same time with other finishes (Nielsen, 2007). In order to **stabilize** upholstery fabrics, manufacturers use a **latex backing**, which prevents seam slippage, fraying, stabilizes the fabric and makes it more durable, keeps the surface yarns from shifting, makes the cutting process very easy and accurate (Selecting Fabric for Upholstery, 2009). **Acrylic backing** is used for upholstery and wall applications (Backing or Back Coatings, 2017). Upholstery fabric with acrylic backing is more flexible, prevents seam slippage, fraying, curling (Nielsen, 2007). Seam slippage strength, abrasion resistance and tendency to surface fuzzing of double woven upholstery fabrics have influence on the weave interlacing coefficient, the average float length, the friction between intersecting yarns and yarn settings (Ozdemir & Yavuzkasap, 2012). The researchers stated that the effect of weft

setting, which is determined by the weave, the yarn count and the yarn type has a major effect on the seam slippage strength of double woven upholstery fabrics.

When analyzing the thermal performance of three different textiles (100% cotton, 50% cotton and 50% acrylic fiber, 100% acrylic fiber) by photopyroelectric technique only from the algorithm of the amplitude pyroelectric signal, it was determined that 100% cotton is the coldest textile (which is requested in summer); on the contrary, 100% acrylic fiber is the warmest textile (Mami, Najoua, Mellouki, & Yacoubi, 2017). **Durablock** is a high performance textile technology that laminates a durable liquid barrier to a textile treated with Nano-Tex (Backing or Back Coatings, 2017). The relevance of this technology is its cleanability and optimum spill/stain prevention of the cushion. Another way of backing upholstery textiles, which is fairly common, is **knit backing**, also used for drapery applications (Backing or Back Coatings, 2017). Knit backing ensures the dimensional stability and enhanced strength of the fabric maintaining the original appearance and touch sensation. The effects of the selected finishing methods on the wrinkle resistance of laminated and non-laminated car seat cover fabrics were investigated by (Degirmenci & Celik, 2013). For the investigation, five types of warp knitted fabrics from 100% PES yarn with different properties were used. It was determined that silicone softener during the dyeing process did not ensure any extra resistance against wrinkles; meanwhile, when the silicone softener was used at the time of the fabric passing from foulard, it gave perfect resistance against wrinkles. Some upholstery manufacturers use a **fray reducing product** *Sprayway No Fray Spray* (Winters, 2012), which is recommended for smooth and shiny polyester and rayon fabrics because of their ability to unravel or minimize fraying.

A composite upholstery panel includes a layer of ticking fabric, a layer of flame and heat-resistant backing fabric, and a layer of resilient flame and heat-resistant cushioning material sandwiched between the layer of the ticking fabric and the layer of the backing fabric (Jones, Small, Walton, Baldwin, & Mikaelian, 2013).

1.1.4. Mechanical behavior of upholstery materials

Upholstery materials during their performance experience biaxial deformations, which are effected by friction in the contact zones: material-to-human skin (Vilhena & Ramalho, 2016), (Derler, Schrade, & Gerhardt, 2007), (Rotaru, et al., 2013), (Tasron, Thurston, & Cerre, 2015), material-to-material (Bertaux, Lewandowski, & Derler, 2007), material-to-inner parts of the furniture: polyurethane (Takuya, Tsuneaki, Soo, & Yuji, 2010) or metal (Das, Kothari, Kumar, & Mehta, 2005). The majority of such investigations are related to the clothing industry with the aim to increase the comfort in contact with the human skin. It is especially important in medicine – for injured or disabled patients who are chained to a wheelchair (Vilhena & Ramalho, 2016), (Rotaru, et al., 2013), in sports – for athletes to reduce the friction between the clothing and the weather conditions, e.g. snow (Nachbauer, Mossner, Rohm, Schindelwig, & Hasler, 2016). New technologies are applied (Dong, Kong, Mu, & Lu, 2015) in innovative textile materials surface treatment HeiQ's Glider, which helps the wearer feel more

comfortable while being involved in summer sports (Phillipp, 2014). A realistic skin model in combination with an objective friction test method allows developing new textiles for sport and medical applications with improved skin-adapted surface and frictional properties (Derler, Schrade, & Gerhardt, 2007).

Different lubricants are also applied in friction studies (Jawale & Patil, 2011), (Gerhardt, Lottenbach, Rossi, & Derler, 2013). Jawale *et al*. applied a lubricant to affect both yarn-to-metal and yarn-to-yarn friction (Jawale & Patil, 2011). (Ujevic, Kovacevic, Wadsworth, Schwarz, & Sajatovic, 2009) analyzed the strength, i.e. the breaking force and elongation, bursting strength and elongation, and the density of two kinds of artificial leather designed for car seat upholstery: artificial leather with woven fabrics on the back side and artificial leather with knitted fabric on the back side. (Koochakzaei, Ahmadi, & Achachluei, 2016) analyzed the influence of lubricants for the mechanical properties of goat leather samples. The researchers obtained that the mechanical strength of untreated leather samples increase after ageing while silicone oil treatment does not affect the mechanical strength of leather. In other investigations, mechanical properties (tensile strength and elongation at break) of chrome-tanned leather were analyzed from the standpoint of the treatment with two different copolymers (Nashy, Essa, & Hussain, 2012). The authors revealed that mechanical properties are higher for leather upon treating if compared to the untreated one. Also, it was determined that tensile strength and elongation at break are higher if compared to the leather treated by a copolymer which contains a higher ratio of the soft butyl acrylate monomer.

It was determined in other publications (Daukantiene & Gutauskas, 2001) that when a PE membrane was punched without any lubricant, the character of the punch deformation curve and the failure of the shell change in the case when specimens have major defects (a defect is a hole cut in the centre of the specimen), i.e. the sizes of defects varied in the range of 0.06–0.22, (the ratio of the defect radius and the specimen radius), but when using a lubricant (water), the changes were observed for all the specimens with defects.

It is known that the main mechanical property for leathers is the tensile strength (Liu, Latona, Lee, & Cooke, 2009). (Schwarz, Kovacevic, & Kos, 2015) analyzed the principal characteristics and the construction parameters of artificial leather with bonded textile fabric on the back side, also by evaluating joining (sewing) and its quality which determines the durability, comfort and aesthetics of the automotive interior design. The most important parameters for upholstery fabrics (artificial leather) durability are the breaking force and the elongation at break, and they were tested in different circular directions. The investigation showed that the longitudinal direction (warp/wale) is denoted by higher breaking properties.

(Schwarz, Kovacevic, & Kos, 2015) carried out a research comparing two groups of upholstery fabrics which were different in terms of the fabric back side structure (woven and knitted) but had similar characteristics (mass per unit area and thickness). The research aims to determine the use of laying cut parts which have significant importance in the construction of car seat covers so that to achieve best results in terms of durability under the influence of stress applied when in use; this is

backed up by testing the fabric breaking properties in different directions when seeking to identify the direction with the greatest strength. Researchers confirmed that structural parameters of the compound material and constructional parameters of the back side fabric (woven or knitted) influence and make a big difference in their properties. Therefore, the highest strength of compound materials is determined in the direction of 0° and 90°, artificial leather samples with woven back side show a higher strength, in all other directions, material strength is greater in artificial leather samples with the knitted back side. Sewing materials reduce the breaking properties in artificial leather samples with the knitted back side. These factors are of great importance in processing the cutting and the laying of cut parts when considering the direction of the greatest strength, i.e. the direction of 90° (warp/wale direction). It is essential to appoint the direction of the highest stress of the car seat cover in actual use, thus improving durability and stability.

The results of the research concerning the properties of cottonized flax/cotton rotor blended yarns and fabrics for upholstery applications are presented in (Sava & Ichim, 2015). The researchers used a double carding technology which was developed for producing rotor-spun yarns of 29.5 tex, 59 tex, and 100 tex linear density from 30/70 and 50/50 cottonized flax/cotton blends. In order to compare cotton yarns, all of them were similar in linear densities. The tensile and tear strength parameters were tested in longitudinal and transverse directions for the 30/70 cottonized flax/cotton rotor blended yarns which were woven into three different ways of fabrics. The evaluation of woven fabrics was performed due to their suitability for upholstery applications.

Lengyel *et al*. analyzed the knitted side of two synthetic leathers of which the first one had a PU matrix, and the second one had a PVC matric. Both materials are used in furniture and automotive upholstering. The researchers calculated the yarn eye by using different geometric models and evaluated the relative surface deformation under biaxial loading. The results revealed that a relative deformation for the PU matrix material was 6.29% while the relative deformation for the PVC matrix material reached 9.41% (Lengyel, Faur, Nes, & Cernescu, 2016).

The key factor (when textiles are used in outdoor architectural applications) which should be considered during the project design is the durability of textile membranes. During the process of coating, the degradation of the polymers promotes the loss of functional performance, especially the mechanical properties. Researchers (Joao, Carvalho, & Fangueiro, 2016) analyzed the durability of two architectural membranes. One of them was made of a PES fiber coated with PVC, whereas the second was made of a glass fiber coated with PTFE. The experiment of in-situ degradation with the testing materials was performed in a real environment and in the context of rapid degradation affected by moisture and ultraviolet radiation; it was performed in an accelerated ageing chamber for 3 months. The influence of these factors on the degradation involving the durability of the membranes was estimated by the loss of mechanical performance performed by the tensile strength test and in terms of the thermal performance levels according to Alambeta test. The testing results showed the unchangeable properties of mechanical

performance of PES/PVC membranes; however, the glass fiber/PTFE membrane showed a reduction of the tensile strength properties. When conducting the accelerated degradation test (the duration was 2,160 hours), the reduction of the membrane was more significant; the decrease reached about 34% in longitudinal and 43% in the transverse direction. No significant differences were shown via SEM images of PES/PVC membranes or via SEM and EDS images of the glass fiber/PTFE membrane except for the case when EDS analysis showed a loss of 52% of the chlorine element.

1.2. Deformational Behavior of Flexible Multilayer Textile Materials

Up to date, the problems of fitting woven and knitted fabrics to three-dimensional surfaces have been analyzed from the standpoint of their mechanical and physical properties. The investigations have been performed with the aim to find out the relationships between the parameters of uniaxial and biaxial behavior (Strazdiene & Gutauskas, 2003a) and to define the effect of materials anisotropy level upon the shapes of spatial objects obtained under biaxial loadings (Klevaityte & Masteikaite, 2008). Other investigations showed that pre-tension is an effective method to improve the quality of shaped composite parts (Bekampiene, Domskiene, & Sirvaitiene, 2011). Still, the problem of practical application remains. The dimensions of furniture upholstery patterns must be adjusted in respect to different mechanical properties of the materials in use.

The problem lies in the fact that the entire range of upholstery materials is denoted by differences in terms of their strength properties and deformational behavior in longitudinal and transverse directions. Thus it is not appropriate to design upholstery patterns with the same ease values for all the materials we make and use. The result of such a practice is evident – furniture coverings of low quality experience significantly high residual deformations during their exploitation. It means that the mechanical characteristics of each applied material must be taken into account individually. Many researchers explore such undesirable deformation as bagging which is significant not only for garment fabrics but also for upholstery furniture production (Jaouachi, 2013), (Hasani, Zadeh, & Behtaj, 2012) and (Baghaei, Shanbeh, & Ghareaghaji, 2010).

A significant amount of research has been done when analyzing the behavior of textiles in uniaxial tension and biaxial loading (Chen, Chen, & Zhang, 2013), (Escarpita, Cardenas, Elizalde, Ramirez, & Probst, 2012), e.g. woven fabrics (Kovacevic, Ujevic, & Brnada, 2010), (Vanclooster, Eshghyar, & Lomov, 2011), (Saceviciene, Strazdiene, Vilumsone, & Baltina, 2012) and knitted materials (Saceviciene, Strazdiene, Vilumsone, & Baltina, 2012), (Dobrich, Gereke, Cherif, & Krzywinski, 2013). Fused textile systems are used not only to perfect the functionality of clothing (Tijuneliene, Strazdiene, & Gutauskas, 1999), but for technical purposes as well, such as the reinforcement of auto window glass (Ancutiene & Strazdiene, 2010), architectural fabrics consisting of a woven base cloth with an impermeable coating providing water-proofness and weave stability (Bridgens, Gosling, Jou, & Hsu, 2012), cellular woven fabrics which can also be

used as technical textiles subjected to bursting and impact forces (Ozdemir & Mert, The Effect of Fabric Structural Parameters on the Tensile, Bursting and Impact Strengths of Cellular Woven Fabrics, 2013). Other researchers investigated the interactive effects between warp and weft in biaxial tension (Chen, Chen, & Zhang, 2013), (Kovacevic, Ujevic, & Brnada, 2010), (Wang, Chen, Cheng, & Li, 2012). Several researches of the effect of pre-tension (pre-stress) have also been conducted (Vanclooster, Eshghyar, & Lomov, 2011), (Yang, et al., 2012), (Bekampiene, Domskiene, & Sirvaitiene, 2011); the issue of the behavior of composite systems with concrete, glass, fibers, etc. was investigated in (Peled, Cohen, Pasder, Roye, & Gries, 2008); (Kruger, Reinhardt, & Fichtlscherer, 2001) discovered that pre-stressing is even more advantageous in the case of high strength fabrics. The limit of proportionality as well as the modulus of rupture and cracking stresses considerably increases with the increase of pre-stressing. Meanwhile, there is no information concerning the effect of pre-tension upon biaxial behavior of fused multilayer textile systems which are often used when manufacturing interior products and upholstery furniture.

It must be noted that the main part of textile materials during their exploitation are affected by forces perpendicular to their surfaces. As a result, the shell, i.e. a spatial surface with the biaxial state of deformation, is developed. Up to date, two biaxial deformation test methods are well-known and widely used for such investigations, i.e. the membrane method (pneumo- and hydro-) and the punch method (Strazdiene & Gutauskas, 2003a), (Strazdiene, Gutauskas, Papreckiene, & Williams, 1997). These methods yield good results of real loading simulation in aerostatic balloons, sails, inflatable building constructions, elements of clothing, soft packing and in other products made from thin materials. Recently, their application has expanded by involving the testing of rubber, leather, textiles, polymer films, paper and other materials (Gutauskas, Papreckiene, Masteikaite, Daukantiene, & Strazdiene, 2000), (Tijuneliene, Strazdiene, & Gutauskas, 1999).

Except for the simulation factor, there is one significant quality of the thin sheet biaxial deformation method compared with the widespread uniaxial tension method. From the technical standpoint, the process of biaxial deformation is simple, and samples never tear close to the clamp (Tijuneliene, Strazdiene, & Gutauskas, 1999). This allows for more reliable assessment of results and a reduction in the expenses related to the number of test samples and their preparation. In spite of the wide range of experiments with various types of materials, there is still significant discrepancy between the theory and the test results. The research work comparing the behavior of the same material in uniaxial and biaxial deformation is fairly limited.

Bagging is a kind of three-dimensional residual deformation that deteriorates the aesthetical appearance of a garment during its wear (Juodsnukyte, Gutauskas, & Cepononiene, 2006). Recently, many researchers have been paying considerably more attention to the exploration of this phenomenon (Juodsnukyte, Gutauskas, & Cepononiene, 2006). (Yeung, Li, Zhang, & Yao, 2002) used a special method to evaluate fabric bagging from the captured images of bagged fabrics by image

processing and abstracting the criteria to recognize the magnitude of bagging. (Juodsnukyte, Gutauskas, & Cepononiene, 2006) analyzed the influence of mechanical parameters to the punch loading process. Kisilak investigated the spatial deformation of fabric under cycle loading by simulating the process taking place in the zones of garment elbows and knees (Juodsnukyte, Gutauskas, & Cepononiene, 2006), (Kisilak, 1999). In many cases, experiments were performed by adhering to the punch loading principle, e.g. such a method is described in (Strazdiene & Gutauskas, 2003a), (Strazdiene, Gutauskas, Papreckiene, & Williams, 1997), (Juodsnukyte, Gutauskas, & Cepononiene, 2006), (Yeung, Li, Zhang, & Yao, 2002), (Kisilak, 1999), (Strazdiene & Gutauskas, 2003b), (Strazdiene, Daukantiene, & Gutauskas, 2003) and (Strazdiene & Gutauskas, 2001).

For the biaxial punch loading tests, different types or sizes of the punch have been used with the intention to investigate the deformational behavior of textile materials. (Rocher, Allaoui, Hivet, & Blond, 2013) presented the results of bias, compaction, bending, friction and forming tests performed in order to characterize the formability of two three-dimensional (3D) fabrics of commingled yarns where a highly double-curved punch with a triple point (a tetrahedral punch) was used for a forming test. (Yin, Peng, Du, & Guo, 2014) used the model where the punch, die and binder were modeled as rigid bodies, and a constant 50 N force was imposed on the binder so that to clamp the plain woven carbon fabric in order to prevent wrinkling. Vanleeuw *et al*. used a double-dome shaped punch to measure the full field displacements (Vanleeuw, Carvelli, Barburski, Lomov, & van Vuure, 2015). When the double-dome punching is being performed (targeting both warp and weft directions), the quasi-unidirectional flax reinforcement does not visualize any significant defects. What concerns to the greater drapability of the flax fabric, it is necessary to reduce the number of intersections. For this reason, during the initial shear deformation, the influence of friction is reduced (Vanleeuw, Carvelli, Barburski, Lomov, & van Vuure, 2015).

(Wu, Zhang, & Wu, 2012) investigated the size-dependent plastic deformation of a Zr-based metallic glass under biaxial loading by conducting the small punch test. The researchers discovered that both the critical shear offset and the density of shear bands decrease with the reduction of the sample thickness. However, the normalized critical shear offset keeps constant, which can well explain the worsened plastic deformation behaviors under small punch loading. (Zhang, Sahraei, & Wang, 2016) analyzed deformation and failure characteristics of four types (PE, three-layer, ceramic-coated, non-woven) of lithium-ion battery separators. Biaxial punching was performed with four punches of different sizes (Fig. 1.3) which were made of Teflon to reduce friction.

Figure 1.3. Punch test simulation with different punch sizes (Zhang, Sahraei, & Wang, 2016)

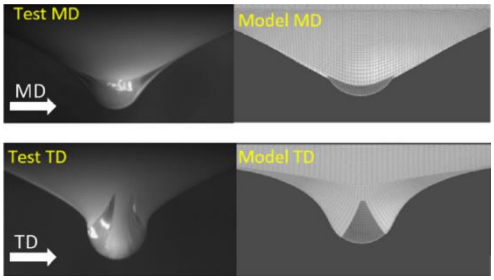

Figure 1.4. Side-view comparison between the test and the simulation from vertical planes along MD and TD (Zhang, Sahraei, & Wang, 2016)

Figure 1.4 shows a comparison of the model and the test during 3.175 mm punch loading in two planes. Due to anisotropic properties, the side views from vertical planes along MD (machine direction) and TD (transverse direction) show different slopes.

1.2.1. Classification of flexible multilayer textile materials deformational behavior assessment methods

The mechanical properties of textile materials have been the object of scholarly studies for a long time. In terms of the relevance for this study, an overview of explorations of the deformation properties of textile materials is essential. In the 1980's, a new point of view was established towards textile fabric experiments, which covers both subjective changes in the behavior of textiles and their objective mechanical properties (Bishop, 1996). In 1972, professor Kawabata carried out analysis of subjective evaluation methods and established the basis for standardization. This analysis was conducted in two stages. The first stage was the determination of the criteria for subjective evaluation while characterizing the properties of textile fabrics. The second stage involved the development of fast, easy to use and accurate experiment basis for textile fabrics investigation. This resulted in manufacturing specific experiment equipment KES-F (Kawabata Evaluation System for Fabrics). The KES-F system consists of four instruments: Tensile and Shear Tester KES-FB-1, Bending Tester KES-FB-2, Compression Tester KES-FB-3, and Surface Friction and Roughness Tester KES-FB-4.

KES-F is more advanced than the earlier methods and equipment used for the investigation of mechanical and physical properties of fabric surfaces. Its advantages are based on the capacity to investigate not only the quality of the fabric, but also the whole product, thus having a significant role in optimization of the manufacturing process.

Another measurement system for textile materials was developed in Australia. It is called SiroFAST (Fabric Assurance by Simple Testing). The latter system differs from KES-F of semicycle testing. It is of lower cost and is easier to use. The SiroFAST system is developed with the objective to measure the mechanical and dimensional properties of textile materials. The system can also be used to predict the performance in garment manufacture by evaluating the mechanical properties of

textile materials in measuring bending, tensile, shear and compression (De Boos & Tester, 1989). It is important to note that both measurement systems were developed to measure at low stress level loads, which correspond to real-life wearing conditions.

The main property of textile materials is the ability to deform without tearing. The external forces and composition of textile materials exert a great influence on this process. The structure of materials and their shape change when external forces are acting. Deformation of fiber and regularities of breaking processes influence the mechanical properties of textile materials. The most important mechanical characteristic of textile materials is their capacity to be tensile as the prevailing loads act in the longitudinal direction. Tensile forces till break and strain are the main characteristics of the tension process (Matukonis, Palaima, & Vitkauskas, 1989).

Textile fabric is a system of threads and fibers. The area of the surface of the textile fabric is very large when compared to the weight, and the system has its own inherent mechanical strength. Woven fabric is a product consisting of two overlaying thread systems (longitudinal and transverse). Longitudinally oriented threads stand for warp whereas transverse threads stand for weft.

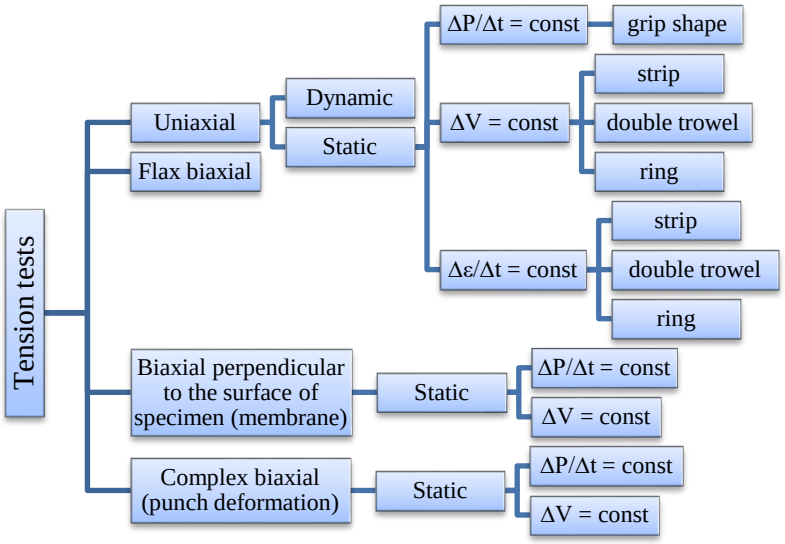

Figure 1.5. Classification of textile materials tensile test (Кобляков, 1973)

The experimental basis of mechanical properties of textile materials simulating their real use conditions is very wide. The forces perpendicular to the surface of the specimen simulate the behavior of textile materials in real wear conditions. All the new methods developed for deformational ability of textile materials are complementary to the previous methods because the uniaxial tensile is the starting point of deformation.

The testing strategies for textile materials tensile are very extensive. They can be classified into 4 types according to the direction of deformation: uniaxial, biaxial

flat, biaxial perpendicular to the surface of the specimen (membrane) and complex biaxial perpendicular to the surface of the specimen (punching). The classification of tensile tests is presented in Figure 1.5, which outlines the main indicators: the character of deformation, the direction, the mode and load parameters. The distribution of deformations and critical stresses under membrane and punch testing methods is different as these methods differ between each other in respect to external load application. During membrane deformation, the normal pressure distributes equally in the entire area of the specimen's surface, though, during punch deformation, the main stresses concentrate in the contact zone between the punch and the specimen (Аронова & Соловьев, 1971).

One of the modes of the tensile should be selected for the tensile test: short-term (dynamic), medium (static) and long-term. In practice, the medium (static) tensile mode is usually used because of lack of time. In this case, only dynamic and static tensile test classes are presented in this classification. According to the selected constant parameter, the tensile tests are divided into the cases when:

- the velocity of clamps is constant (ΔV = const) while the velocity of strain and deformation changes with their increase;
- the strain increase of the specimen remains constant (ΔP = const);
- the velocity of specimen deformation remains constant (ε_c = const).

In terms of specimens of different shapes and various fastening techniques in the clamps of the tensile machine used in the course of tensile tests, the tests are classified into 4 groups:

- the 'strip' method is used when rectangular specimens are stretched along the entire width;
- the 'grip shape' method is used when a certain area of the specimen is stretched along the width;
- profiled or ring specimens;
- closed circuit specimens.

Loadings acting in the course of product manufacturing and exploitation are significantly lower compared to breaking forces. Therefore, the investigations which are aimed to determine the level of such loads are very important (Makinen & Meinander, 2005). It is known that, during garment wear, fabrics experience tension forces which can vary from 7 N to 90 N (for the specimen width of 5 cm). Even more, certain clothing zones can experience external loadings which comprise 18% ÷ 25% of the breaking force, whereas in other zones they only reach 5% – 10% of the breaking force.

Numerous scientists have investigated a sizable number of different textiles by evaluating the parameters of these materials and comparing them with different kinds of measurement systems identified by the measurement system KES-F as a highly correctly performing evaluation system characterizing the processes of textile deformation (Bahadir, Kalaoglu, Jevsnik, Eryuruk, & Saricam, 2015), (Ancutiene, Strazdiene, & Nesterova, 2010), (Apurba, Abhijit, & Sukumar, 2016). Tokmak *et al*. used objective evaluation techniques for mechanical and performance analyzes of 21 woven fabrics. They found strong correlations between each pair of parameters of

the KES-FB and FAST systems (Tokmak, Berkalp, & Gersak, 2010). Some experiments for cotton (woven and knitted) fabrics which underwent reaction with sodium hydroxide, morpholine and cellulose enzyme involved analysis of mechanical and surface properties by using the KES-F evaluation system (Moses & Venkataraman, 2014).

The KES-F system can be used not only for fabrics, and interesting investigations were conducted with paper towels (Kan, Leung, & Mongkholrattanasit, 2016). These authors evaluated the bending properties of paper towels and revealed significant statistical relationship between the weight and bending rigidity *B* but no relationship between the thickness and *B*. The deformability of multiaxial multiply stitched carbon preforms was also studied at low loads by using the KES-F evaluation system (Lomov, Verpoest, Barburski, & Laperre, 2003). The results of the test regarding tension, shear, compression, bending and friction showed that both bi- and quadriaxial fabrics displayed a sufficiently uniform behavior. The general properties of deformability were formulated, and the generic values of parameters for evaluation purposes were suggested (Lomov, Verpoest, Barburski, & Laperre, 2003).

Nowadays, furniture manufacturers encounter extremely high competition in the global marketplace where differentiation, time to market and cost management are the most important factors to success.

Lectra is the world leader in integrated technology solutions designed for industries using fabrics, leather, technical textiles and composite materials in terms of garment manufacturing. The parameters of upholstery materials determined by KES-F or FAST systems are used in Lectra's software *DesignConcept Furniture V3R1* with its 2D/3D collaborative design, cost calculation and virtual prototyping solution for upholstered furniture (Globe news wire, 2016). Such processes as even stitching, buttoning, etc. used in upholstery manufacturing can be virtually prototyped by establishing the cost and preparing for production. This software was created to shorten process times – up to 20% in preparing design reviews, 25% in physical prototyping and 25% in developing stitched and buttoned models. The key to the increase in effectiveness is mutual product development, pre-production planning and preparation processes enabling different teams to organize simultaneous work on the cover, frame and foam.

A virtual simulation of new models helps to cut by half the number of physical prototypes which are expensive and time-consuming to manufacture. A simple sofa could serve as an example. The usual manufacturing time of the prototype of the traditional sofa is 15 working days, while with the use of the software features, it could be cut down to 11 working days. Obviously, this stands for a significant change of time consumption. The current new version is integrated with the options for wide use of standardization; this particularly encourages the creation of a library of different standardized component 3D models which are easily accessible and compatible for use in the upcoming model design and manufacturing. An especially effective feature is the automatic conversion and application of modifications made to the 3D model regarding the 2D manufacturing data; furthermore, the program

generates technical documentation, material bills, CNC (computer numerical control) data for material quantities and dimensions, detailed assembly specifications. *DesignConcept Furniture* helps avoid production errors and reduces costs throughout the manufacturing processes.

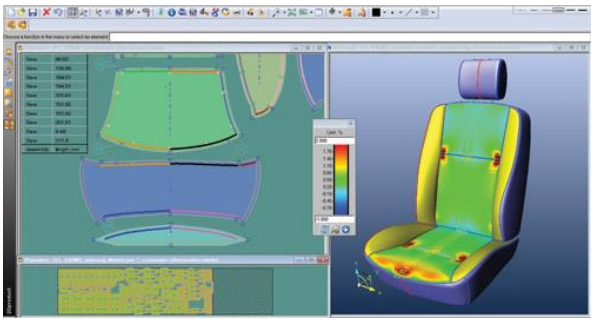

Figure 1.6. Pattern-making and documentation in the *DesignConcept Auto V4R2* suite for a car seat (Gardner Business Media, 2012)

DesignConcept Auto V4R2 (Fig. 1.6) is a virtual prototyping system. It determines specifications for textile and leather prototypes while building the 3D virtual model, thus enabling the manufacturers to obtain more accurate estimates of the total production costs. It is possible to analyze not just one but even a few virtual models side by side, compare the specifics of each design, define the pros and cons, and ultimately find the most suitable one. The *DesignConcept* software has an auto export function for finalized patterns and assembly instructions. Various material prototypes can be managed including leather, composite materials and other industrial fabrics. The pattern preparation process can be used as an example of the proper and beneficial use of the software, i.e. after the seam locations are confirmed on the 3D model, the software improves the quality of the initial 2D patterns thus rendering them into production-ready patterns. This is how the software aids in reducing the number of unexpected imperfections in the prototypes and later processes.

1.2.2. Flexible multilayer textile materials behavior modeling

Usually, textile materials are made from viscoelastic polymers whose mechanical behavior may depend on the usage time factor. Investigations concerning the viscoelastic behavior of such materials as creep and relaxation processes, are still of great importance. Creep is a process when materials under constant stress increase continuously in strain and, vice versa, if a material is kept at constant strain, stresses decrease continuously, and this process is called relaxation (Patil & Nachane, 2009), Several research works deal with the problems of creep and relaxation behavior modeling (Urbelis, Petrauskas, & Vitkauskas, 2005), (Scarborough, Fredrickson, Cadogan, & Baird, 2008) in multilayer materials (Asayesh & Jeddi Ali, 2010), (Gao, Sun, Meng, & Sun, 2012), fused textile systems

(Abid, Dhouib, & Sakli, 2011) and textile composites (Mourid, Ganesan, & Levesque, 2013), (Branke, Kastner, Pohl, & Ulbricht, 2014).

Textile-reinforced composites are of great importance due to the increasing importance of constructive lightweight in the modern engineering science (Branke, Kastner, Pohl, & Ulbricht, 2014). An essential target for manufacturers is the reduction of development costs; for this purpose, the modeling of the macroscopic behavior of the final product featuring numerical simulations is required. (Hufenbach, Mader, Ulbricht, Branke, Kastner, & Pohl, 2013) in their paper presented the investigation of the long-term behavior of modified textile reinforced polypropylene and found that its deformational behavior depends on the asymmetry between the material behavior under tension and compression (dependence is valid only for non-reinforced PP). To predict the behavior of a material, a two-step (the first step is micro-meso, while the second step is meso-macro) homogenization is performed (Branke, Kastner, Pohl, & Ulbricht, 2014), (Hufenbach, Mader, Ulbricht, Branke, Kastner, & Pohl, 2013). During the first step, Hufenbach *et al*. computed the anisotropic viscoelastic behavior of areas with roving (i.e. high fiber volume fraction) by using homogenization procedures applied to linear viscoelastic material behavior. During the second step, they set out a geometric model for a textile-reinforcing structure from CT scans. After that, by using a mesoscopic RVE model, the composite behavior was simulated and then compared to the static (long-term) compression experiments. The results of the experiments revealed deviations between the geometric model and the real structure of the composite as well as asymmetry between the tension and compression of the matrix material.

Another research showed (Renaud, Vernet, Ruiz, & Lebel, 2016) that there is an option to increase the compaction ability of 3D carbon interlock fabrics with water lubrication according to the experiment results which determined faster compactions and higher V_f (compared to dry compaction). The creep process remains stable after 48% of water saturation; consequently it is not necessary to fully saturate the fabric. Another improvement of compaction ability is the increase of the compaction temperature for dry fabrics. During this experiment, it was found out that the stabilization time for the creep process has a stronger impact on dry fabrics compared to the lubricated ones. With the temperature of 160° C, instantaneous compaction to final V_f was reached. Polymer sizing on the fibers influenced the temperature regarding the creep compaction behavior. It is believed that viscosity was achieved at a high temperature because of the friction coefficient decrease between the fibers.

Analysis of the creep properties of non-woven fabrics based on mechanical models was done by (Gao, Chen, & Sun, 2015). Four mechanical models were used for the creep investigation: one-term generalized Kelvin model, two-term generalized Kelvin model, Burger's model and Zurek's model. The suitability of a model for the experiments was checked and confirmed by investigating the creep of non-woven fabrics, then by fitting the data by the above mentioned four models and obtaining their parameter values for Marquardt algorithm for nonlinear regression. Burger's model fitted the experimental creep curves better than the other 3 models.

The suitability of Burger's model to describe the creep behavior of non-woven fabrics was confirmed by conducting evaluation: the residual sum of squares and the correlation coefficient squares were almost equal to each other. The viscoelastic model turned out to be suitable for use when predicting the creep elongation of non-woven fabric.

Iranian researchers (Jafari & Ghane, 2016) presented a viscoelastic model describing the recovery behavior of a machine-made carpet. The mechanical behavior of textile materials by default is modeled by using combinations of spring and dashpot systems. The trend of a carpet sample's loss of thickness at different relaxation times was established by using Jeffery's mechanical model, which is comprised of two bodies representing viscoelastic behavior (Voigt-Kelvin body) and permanent deformation (plastic body), both being set in series to each other. The experimental curves were adjusted to the theoretical model based on the least square method together comparing with the standard linear model. It was revealed that Jeffery's model describes the experimental data while the linear standard model demonstrates poor regression for the recovery properties after unloading. The explanation of such results is that the standard linear model was completely elastic, without secondary creep, whereas the recovery after unloading showed regular creep.

Regarding the stretching load being applied/released, (Jung, Lee, Kim, Ryu, & Ko, 2016) noted that a certain part of deformation/recovery does not occur immediately, and a certain part of deformation is never recovered. It was found out that, during modeling, the inelastic stretch of cloth, the decomposition of stretch deformation considering the time intended for the stretch/recovery is significant since the modeling of separate components (sudden elastic, viscoelastic, and plastic) is easier to formulate than the combined deformation. The process when the extension increases within time while the stretching force is constant is called the creep. When the force creep is maintained constant, the deformation is classified into 3 components:

- Immediate Elastic Deformation (IED) is considered at the moment when the deformation occurs instantly after the loading/unloading.
- Viscoelastic Deformation (VED) begins after IED starting with constant force stretch. The same happens after unloading (the recovering part).
- Permanent Deformation (PD), compared to the total extension during a stretch deformation, never allows recovery.

When considering the proportion between viscoelastic and plastic components which are invariant during the loading, it is possible to predict decomposition (Jung, Lee, Kim, Ryu, & Ko, 2016). What regards this statement, a non-elastic stretch model based on Kelvin's equation was developed. According to experimental results, it is possible to control the non-elastic nature of stretch deformation reproduction.

A method developed by (Jung, Lee, Kim, Ryu, & Ko, 2016) was aimed to identify the parameters of the non-elastic model (based on Kelvin's equation) in

order to avoid the sensitivity of measurements and complexity in the optimizing process.

The computational parametric model (Farukh, Demirci, Sabuncuoglu, Acar, Pourdeyhimi, & Silberschmidt, 2013) was used to analyze extensive deformation of low density non-woven fabrics. This model comprises elastic and viscous properties of the fibers. It resulted in the model being capable to accurately simulate the mechanisms which are present in deformation up to the appearance of damage, fabric's anisotropy, effect of constraints conditioned by the clamps, and the uniform stress and strain behavior. Furthermore, the model captures the load jumps due to the tensile strain rate being changed. The parametric modeling technique was used to model the fiber network structure, and the findings were expected to determine the mechanisms in act at the damage initiation and progress with the intention to introduce the corresponding changes in the network topology. The model can aid in finding the areas of the initial damage appearance, and is based on the prediction of stress levels in the fiber network elements. It was confirmed that the model may serve as a proper tool for the analysis of non-woven network elastic, plastic and viscous properties.

The mechanics of the embedded reinforcement structure influences the performance of composite materials (Dobrich, Gereke, & Cherif, 2016). The reinforcements in high-performance composites and textiles are generally composed of continuous fibers, i.e. glass or carbon. When modeling the textile structure, the digital element approach was used on a near micro-scale resolution aiming at the analysis of reinforcement (Dobrich, Gereke, Cherif, & Krzywinski, 2013). The simulation was compared with the testing results and revealed a very good agreement with the approach presented above. The near micro-scale approach takes a near micro-scale textile model with precise geometry and actual mechanical behavior as its fundamentals. Supplementary investigations such as load distribution analysis in the composite are enabled by digital simulation. Textile structures can be established by considering the textile process while knowing the mechanics of yarn.

1.3. Literature Review Summary

High quality soft furniture upholstery must meet the user's needs, fulfill expectations for wear-off, and maintain aesthetic and functional properties as long as possible. The covering fabric must be stable, low-wrinkling, wear resistant and low-punching on the seat zone. Considering the above, manufacturers must use newly introduced modern furniture textiles with the aim to produce items meeting high quality and design trend expectations. The textiles to be applied for a product must be thoroughly investigated on their tensile and deformational properties, and their designated use on different parts of the furnishing product must be correctly determined and assessed. A frequent problem is that the product loses quality as early as in the state of production if the textiles are selected without adequate consideration and investigation of the tensile and deformational properties. Obvious quality defects, such as unintended stretches or shape deformation, are likely to appear in the upholstering process. Analysis of different studies on the subject

shows that the strength properties are the main aspect when furniture and vehicle textiles are being evaluated and selected for production. Scholarly studies highlight that the main load carrying direction is the longitudinal direction. It is not appropriate to evaluate the deformational behavior of materials only from the standpoint of their strength properties due to the fact that, most commonly, the main load carrying direction is not the longitudinal direction but rather the weaker and more deformable transverse direction, which influences the deformational behavior of the materials. On the other hand, the sole evaluation of tensile properties is not sufficient because furniture experiences biaxial deformation upon constant punching (a 3D load is applied), relaxation deformation (when the load is removed), friction between the face side and human skin or clothing as well as the friction which is present between different materials in the inside of the furniture. Furthermore, furniture upholstery in the course of production and when in use seldom endures loads that are at or near the break load; hence it is purposeful to evaluate the fabric's mechanical properties under lower level loads simulating the ones appearing in the everyday use of furniture.

Many researches have been done while analyzing the mechanical properties of light thin textile materials used in clothing by employing the KES-F system. Unfortunately, lack of information is evident regarding mechanical and deformational processes of upholstery materials performed by the KES-F system. It is known that software package *DesignConcept Furniture V3R1* by Lectra company uses the KES-F and FAST system parameters; thus it is essential to determine the deformational behavior of the most problematic upholstery textiles.

Detailed analysis was carried out in the literature review about the materials most frequently used in furniture upholstering, that is, natural and synthetic fiber textiles. Three types of upholstery fabrics are used: woven, non-woven (flock) and knitted (tricot). Woven upholstery materials are jacquard materials (14 types), tapestry, chenille fabrics, velour and corduroy (V-shape and W-shape). The latter type used in upholstering is of a lower number of wales per 2.5 cm. Vinyl fabrics are classified into grades according to their uses (marine, automotive, decorative, PVC coated vinyls). In furniture upholstering, especially in automotive textiles, synthetic leather of different sizes and geometry perforations (there are 8 standard patterns) is used.

Coating and lamination are the main processes used to complete a finishing of an upholstery material. Laminated upholstery fabrics are denoted by higher strength and reduced elasticity compared to the basic upholstery fabrics. In upholstering, the most frequently used lamination techniques are vinyl lamination, moisture-barrier backing, water-repellent finish, stain protection (siliconizing), moth and mildew resistance. In order to stabilize upholstery fabrics, in most cases, manufacturers use latex backing, acrylic backing and knit backing. The less frequently used options are durablock, paper backing and canvas backing.

A lot of research has been done about analyzing the creep and relaxation deformation or using mathematical models since the investigations of creep-relaxation deformations are of great importance and are widely used for various

purposes of textile materials as well as for the evaluation of the deformational behavior of fibers. The elasticity of materials is frequently emphasized, i.e. the ability of a stretched material to regain the initial shape straight after the tensile load has been removed is considered to be of importance. The main researches are performed when a constant load is applied to the material and the creep process is assessed, or, after unloading, the relaxation process is analyzed by taking into account all the constituent parts of creep-relaxation deformation. The conducted literature review allowed modeling deformational processes for upholstery materials by using classical models, such as Maxwell-Thompson and Kelvin-Voigt models.

During their performance, upholstery materials experience biaxial deformations which are effected by friction in contact zones. Different lubricants are also applied in friction studies: silicone oil treatment, water, different copolymers. In some researches, lubricants affect the mechanical properties for the investigated materials, while in others the treatment does not affect the mechanical properties. Lubricants were applied to affect yarn-to-metal and yarn-to-yarn friction. Friction was analyzed in various contact zones such as material-to-human skin, material-to-material, and material-to-inner parts of the furniture (PU, metal).

Many researchers have explored such undesirable deformation as bagging (punching), which is substantial not only for garment fabrics but also in upholstery furniture production. Deformational behavior of various textile materials, polymers, fused systems, woven, knitted and non-woven materials was analyzed in the course of the biaxial punching process with differently sized and shaped punches (tetrahedral, double-dome).

A significant number of researches has been done when analyzing the behavior of textiles in uniaxial tension and biaxial loading, i.e. woven fabrics, knitted materials as well as knitted and woven backgrounds of two-layer materials. Fused textile systems are used not only to boost the functionality of clothing but for technical purposes as well. They are also used for the reinforcement of auto window glass, architectural fabrics (which consist of a woven base cloth with an impermeable coating providing water-proofness and weave stability). Besides, cellular woven fabrics can be used as technical textiles subjected to bursting and impact forces. Several researchers have analyzed the effect of pre-tension (pre-stress) upon the behavior of composite systems with concrete, glass, fibers, etc. They have found out that pre-stressing is even more advantageous in the case of high strength fabrics. Meanwhile, there is no information concerning the effect of pre-tension upon biaxial behavior of fused multilayer textile systems which are often used for interior products and upholstery furniture production. Only limited research work comparing the behavior of the same material in uniaxial and biaxial deformation is available.

2. Methodology of the Work

2.1. Research Object

The research object was selected according to the practical problems which are the most common in furniture upholstering. Manufacturing company *Kauno baldai* selected a variety of most problematic upholstery fabrics. The research object was 27 upholstery textiles which are different in terms of fiber composition, structure, physical and mechanical properties. The textiles were marked with corresponding codes according to their structure: woven fabrics (one-layer and two-layer) correspond to M1–M21, knitted fabrics are referred to as K1, K2 while synthetic leathers are denoted by L1–L4. Surface and yarn characteristics for the investigated upholstery materials are presented in Table 2.1.

Table 2.1. Surface and yarn characteristics of upholstery materials

Material code	Surface density ρ, g/m^2	Linear density D_L, tex 1st layer (2nd layer)		Stitch density D, dm^{-1} 1st layer (2nd layer)		Thickness T, mm
		Long.	Trans.	Long.	Trans.	
M1	305	61	101	290	120	0.71
M2	528	20	262, 454	680	110	1.69
M3	548	153	211	240	180	1.57
M4	532	34 (30)	37, 149 (67)	260 (160)	150 (150)	3.12
M5	376	18 (30)	14 (66)	800 (160)	340 (160)	1.02
M6	272	71	77	200	150	0.54
M7	378	38 (38)	45 (76)	280 (150)	280 (100)	1.25
M8	320	21	80, 252	600	100	1.59
M9	371	41 (30)	41 (72)	320 (150)	270 (100)	1.25
M10	548	45, 250, 470	54, 236, 434	340	70	2.33
M11	672	152, 430	74, 330	140	130	2.41
M12	320	21	21, 149, 250	700	110	1.33
M13	404	18	36, 400	620	150	1.99
M14	347	126	134	160	120	1.18
M15	380	38	256, 423	320	100	1.62
M16	519	316	340	90	90	1.13
M17	483	56	47, 180	280	160	2.17
M18	303	60	100	280	120	0.66
M19	637	20 (36)	279 (130)	700 (360)	160 (140)	2.89
M20	399	228	290	100	60	1.66
M21	298	192	258	70	60	1.20
L1	401	(27)	(64)	180	160	0.98
L2	580	-	-	220	180	1.23
L3	417	(24)	(65)	180	160	0.98
L4	595	(35)	(93)	180	120	1.14
K1	186	-	-	140	200	0.89
K2	291	-	-	160	140	1.60

Notes: linear density and stitch density of the second layer of two-layer materials is presented in the brackets

Upholstery materials used for the investigation are different in structure and weave type (Table 2.2, Figs. 2.1, 2.2). The investigated one-layer upholstery textiles are woven in plain weave (M1, M3, M6, M7, M9, M16, M18, M20), basket weave

2/2 (M10) and twill weave 2/2 (M14). Two-layer upholstery fabrics are woven in plain weave (M7, M9, M21) and bedford cord (M5) and fused with woven fabrics of plain weave (M5, M7, M9) whereas one sample is fused with non-woven interlining (M21).

Complex weaves are specific to chenilles (M2, M8, M11–M13, M15), jacquard material of the brocatelle type (M19) and W-type corduroys (M4, M17) of 2.5 wales/2.5 cm. Different weaves are used in chenille fabrics such as plain weave (for M2 and M12 materials), woven braided rib (M8 and M15 materials), bedford cord (for M13) and combined weave (for M11).

Synthetic leathers L1, L3 and L4 are fused with plain weave wovens, except for L2 which is fused with the knitted background of plain jersey weave. The composition of synthetic leathers with PVC coating (L1, L2, L4) is 75% polyvinyl chloride, 15% polyolefin, 8% cotton and 2% polyurethane. The composition of synthetic leather L3 is 65% polyurethane and 35% polyester.

Knitted fabrics K1 and K2 in weft knitting of the plain jersey weave type differ in surface density as well as in stitch density and thickness (Table 2.1).

Table 2.2. Structure and weave types of the investigated upholstery materials

No.	Material code	Structure		Weave type	
		1st layer	2nd layer	1st layer	2nd layer
1	M1	woven		plain	
2	M2	woven		plain	
3	M3	woven		plain	
4	M4	woven	woven	corduroy plain	plain
5	M5	woven	woven	bedford cord	plain
6	M6	woven		plain	
7	M7	woven	woven	plain	plain
8	M8	woven (napped back side)		woven braided rib	
9	M9	woven	woven	plain	plain
10	M10	woven		basket 2/2	
11	M11	pile woven		combined	
12	M12	woven	non-woven	plain	-
13	M13	woven		bedford cord	
14	M14	woven		twill 2/2	
15	M15	woven (napped back side)		woven braided rib	
16	M16	woven (latex backing)		plain	
17	M17	woven		corduroy plain	
18	M18	woven		plain	
19	M19	woven	woven	jacquard	jacquard
20	M20	woven (latex backing)		plain	
21	M21	woven	non-woven	plain	-
22	L1	PVC coating	woven	-	plain
23	L2	PVC coating	knitted	-	plain jersey
24	L3	PU coating	woven	-	plain
25	L4	PVC coating	woven	-	plain
26	K1	knitted		plain jersey	
27	K2	knitted		plain jersey	

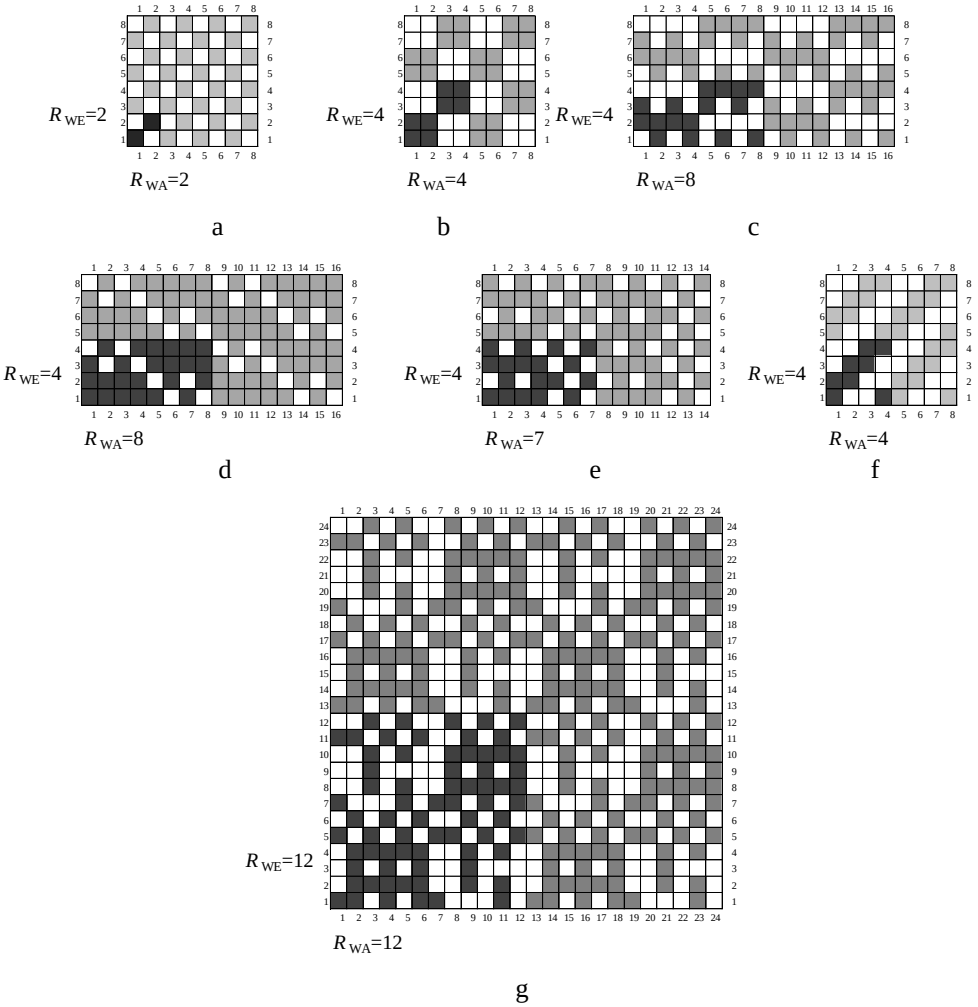

Figure 2.1. Weave types of the investigated upholstery materials: a – plain weave (M1–M3), b – basket weave 2/2 (M10), c – woven braided rib (M8, M15), d – bedford cord (M5), e – bedford cord (M13), f – twill weave 2/2 (M14), g – combined (M11), where R_{WA} and R_{WE} – the number of warp and weft yarns in reports of fabric, ▭ – longitudinal direction and ▭ – transverse direction

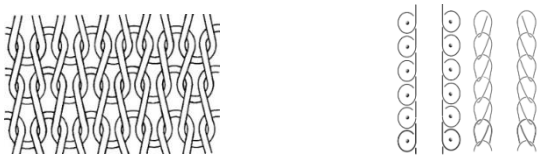

Figure 2.2. Knitting types of the investigated materials: a – single jersey (of knitted upholstery materials K1, K2), b – closed pillar stitch (of knitted interlinings W4, W5)

For the investigations of the effect of fusing material structure upon the variations of flexible multilayer systems spatial shape and for the investigations of the pre-tension level upon biaxial behavior of fused systems, 100% cotton fabric of plain weave was used as the basic layer. For the second layer, five types of 100% PES-fused interlinings of woven, knitted and non-woven structure were used (Table 2.3, Fig. 2.1, f, Fig. 2.2, b). The density of the adhesive was 52 and 76 dots/cm^2, the surface density varied from 36 up to 53 g/m^2.

Table 2.3. Characteristics of the investigated materials (components of fused systems)

Material code	Thick-ness *T*, mm	Surface density ρ, g/m^2	Material structure	Adhesive density, dots/cm^2	Stitch density, dm^{-1}	
					long.	trans.
W1	0.30	44	Woven, twill weave 2/2	52	360	150
W2	0.31	53	Woven, twill weave 2/2	76	240	140
W3	0.26	50	Non-woven	52	-	-
W4	0.39	50	Knitted, closed pillar stitch	52	70	130
W5	0.16	36	Knitted, closed pillar stitch	76	130	200
M	0.31	136	Woven, plain weave	-	250	190

Specific tensile strength of the base fabric M in the warp direction was f = 0.065 N/tex whereas in the weft direction it was f = 0.057 N/tex.

For the biaxial deformation, interlinings were fused with base material M. The fusing conditions for all the samples were: temperature 140 ºC, duration 16 s, pressure 1–3 bar (5–35 N/cm^2). Eighteen samples of each fused system of 250 × 320 mm were cut out in longitudinal and transverse directions. The tested samples were kept in standard atmosphere conditions (20±2 ºC and 65±4% humidity) for 24 h according to the requirements of ISO Standard 139:2005.

For further investigations, two types of commercial synthetic leathers were selected: non-perforated L5 and perforated L6 (Fig. 2.3). They were vinyl-coated PVC from the face side and had the plain jersey background, the composition of which was cotton and polyester. Both investigated vinyl leathers L5 and L6 are commonly used for car interior installations – seats, front and lateral panels, etc.

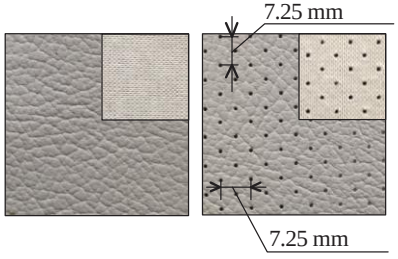

a b

Figure 2.3. Samples of investigated commercial synthetic leathers L5 (a) and L6 (b)

Perforated leather is often paired with other fabrics for adjustable temperature controlled car seats. The perforation diameter of L6 leather was 1.32 mm, whereas the density was 25 holes in 2.5 cm^2, and the distance between the holes in the longitudinal and transverse directions was 7.25 mm (Fig. 2.3). The characteristics of synthetic leathers L5 and L6 are presented in Table 2.4.

Table 2.4. Characteristics of synthetic leathers L5 (non-perforated) and L6 (perforated)

Parameter	Direction	Dimension	Method	Material	
				L5	L6
Thickness *T*		mm	EN ISO 5084:2000	1.06	1.01
Reverse side textile ρ		g/m^2		80–90	80–90
Surface density ρ		g/m^2	EN 12127:1999	674.8	629.0
Strength parameters	Longitudinal	F_{max}, N	LST EN ISO 13934-1:2000	342.8	170.0
		ε_{max}, %		23.9	23.4
	Transverse	F_{max}, N		282.8	118.4
		ε_{max}, %		127.6	50.6
Coefficient of anisotropy c_a				0.19	0.46

2.2. Research Method

2.2.1. KES-F: characterisation of the deformability of the preforms when using low loads measurement method

For the investigations of upholstery material deformability at low loads, the KES-F system was used which allows determining such parameters as tensile load – elongation, bending moment – curvature, shear force – shear angle, compression load – deformation and surface roughness as well as friction. KES-F testing parameters were measured in *cgs* units (centimetre, gram, second) – thus the measurement units were recalculated to the SI system units (Appendix 1, Table A1.1). Before the experiments, the specimens of upholstery materials were kept in standard atmosphere conditions (temperature – 22.2º C, humidity – 47.7%) for 24 hours. Sample dimensions for all the properties of KES-F were 200 x 200 mm. Primarily, the surface and compression properties were measured, then bending, shear and, finally, the tensile parameters were determined. By using the same single sample, 17 parameters of KES-F were detected (Table 2.5). The samples were tested in longitudinal and transverse directions.

For establishing tensile properties, a sample is stretched until 490 N/m has been reached, after which, the sample is relaxed until it returns to the original length. The load extension curve (hysteresis) is registered (Fig. 2.4). The coefficient of variation *v* for the results of the tensile test did not exceed 12.46%.

Tensile parameters are defined from tensile hysteresis (Fig. 2.4). The resilience of tensile *RT* (%) is thus calculated:

$$RT = \frac{WT'}{WT}100\%, \quad (2.1)$$

where *WT*' is the tensile energy in the return process (Nm/m^2) which is determined as the area under the tensile curve's reversible part, *WT* is the tensile energy (Nm/m^2) which is determined as the area under the curve of the loaded part (Fig. 2.4).

The tensile linearity is defined as follows:

$$LT = \frac{WT}{WOT}; \tag{2.2}$$

where *WOT* is the area of triangle *0AB* (Nm/m^2) which is comprised of the beginning point of the coordinates, determined tensile force F_{max} (490 N/m) and strain EMT_{max}:

$$WOT = \Delta 0AB = \frac{F_{max} EMT_{max}}{2}; \tag{2.3}$$

The relation between strain deformation EMT_{max}, tensile energy *WT* and linearity *LT* when the tensile load is F_{max} = 490 N/m is then estimated:

$$EMT_{max} = \frac{2[WT]}{[LT] \cdot F_{max}} = \frac{[WT]}{250[LT]} \tag{2.4}$$

Table 2.5. Characteristics of KES-F parameters

Parameter	Property	Characteristics	Mode
KES-FB1	Tensile	*LT*, Linearity	Maximal load – 490 N/m, tensile velocity – 0.2 mm/s. Sample width – 200 mm, distance between the clamps – 50 mm
		WT, Tensile energy, Nm/m^2	
		RT, Resilience, %	
		EMT, Tensile strain, %	
	Shear	*G*, Shear stiffness, N/m°	Shearing velocity 0.417 mm/s, maximal shear angle φ = ±8º, sample width – 200 mm, distance between the clamps – 50 mm shearing is taken along the weft direction
		2HG, Hysteresis at shear angle φ = 0.5º, N/m	
		2HG5, Hysteresis at shear angle φ = 5º, N/m	
KES-FB2	Bending	*B*, Bending rigidity, Nm^2/m	Pure bending between the curvatures K= -2.5 and 2.5 (cm^{-1}), the rate is – 0.5 cm^{-1}/s
		2HB, hysteresis of bending rigidity, Nm/m	
KES-FB3	Compression	*LC*, Linearity	The compressed area is 2 cm^2 of a circle, the maximal pressure equals 0.45 N/cm^2, the velocity is 20 μm/s. The dimensions of the specimens were 200 × 200 cm
		WC, Energy required for the compression, Nm/m^2	
		RC, Resilience, %	
		T_m, Thickness of specimen at pressure, mm	
		T_0, Thickness of unpressed specimen, mm	
KES-FB4	Surface	*MIU*, Mean value of the coefficient of friction	The friction compressional force was 25 N/cm^2, whereas the roughness equaled 5 N/cm^2. The measured surface was 20 mm long and 5 mm wide. The velocity was 0.1 cm/s. The dimensions of the specimens were 200 × 200 cm
		MMD, Mean deviation of coefficient of friction	
		SMD, Mean deviation of surface roughness, μm	

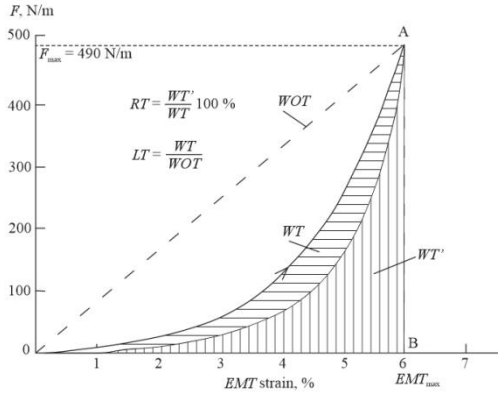

Figure 2.4. Typical force-extension tensile curve for fabric

Shear stiffness *G* and shear hysteresis *2HG* at shear angle 0.5° and shear hysteresis *2HG5* at shear angle 5° were determined by using the same tensile property of KES-F1. The parameters were determined from the shear force–shear angle curve (Fig. 2.5). The curve was obtained by applying constant tension F_{sh} to the sample till the shear angle has reached θ = 8° in the positive direction and θ = –8° in the negative direction, respectively, when the clamps moved along each other while keeping the uniform distance between them which resulted in shear deformation. The tensile load of 10 N/m was applied for this purpose.

The shear for the investigated upholstery materials was tested in the longitudinal and transverse directions. Coefficient of variation *v* for the results of the shear test never exceeded 14.90%.

The coefficient of shear rigidity *G* is determined by the ratio of shear force to the unit of width and shear angle, i.e. it is determined by the slope of the curve between shear angle θ at 0.5° and at 2.5°:

$$G = \frac{|A-B|}{2.5^{\circ}-0.5^{\circ}} \tag{2.5}$$

where $|A - B|$ is the value of shear force F_{sh} between points *A* and *B* which is obtained from the shear curve by setting the perpendicular at 0.5° and at 2.5° shear angles (Fig. 2.5).

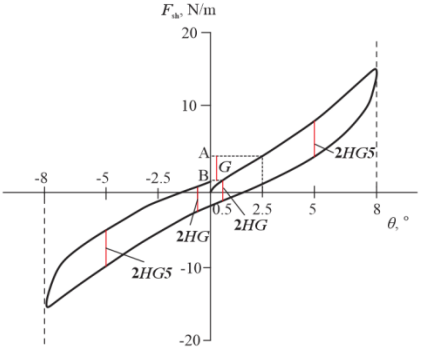

Figure 2.5. Shear force–shear angle curve in the KES-F system

When taking the shear strain instead of the shear angle for defining G, the value is equal to the shear modulus and is re-calculated as:

$$G(\mathrm{N/m}) = 57.3\, G(\mathrm{N/m°}) \tag{2.6}$$

In bending, the effective dimension of a specimen is 25 mm long and 10 mm in width (it is the width that is bent). The standard of the longitudinal length of the specimen is 200 mm but it can be chosen between 20 mm and 200 mm according to the material. During the experiment, bending rigidity B and bending hysteresis HB are determined. The specimen is bent at a constant rate, from a curvature of 2.5 to –2.5 cm^{-1}. One side of the specimen is clamped to a fixed clamp while the other side is fixed to a moving clamp which bends the specimen following a circular path. The angular momentum is recorded during the bending deformation. The momentum–curvature curve shows the typical hysteresis behavior (Fig. 2.6). Bending rigidity B is obtained as a slope of the M–K curve where M is the bending moment per unit length of the specimen. B is defined by the slope of the curve between K = 0.5 and 1.5 cm^{-1} and K = –0.5 and –1.5 cm^{-1}, respectively. The bending property for the investigated upholstery materials was tested in the longitudinal and transverse directions.

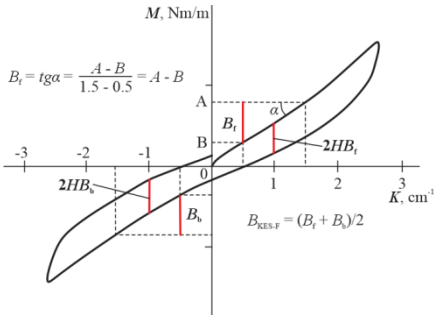

Figure 2.6. Bending curve in the KES-F system

The bending method as developed by Pierce was used for upholstery materials; when applying this method, a specimen of 25 mm width is pushed on a horizontal platform towards a slanted plane of the angle equaling 41.5° (Fig. 2.7). At the moment when the specimen reaches the slanted plane, bracket length l (mm) is measured. Slope length e of the material is calculated:

$$e = l\left(\frac{cos\left(\frac{\theta}{2}\right)}{8tan\theta}\right)^{\frac{1}{3}} \approx \frac{l}{2} \tag{2.7}$$

After measuring slope length e in longitudinal and transverse directions e_1 and e_2, the mean of e value and average bending rigidity B_P are calculated:

$$\bar{e} = \sqrt{e_1 e_2}; \tag{2.8}$$

$$B_P = \rho e^3 \tag{2.9}$$

where ρ is the surface density (g/m^2).

Coefficient of variation *v* for the results of the bending test (by employing Pierce's method) never exceeded 8.57%.

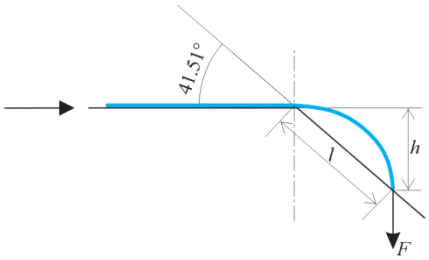

Figure 2.7. Scheme of bending rigidity measuring method by Pierce

The compression behavior in the KES-F system is determined by compressing the specimen with a 2 cm^2 flat circular head until the pressure has attained 50 g/cm^2 (Fig. 2.8). Compression linearity *LC*, that is, the energy required for compression *WC* (Nm/m^2) and resilience *RC* (%) are calculated from the hysteresis as follows (Fig. 2.8):

$$LC = \frac{WC}{W0C}; \tag{2.10}$$

$$WC = \int_{T_m}^{T_0} PdT; \tag{2.11}$$

$$RC = \frac{WC\prime}{WC}; \tag{2.12}$$

where *T* is the thickness of the specimen (mm), T_0 stands for the thickness of the specimen at the maximum pressure of 49 N/m^2; T_m denotes the thickness of the specimen at the maximum pressure of P_m = 4903.3 N/m^2; *WC*' is the recovering energy given by the pressure of the recovering process.

$$W0C = \frac{P_m(T_0 - T_m)}{2}; \tag{2.13}$$

The coefficient of variation *v* of the compression test never exceeded 9.30%.

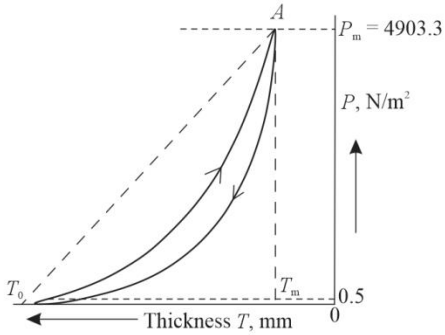

Figure 2.8. Scheme of the compression test in KES-F system

The surface characteristics – coefficients of friction *MIU* and roughness *SMD* (μm) – are determined by employing the KES-F test. Here, the specimen is moved in 2 cm intervals at a constant velocity of 0.1 cm/s on a smooth steel plate which is placed horizontally thus keeping the tension of the specimen at 19.6 N/m and keeping the contactor in its position. The friction force is recorded, and the average and variation of the friction coefficient is obtained:

$$MIU = \frac{1}{X}\int_0^X \mu dx; \tag{2.14}$$

$$MMD = \frac{1}{X}\int_0^X |\mu - \bar{\mu}| dx; \tag{2.15}$$

where μ is the frictional/compressional force; x represents the displacement of the contactor on the surface of the specimen; X is the distance of 2cm.

Roughness is determined with a wire sensor of 5 mm length; the sample is compressed with a force of 1961 N/m^2. The sample (which is under the sensor) is moved over a distance of 30 mm, and the vertical displacement of the sensor, the sample roughness, is recorded:

$$SMD = \frac{1}{X}\int_0^X |T - \bar{T}| dx; \tag{2.16}$$

where T (mm) is the thickness of the specimen at position x which is measured by this contactor; $\bar{T}$ is the mean value of T.

Coefficient of friction *MIU* and surface roughness *SMD* (μm) for the investigated upholstery materials were tested in longitudinal and transverse directions. Coefficient of variation v for the results of the surface test did not exceed 8.00%.

2.2.2. Creep and relaxation deformation research method

Solving the practical problem of furniture upholstery materials deformational behavior requires determining the deformational behavior of upholstery materials during the covering (upholstering the furniture). The upholstery pattern was sewn and pulled on the pouffe whose construction and shape are very simple. All the corners were set in the right position, smoothing the puckers and seams. During the covering (pulling) process, a special manual strength meter was hooked onto the edge of the pattern, which allowed to measure the tension force when the pattern is stretched to cover the pouffe. The tension force of 100 N was determined for upholstering the simple-shaped furniture. This tension was measured for further investigations in order to perform the creep and relaxation deformation research for upholstery materials.

Before the experiments, the specimens of upholstery materials were kept in standard atmosphere conditions (the temperature of 22.2º C, and the humidity equaling 47.7%) for 24 hours. The dimensions of the specimens for the analysis of creep and relaxation deformation processes were 50 mm width and 200 mm length. One end of the specimen was fixed in the clamp, and the load of 100 N was applied on the second end of the specimen, after which the deformational process started

immediately (Fig. 2.9). The tensile strain was registered straight after the loading, i.e. about 5–7 s after applying the load; during the following 5 minutes, the extension of the specimen was being registered each minute, afterwards, the extension was measured every 5 minutes. After half an hour, the load was removed, and the recovery process was being registered in the same way (in accordance with the same time intervals of measuring) as tensile strain. In general, the load duration was 1800 s; also, the relaxation (recovery) load duration was 1800 s. The constituent parts of creep and relaxation deformation processes are determined from the obtained results involving general deformation ε_G, sudden ε_s, creep ε_c, elastic ε_e, viscoelastic ε_v, residual ε_r, and reversible ε_R deformations (Fig. 2.10). For testing the loadings that typically act in production processes and exploitation of upholstery furniture were chosen. Therefore, the decision was made to perform the uniaxial tension test up to 25 N, i.e. low wearing level load according to the KES-F methodology and up to 100 N, i.e. the production level load was applied for upholstery pulling on furniture.

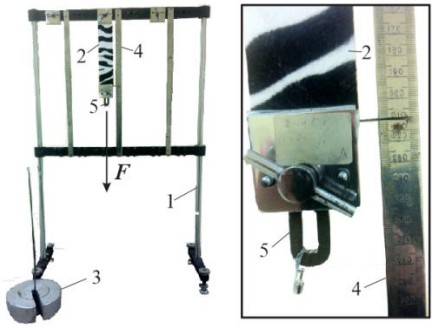

a b

Figure 2.9. Measurement device (a) for creep and relaxation deformation process with a zoomed view (b) of measuring: 1 is the stand, 2 is the sample, 3 is the hanging weight of 100 N, 4 is the ruler, 5 is the hook for hanging the weight

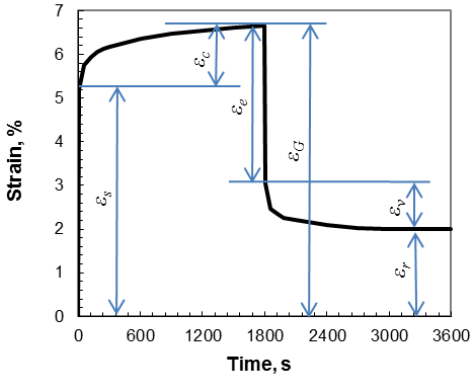

Figure 2.10. Creep and deformation relaxation process with its constituent parts: ε_s – sudden deformation, ε_c – creep deformation, ε_e – elastic deformation, ε_G – general deformation, ε_v – viscoelastic deformation, ε_r – residual deformation

The creep and relaxation deformation test was performed in longitudinal and transverse directions. Five specimens were tested for each material sample, coefficient of variation v for the results of the creep and relaxation deformation test when the load was 25 N did not exceed 5.4%, and when the load of 100 N was being applied, v did not exceed 6.8%.

Maximal uniaxial tension characteristics were defined for the investigated fabrics by using the standard tensile testing machine Tinius Olsen 10KT (Fig. 2.11) and following the requirements of standard LST EN ISO 13934 – 1:2000 Textiles. The tensile properties of fabrics were the following: Part 1: Determination of the maximum force and the elongation at the maximum force when using the strip method. The initial gauge was 100 mm, the specimen width was set at 50 mm, whereas the tensile velocity was 100 mm/min. The force–strain curves were digitally recorded on the basis of which, specimen breakage force F_{max} (N), elongation ε_{max} (%) and anisotropy coefficient c_a (2.17) were defined.

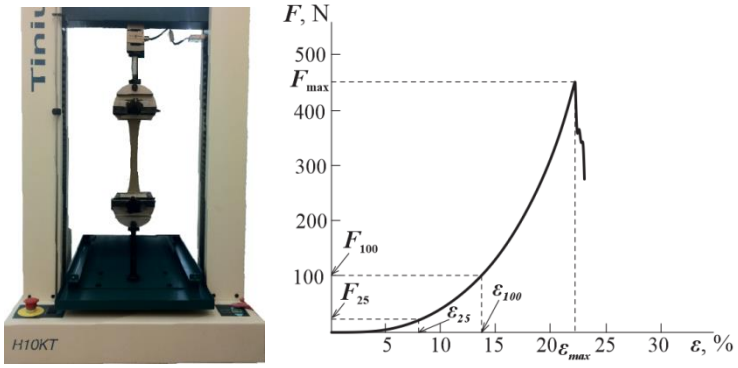

a b

Figure 2.11. Standard tensile testing machine (a) and typical tensile curve (b)

$$c_a = \frac{\varepsilon_{long}}{\varepsilon_{trans}} \tag{2.17}$$

As one of the tasks of the research was to analyze upholstery materials relaxation behavior at low level loads, instantaneous rigidity modulus (2.18) as well as anisotropy coefficients in terms of the two exploitation loadings (25 N and 100 N) were calculated: E_{m25} – that is, the rigidity modulus at 25 N; E_{m100} – the rigidity modulus at 100 N; c_{a25} stands for the anisotropy coefficient at 25 N, c_{a100} denotes the anisotropy coefficient at 100 N:

$$E_m = \frac{F_{max}}{\varepsilon_{max}} \tag{2.18}$$

The coefficient of the measurement variation for the investigated fabrics did not exceed 7.95%. The surface density and thickness characteristics of the investigated fabrics were defined by referring to the requirements of standards LST EN ISO 5084:2000 Textiles – *Determination of thickness of textiles and textile*

products and LST EN 12127:1999 Textiles – Fabrics – *Determination of mass per unit area using small samples*.

The theoretical modeling of the creep process was applied by employing power equation (2.19); determination coefficient R^2 varies within the limits of 0.95 and 0.99:

$$y = g + kx^j \tag{2.19}$$

where *g, k, j* are the variables, *x* denotes time (s), and *y* stands for deformation (mm).

The relaxation deformation process was analyzed by approximating and using exponent equation (2.20); determination coefficient R^2 varies within the limits of 0.93 and 0.99:

$$y = g + k\exp(-\frac{x}{j}) \tag{2.20}$$

For the mathematical analysis of creep and relaxation deformation processes, the classical models were used. The solution of Maxwell-Thompson equation is obtained when the specimen is loaded F = const, i.e. when the creep process takes place. The calculation of this modeling is as follows:

$$\varepsilon_{(t)} = \varepsilon_G \cdot \left[1 - \frac{H - E}{m \cdot H} \sum_{i=1}^{m} a_i e^{-\frac{t}{b_i}}\right] \tag{2.21}$$

where b_i is the i-th element time coefficient of relaxation duration; ε_G represents the maximal strain of the specimen (general deformation); E stands for the long-term modulus of elasticity ($E = F / \varepsilon_G$); H denotes the instantaneous modulus of elasticity ($H = F / \varepsilon_s$, ε_s shows the sudden deformation when the specimen is provided under constant load F); m is the quantity of duration of relaxation coefficients ($m = 5$).

As soon as the load has been removed, the relaxation process begins by the solution of the Maxwell-Thompson system and is equal to:

$$\varepsilon'_{(t)} = \varepsilon_G - (\varepsilon_G - \varepsilon_r) \cdot \left[1 - \frac{H' - E'}{m \cdot H'} \sum_{i=1}^{m} a_i e^{-\frac{t}{b_i'}}\right] \tag{2.22}$$

where H' is the instantaneous modulus of elasticity after unloading ($H' = F / (\varepsilon_G - \varepsilon_0)$); E' denotes the long-term modulus of elasticity after unloading ($E' = F / \varepsilon_R$); ε_R stands for the general reversible deformation ($\varepsilon_R = \varepsilon_G - \varepsilon_r$); ε_r is the residual deformation ($\varepsilon_r = \varepsilon_G - \varepsilon_v - \varepsilon_e$); ε_e provides the sudden reversible deformation ($\varepsilon_e = \varepsilon_G - \varepsilon_0$).

Equations (2.21) and (2.23) describe creep deformations while equations (2.22) and (2.24) describe relaxation deformation. Mechanical modeling based on Kelvin-Voigt elements is calculated as follows:

$$\varepsilon = \frac{F_0}{E_1} + \sum_{i=1}^{n} \frac{F_0}{E_2^i}\left(1 - e^{-\frac{E_2^i}{\eta_2^i}\cdot t}\right) + \frac{F_0}{E_3} + \frac{F_0}{E_4}\left(1 - e^{-\frac{E_4}{\eta_4}\cdot t}\right) \quad (2.23)$$

$$\varepsilon_2 = \sum_{i=1}^{n} \frac{F_0}{E_2^i}\left(e - 1^{-\frac{E_2^i}{\eta_2^i}\cdot t_1}\right)\cdot e^{-\frac{E_2^i}{\eta_2^i}\cdot t^*} \quad (2.24)$$

2.2.3. Measurement method of the pre-tension level upon biaxial punching

A new method was created in order to solve the practical problem of furniture upholstery materials deformational behavior allowing to determine the deformational behavior of upholstery materials during the covering process (i.e. upholstering the furniture). For the investigations of the effect of fusing materials structure upon the variations of flexible multilayer systems spatial shape and for the analysis of the pre-tension level upon biaxial punching of fused systems, the new method – as described above – was applied (Fig. 2.12, a).

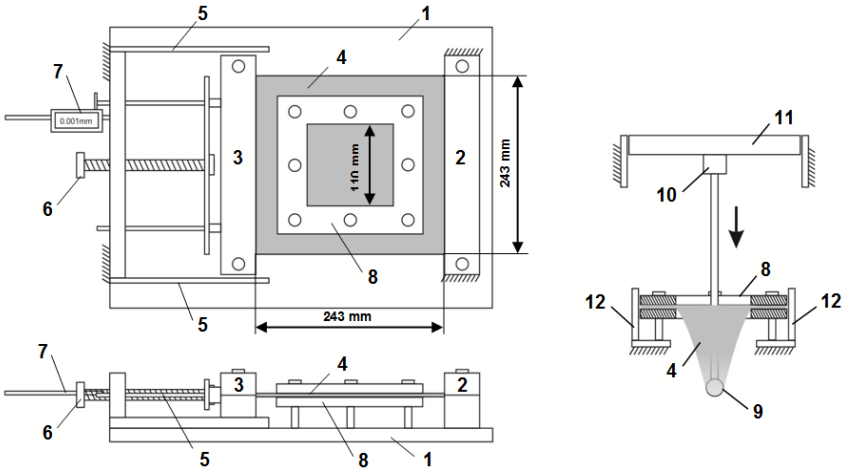

a b

Figure 2.12. The device for specimens initial pre-tension (a) and the device for specimens biaxial punching (b): 1 – the platform; 2 – the fixed clamp; 3 – the moving clamp; 4 – the specimen; 5 – the guides of the moving clamp; 6 – the threaded drive for specimen pre-tension; 7 – the strain gauge; 8 – square shaped clamps; 9 – the punch; 10 – the tensometer; 11 – the standard drive of the tensile testing machine; 12 – the fixed holder

For biaxial punching, interlinings were fused with base material M. The fusing conditions for all the samples were: temperature 140 ºC, duration 16 s, pressure 1–3 bar (5–35 N/cm^2). Eighteen samples of each fused system of 250 × 320 mm were cut in longitudinal and transverse directions. Coefficient of variation *v* for the pre-tension level upon biaxial behavior measurement did not exceed 19.09% except for basic fabric M when coefficient of variation *v* reached 26.9%. First of all, specimen

4 of the fused multilayer system was fixed in a special device for uniaxial pre-tension with the help of clamps 2 and 3 (Fig. 2.12). Certain initial pre-tension is applied by thread drive 6. The displacement of moving clamp 3 is controlled by digital gauge 7 (the accuracy of the measurement is 0.01 mm). During these investigations, the specimens were pre-tensioned by 0.0%, 1.2%, and 2.1%. After that, stretched specimens were clamped into square-shaped clamp 8 of inner dimensions 110 x 110 mm which was placed into special holder 12 mounted on the standard tensile testing machine. Drive 11 pulled down punch 9, which broke stretched specimen 4. Tensometer 10 recorded breaking force P_{max}, N, while the strain gauge detected maximal punching height H_{max}.

For the analysis of the pre-tension level upon biaxial behavior of fused systems, coefficient of variation v did not exceed 8.2%. The samples of fused systems were punched from the side of the main cotton fabric in order to maintain the same friction force between the punch and the specimen. During these investigations, the specimens were pre-tensioned by 0.0%, 0.4%, 0.8%, 1.2%, 1.7% and 2.1%. After pre-tension, stretched specimens were clamped into a flat circular shaped clamp (the radius of the inner specimen was 110 mm). Such pre-tension levels were chosen in order to make them closer to the testing conditions of the previously performed research work (Zubauskiene, Strazdiene, Urbelis, & Saceviciene, 2012). In order to obtain more evident dependencies in respect to the earlier results, the number of pre-tension steps was increased from three to five.

The specific tensile strength of base fabric M was determined:

$$f = \frac{F_{max}}{D \cdot b_0 \cdot D_L}, \text{ (N/tex)}, \tag{2.25}$$

where F_{max} is the maximal force at break (N), D are the density stitches (dm^{-1}), b_0 denotes the specimen width (cm), D_L stands for the linear density (tex).

Uniaxial tension tests were performed with the same standard tensile testing machine. The tensile velocity was 100 mm/min. Fifteen specimens of each tested sample (separate components and their fused systems) of 50 × 200 mm were tensioned in longitudinal and transverse directions. The average values of sample tensile strength F_{max} and elongation at break ε_{max}, were established. Coefficient of variation v of all the fusing interlinings did not exceed 23.97%, and v of their systems did not exceed 5.87%.

During the research, the evaluation of the effect of the pre-tension level upon the total deformability of all the tested samples was performed on the basis of complex criterion S (Fig. 2.13). It was calculated as the ratio between the area of polar diagram d which was outlined by punching height H_{max} values of non-tensioned samples and by area c which was outlined by tested samples punching heights H_{max} at each pre-tension level:

$$S = \frac{c}{d} \tag{2.26}$$

where c is the area of any pre-tension level except for 0.0%; d is the area determined by the tested systems deformability without pre-tension.

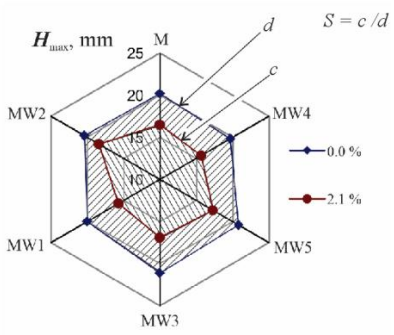

Fig. 2.13. Complex criterion *S* for the evaluation of the total deformability of the tested samples

2.2.4. Biaxial punching research method

Biaxial punching was performed with a special test unit attached to the standard tensile testing machine Tinius Olsen (load cell – 500 N) featuring a special punching device (Fig. 2.14).

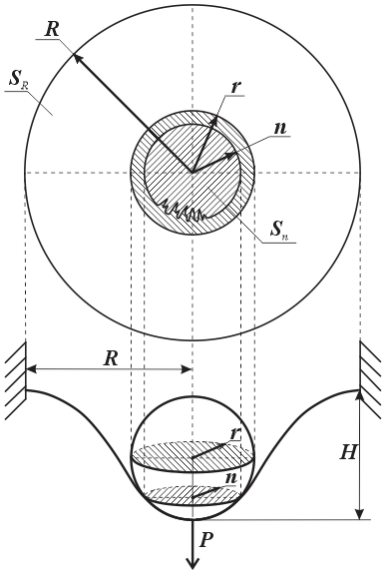

Figure 2.14. The principal scheme of specimen tearing location S_n parameter calculation: *R* is the radius of the specimen work zone, *r* denotes the radius of the punch, *n* represents the radius of the tearing zone, S_R is the area of the specimen work zone, S_n is the area of the tearing zone, *H* is the punching height, *P* is the punching force

The tensile velocity of the upper clamp was 100 mm/min. For the investigations, ten specimens (180 x 180 mm) were cut out from each sample of synthetic leather. The radius of the clamped specimens was R = 60 mm. Punching was performed from both sides of the specimens by using punches of three different sizes: r_1 = 9.0 mm (r_1/R = 0.15), r_2 = 23.5 mm (r_2/R = 0.39) and r_3 = 31.0 mm (r_3/R

= 52.0). Typical punching curves *P/H* until complete crack were registered during the experiment. The number of specimens in the experiment was 4, and coefficient of variation *v* of biaxial punching reached 9.19% when punching with the smallest punch r_1; it did not exceed 7% when punching with the other punches r_2 and r_3. Coefficient of variation *v* was 6.82% and 4.89%, respectively.

For the investigation of the friction phenomenon, four different types of lubricants were applied: L_A – pure water; L_B – commercial cleaner *Arexons* which is developed for car seats and upholstery cleaning, polishing and protecting and is enriched with glycerin and natural waxes; L_C – industrial silicone; L_D – commercial leather cleaner and conditioner *Turtle Wax* whose ingredients are water, silicone, emulsifiers and additives.

All the four types of lubricants were used not only in order to determine the friction parameters but also to define and to analyze the effect of friction between the punch and the specimen upon deformational behavior of the researched synthetic leathers. In all the cases, the lubricant was spread over metal surfaces with the help of a rubber brush. After each test, the surfaces were cleaned, and the appropriate lubricant was re-applied.

Area S_n of the punch-to-specimen contact zone during tearing was defined according to the scheme presented in Figure 2.14 and was calculated according to the following equation:

$$S_n = \pi n^2, \tag{2.27}$$

where S_n is the area of the tearing zone (mm^2), *n* is the radius of the tearing zone (mm).

2.2.5. Friction research method

Friction testing (Fig. 2.15) was performed in accordance with the requirements of Standard DIN EN ISO 8295 Plastics – Film and sheeting – Determination of the coefficients of friction.

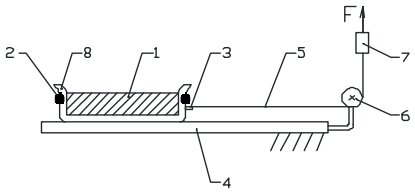

Figure 2.15. The scheme of friction testing: 1 – the scotch, 2 – the holders of the specimen (carriage), 3 – the hook, 4 – the metal tray, 5 – the thread, 6 – the sheave, 7 – the clamp, 8 – the specimen

For the investigation, 10 specimens (60 × 100 mm) were cut out from each sample of synthetic leathers L5 and L6. The working area was 60 × 60 mm, the weight of the specimen carrier was 1.96 N, the length of the path was 150 mm. The tensile velocity of the upper clamp was 100 mm/min.

Friction curves *l*–*F* (path–force) were registered during the friction experiment in which static F_S and dynamic F_D friction forces, as well as static μ_S and dynamic μ_D friction coefficients were defined (Fig. 2.16). Coefficient of variation v of the obtained results did not exceed 5.54%.

As well as in the punching test during the friction experiments, the lubricant was spread over the metal surface of the tray with the help of a rubber brush. After each test, the surface was cleaned, and the appropriate lubricant was re-applied.

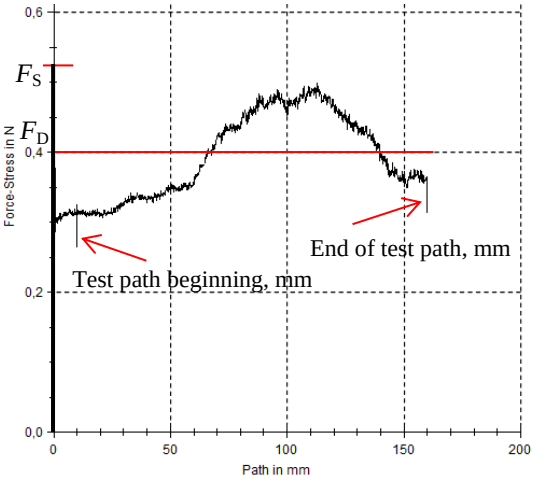

Figure 2.16. A typical scheme of friction where the test path beginning was at 10 mm, the end of the test path was at 159.95 mm

2.2.6. Statistical analysis method for experiment results

Mathematical statistical processing was performed for all the obtained results during investigations. Arithmetic mean $\bar{X}$ (2.28), variance σ^2 (2.29), standard deviation σ (2.30), coefficient of variation v (2.31), absolute random error Δ (2.32), relative error δ (2.33), and confidence interval I_β (2.34) were calculated for various research parameters by using the *Microsoft Excel* software. The statistical parameters of the research results for the investigated materials are presented in Appendices.

$$\bar{X} = \frac{1}{n}\sum_{i=1}^{n} X_i \tag{2.28}$$

where X_1, X_2, X_3, …, X_n are individual observations of the variable, $\sum X$ stands for the sum of all the observations of the variable, n is the number of observations.

$$\sigma^2 = \frac{1}{n}\sum_{i=1}^{n}(X_i - \bar{X})^2 \tag{2.29}$$

$$\sigma = \sqrt{\frac{1}{n}\sum_{i=1}^{n}(X_i - \bar{X})^2} \tag{2.30}$$

Variance is defined as the sum of the squared distances of each term in the distribution from mean $\bar{X}$ divided by the number of terms in distribution *n*.

$$\nu = \frac{\sigma}{\bar{X}} \cdot 100\% \tag{2.31}$$

The absolute random error is found in the calculation of individual measurement deviations from the mean:

$$\Delta = X_i - \bar{X}_\iota \tag{2.32}$$

where the measured value was obtained during the i-th measurement.

The absolute random error does not show the exact margin of error. Therefore, the relative error is generally used. The relative error is calculated as the ratio of the absolute random error and the arithmetic mean expressed as percentage:

$$\delta = \frac{\Delta}{\bar{X}} \cdot 100\% \tag{2.33}$$

The beginning and the end of confidence interval I_β were calculated:

$$I_\beta = (\bar{X} - \Delta;\ \bar{X} + \Delta) \tag{2.34}$$

The representative curves were selected after the statistical calculation and used in the analysis of the results.

3. Results

3.1. KES-F Characterization of the Deformability of Upholstery Materials

3.1.1. Tension

During the testing, 23 samples of upholstery materials were grouped into four groups by taking into account their structure:

Group I – synthetic leathers;

Group II – one-layer woven fabrics and knitted materials;

Group III – two-layer fused textile systems;

Group IV – jacquard, chenille and corduroy materials which are characterized by complex weave type. In the presented figures, they are marked as follows: jacquard fabric M19 in red color, chenille fabrics M2, M8, M11–M13 in orange color, and corduroys M4, M17 are in grey color.

The deformational behavior of the investigated upholstery materials is different not only between the groups of the investigated materials, but in their longitudinal and transverse directions as well (Tables 3.1, 3.2). Figure 3.1 shows that the most deformable upholstery materials in the longitudinal direction were chenilles M12 (8.39%) and M11 (6.22%), one-layer materials M3 (6.78%), M10 (6.42%) and M6 (6.27%), synthetic leather L3 (6.97%), and a slightly less deformable material was synthetic leather L2 (5.83%). The lowest deformation in the longitudinal direction was characteristic for one-layer material M20 (1.39%). The most deformable in the transverse direction were synthetic leathers, i.e. L3 (21.33%), L2 (14.10%) and L1

(8.56%). Figure 3.1 also reveals evident differences of the investigated materials deformability in the transverse and longitudinal directions. High anisotropy characterized not only all the investigated synthetic leathers: L3 (0.33), L2 (0.41), L1 (0.42) and L4 (0.46) but also chenille material M2 (0.38), corduroy materials M4 (0.45), M17 (0.46) and knitted material K1 (0.48). There were also several orthotropic samples: one-layer materials M1 (0.88), M18 (0.89); two-layer materials M5 (0.95), M9 (0.89), M21 (0.87); jacquard M19 (0.96) and chenille materials M8 (0.91), M11 (0.85), M12 (0.84).

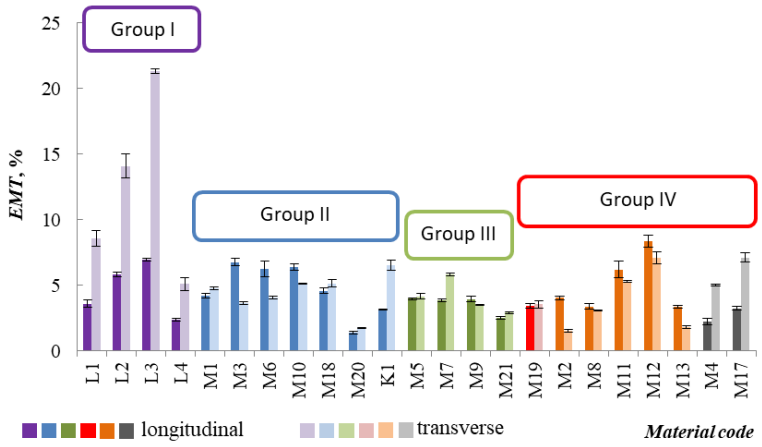

Figure 3.1. The difference between upholstery materials tensile strain *EMT* (%) in longitudinal and transverse directions

Furthermore, the obtained results show that tensile strain *EMT* for jacquard and chenille materials is higher in the longitudinal direction contrary to the synthetic leathers which are more deformable in the transverse direction.

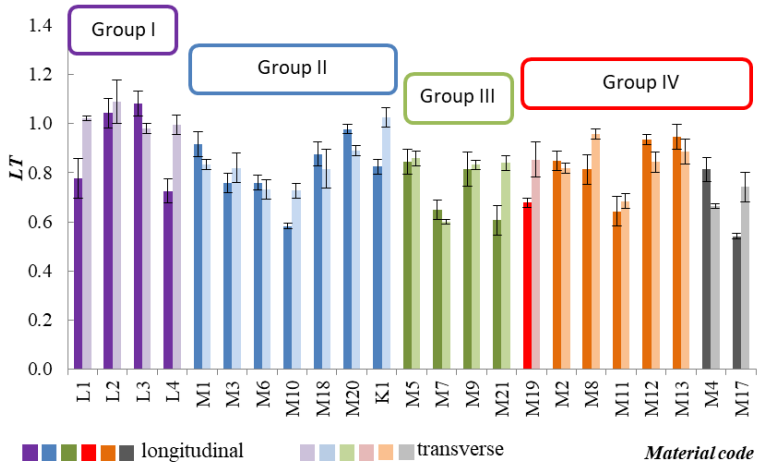

Figure 3.2. The difference between materials linearity *LT* in the longitudinal and transverse directions

Table 3.1. The parameters of KES-F tension and shear for the investigated upholstery materials in the longitudinal direction

Material code	Tension								Shear					
	LT		*WT*, Nm/m^2		*RT*, %		*EMT*, %		*G*, (N/m °)		*2HG* at 0.5° (N/m)		*2HG5* at 5° (N/m)	
M1	0.92	±0.08	9.47	±0.5	46.11	±2.36	4.22	±0.31	4.55	±0.60	7.75	±0.98	17.58	±0.91
M2	0.85	±0.06	8.44	±0.6	43.12	±3.11	4.05	±0.22	3.06	±1.44	11.60	±0.42	18.22	±5.67
M3	0.76	±0.05	12.61	±0.4	37.35	±2.10	6.78	±0.13	1.98	±0.19	8.46	±0.47	11.28	±0.05
M4	0.81	±0.05	4.46	±0.2	47.25	±2.15	2.24	±0.14	1.36	±0.28	3.27	±0.13	7.60	±0.59
M5	0.84	±0.05	8.24	±0.1	51.79	±4.11	4.00	±0.22	2.38	±0.28	6.26	±0.32	8.66	±0.32
M6	0.76	±0.04	11.67	±0.6	44.12	±2.74	6.27	±0.31	1.25	±0.41	1.70	±0.32	5.23	±1.21
M7	0.65	±0.03	6.13	±0.5	54.40	±3.64	3.86	±0.64	2.77	±0.22	6.62	±0.83	11.08	±1.13
M8	0.81	±0.05	6.77	±0.4	45.65	±2.56	3.39	±0.21	0.71	±0.22	1.84	±0.03	2.50	±0.74
M9	0.82	±0.02	7.90	±0.2	49.60	±4.81	4.00	±0.09	2.09	±0.34	5.42	±0.32	7.99	±0.64
M10	0.58	±0.03	9.17	±0.7	42.25	±4.27	6.42	±0.04	1.51	±0.19	5.28	±0.13	7.11	±0.44
M11	0.64	±0.05	9.81	±0.6	38.50	±2.67	6.22	±0.09	0.87	±0.24	4.05	±0.08	5.33	±1.06
M12	0.93	±0.04	19.23	±0.3	40.31	±2.63	8.39	±0.13	1.81	±0.2	3.87	±0.10	6.86	±0.39
M13	0.95	±0.07	7.75	±0.4	42.41	±2.94	3.34	±0.22	1.46	±0.38	7.29	±0.28	8.81	±1.60
M17	0.54	±0.06	4.32	±0.3	48.86	±2.43	3.25	±0.13	4.70	±1.24	11.28	±0.98	16.03	±0.93
M18	0.88	±0.04	9.86	±0.6	41.79	±2.55	4.59	±0.12	3.90	±0.15	6.50	±0.91	13.88	±1.23
M19	0.68	±0.01	5.69	±0.2	54.31	±2.61	3.42	±0.24	3.14	±0.54	7.63	±0.28	11.45	±1.01
M20	0.98	±0.02	3.34	±0.6	54.41	±1.49	1.39	±0.17	4.20	±0.69	8.83	±0.69	15.03	±0.23
M21	0.61	±0.06	3.78	±0.8	55.84	±5.10	2.54	±0.19	4.87	±0.61	10.87	±0.67	13.86	±0.47
L1	0.78	±0.06	6.87	±0.4	45.00	±1.36	3.61	±0.61	14.78	±1.31	26.02	±4.30	22.00	±0.18
L2	1.04	±0.02	14.91	±0.9	42.11	±1.48	5.83	±0.47	11.30	±1.74	24.61	±3.97	20.99	±1.86
L3	1.08	±0.05	13.98	±0.3	23.51	±1.20	7.00	±0.11	8.88	±0.52	17.70	±0.93	14.91	±0.05
L4	0.73	±0.05	4.22	±0.1	44.19	±3.69	2.37	±0.23	18.75	±4.92	35.25	±8.24	31.48	±1.91
K1	0.83	±0.01	6.38	±0.2	51.54	±1.30	3.15	±0.16	5.12	±0.17	13.29	±1.62	12.48	±0.13

Table 3.2. The parameters of KES-F tension and shear for the investigated upholstery materials in the transverse direction

Material code	Tension								Shear					
	LT		*WT*, Nm/m^2		*RT*, %		*EMT*, %		*G*, (N/m °)		*2HG* at 0.5° (N/m)		*2HG5* at 5° (N/m)	
M1	0.83	±0.01	9.76	±1.23	37.19	±1.2	4.78	±0.61	4.80	±0.11	6.60	±0.18	18.17	±0.81
M2	0.82	±0.09	3.09	±3.25	48.59	±3.6	1.54	±0.92	2.95	±0.52	9.56	±0.49	17.19	±1.11
M3	0.82	±0.02	7.31	±5.24	34.23	±1.1	3.64	±0.23	1.97	±0.32	7.65	±0.34	11.01	±0.77
M4	0.66	±0.04	8.19	±1.20	61.08	±1.2	5.03	±0.52	1.19	±0.32	2.63	±0.03	6.60	±1.26
M5	0.86	±0.02	8.78	±0.27	42.46	±1.9	4.17	±0.11	2.15	±0.06	6.06	±0.18	7.99	±0.20
M6	0.73	±0.06	7.31	±0.23	40.27	±1.8	4.07	±0.10	1.27	±0.15	1.08	±0.05	5.13	±0.42
M7	0.60	±0.04	8.63	±0.61	42.61	±2.3	5.86	±0.12	2.66	±0.47	6.99	±0.77	10.79	±0.49
M8	0.96	±0.08	7.21	±0.41	39.46	±5.4	3.07	±0.33	0.63	±0.06	1.32	±0.05	2.21	±0.10
M9	0.83	±0.02	7.16	±0.08	52.05	±3.6	3.51	±0.05	1.91	±0.15	5.03	±0.42	7.21	±0.05
M10	0.73	±0.04	9.12	±0.64	43.01	±2.6	5.12	±0.42	1.48	±0.23	5.00	±0.54	6.85	±0.08
M11	0.68	±0.03	8.88	±0.31	38.12	±1.7	5.29	±0.23	0.81	±0.08	3.27	±0.44	4.44	±0.08
M12	0.84	±0.01	14.62	±0.22	38.67	±1.2	7.08	±0.12	1.76	±0.04	3.19	±0.29	6.37	±0.15
M13	0.89	±0.02	3.97	±0.52	58.02	±2.5	1.83	±0.04	1.55	±0.20	6.33	±0.39	8.71	±0.18
M17	0.74	±0.03	12.95	±0.36	52.27	±1.6	7.12	±0.06	4.26	±0.38	11.28	±0.79	18.32	±1.70
M18	0.82	±0.02	10.30	±0.14	43.33	±2.3	5.15	±0.08	4.01	±0.06	5.82	±0.42	13.39	±0.49
M19	0.85	±0.03	7.46	±0.25	42.76	±1.6	3.56	±0.06	3.26	±0.12	7.35	±0.74	11.52	±0.93
M20	0.89	±0.07	3.78	±0.33	36.13	±3.2	1.73	±0.29	3.90	±0.72	9.15	±0.23	15.47	±1.06
M21	0.84	±0.02	6.03	±0.61	52.03	±4.8	2.93	±0.04	5.07	±0.82	11.94	±0.62	15.30	±0.79
L1	1.02	±0.03	21.43	±0.48	45.31	±1.0	8.56	±0.08	13.87	±1.31	22.70	±0.15	20.59	±1.52
L2	1.09	±0.04	37.67	±0.99	41.28	±4.1	14.1	±0.45	12.93	±2.04	23.49	±2.65	21.48	±2.31
L3	0.98	±0.05	51.21	±0.18	28.64	±1.2	21.33	±0.10	8.62	±0.75	17.88	±1.26	15.72	±0.96
L4	1.00	±0.01	12.46	±0.84	38.58	±2.5	5.1	±0.09	15.72	±2.14	36.56	±6.06	32.56	±5.84
K1	1.02	±0.06	16.48	±0.63	45.54	±1.8	6.56	±0.35	7.24	±0.08	17.60	±1.32	17.21	±0.59

Table 3.3. The parameters of KES-F compression and surface for the investigated upholstery materials

Material code	Compression										Surface							
	LC		*WC*, Nm/m^2		*RC*, %		T_0, mm		T_m, mm		*MIU*				*SMD*, µm			
											Longitudinal		Transverse		Longitudinal		Transverse	
M1	0.45	±0.02	0.27	±0.01	53.57	±2.81	0.79	±0.01	0.54	±0.02	0.16	±0.01	0.16	±0.01	13.96	±1.05	3.948	±0.17
M2	0.45	±0.03	0.59	±0.04	39.40	±1.11	1.86	±0.13	1.32	±0.08	0.34	±0.01	0.33	±0.01	12.55	±0.54	6.011	±0.14
M3	0.49	±0.01	0.41	±0.02	43.61	±1.64	1.61	±0.10	1.27	±0.09	0.26	±0.01	0.32	±0.01	13.43	±0.94	20.290	±0.94
M4	0.48	±0.01	2.00	±0.08	41.11	±1.52	3.57	±0.21	2.05	±0.15	0.47	±0.02	0.50	±0.02	2.20	±0.15	8.678	±0.35
M5	0.43	±0.04	0.31	±0.01	58.81	±3.41	1.11	±0.02	0.81	±0.03	0.42	±0.01	0.37	±0.01	1.99	±0.03	1.992	±0.15
M6	0.50	±0.02	0.16	±0.01	62.35	±2.59	0.62	±0.03	0.49	±0.02	0.18	±0.01	0.27	±0.02	14.83	±0.67	6.430	±0.28
M7	0.38	±0.01	0.37	±0.02	48.81	±1.52	1.46	±0.09	1.07	±0.02	0.30	±0.02	0.25	±0.02	13.23	±0.57	6.712	±0.14
M8	0.51	±0.04	0.84	±0.07	51.56	±1.64	1.65	±0.03	1.17	±0.02	0.32	±0.01	0.32	±0.02	16.32	±0.24	5.594	±0.21
M9	0.32	±0.02	0.44	±0.03	53.91	±1.25	1.58	±0.11	1.03	±0.07	0.27	±0.01	0.27	±0.01	9.92	±0.56	14.720	±0.58
M10	0.53	±0.02	1.77	±0.09	42.86	±1.51	2.41	±0.10	1.77	±0.08	0.30	±0.01	0.35	±0.01	14.46	±0.22	13.901	±0.94
M11	0.63	±0.03	0.84	±0.03	37.06	±1.52	2.19	±0.15	1.65	±0.09	0.35	±0.01	0.41	±0.01	9.78	±0.43	13.392	±0.48
M12	0.37	±0.02	0.48	±0.04	65.03	±1.63	1.41	±0.02	0.89	±0.06	0.20	±0.01	0.20	±0.01	2.96	±0.14	2.599	±0.14
M13	0.65	±0.05	0.98	±0.05	36.08	±1.94	1.97	±0.13	1.36	±0.08	0.40	±0.03	0.38	±0.02	7.64	±0.05	5.980	±0.24
M17	0.51	±0.01	0.58	±0.02	40.69	±2.51	3.56	±0.18	1.95	±0.14	0.45	±0.01	0.58	±0.01	2.85	±0.14	7.120	±0.24
M18	0.55	±0.03	0.42	±0.04	51.76	±3.05	0.89	±0.01	0.58	±0.03	0.19	±0.01	0.19	±0.01	14.19	±0.47	4.598	±0.15
M19	0.56	±0.02	0.60	±0.03	47.28	±2.13	1.67	±0.11	1.25	±0.08	0.36	±0.02	0.33	±0.02	19.88	±0.45	4.688	±0.24
M20	0.41	±0.01	0.67	±0.04	50.00	±2.64	1.67	±0.10	1.01	±0.02	0.31	±0.02	0.33	±0.01	13.66	±0.67	6.339	±0.27
M21	0.51	±0.01	0.56	±0.04	57.29	±2.21	1.42	±0.10	0.97	±0.02	0.32	±0.02	0.29	±0.02	12.26	±0.16	12.851	±0.27
L1	0.58	±0.05	0.30	±0.02	71.38	±2.15	1.05	±0.05	0.84	±0.05	0.37	±0.02	0.41	±0.01	1.27	±0.05	0.921	±0.04
L2	0.49	±0.01	0.53	±0.01	62.13	±3.54	1.40	±0.10	0.96	±0.04	0.48	±0.02	0.44	±0.02	1.07	±0.06	1.189	±0.06
L3	0.44	±0.02	0.29	±0.02	59.93	±2.17	1.10	±0.04	0.84	±0.03	0.23	±0.01	0.31	±0.01	2.79	±0.04	2.609	±0.05
L4	0.57	±0.03	0.38	±0.03	70.47	±3.61	1.27	±0.03	1.00	±0.02	1.09	±0.03	0.93	±0.02	0.83	±0.05	1.150	±0.08
K1	0.61	±0.05	0.52	±0.03	58.49	±2.81	0.90	±0.03	0.55	±0.01	0.33	±0.01	0.33	±0.01	3.34	±0.01	3.669	±0.17

Tensile linearity signifies the uniformity in the tensile load-bearing capacity (Raj & Sreenivasan, 2009). Synthetic leather L2 is denoted by the highest value of linearity compared to all other materials. Figure 3.2 shows that the tensile diagrams are linear enough for synthetic leathers L1–L4 (linearity 0.73–1.09) and one-layer materials (linearity 0.73–1.02) in the longitudinal and transverse directions. Meanwhile, to the contrary, linearity *LT* is low for one-layer material M10 (*LT* = 0.58; 0.73), two-layer material M7 (*LT* = 0.65; 0.60), chenille M11 (*LT* = 0.64; 0.68) and corduroy M17 (*LT* = 0.54; 0.74).

Low tensile energy causes low extension at a low stress level. It is evident from Figure 3.3 where tensile energy *WT* is the highest for synthetic leather L3 and L2 (*WT* = 13.98–51.21 Nm/m^2) while the lowest level is obtained for one-layer material M20 (*WT* = 3.34 Nm/m^2) and two-layer material M21 (*WT* = 3.78 Nm/m^2).

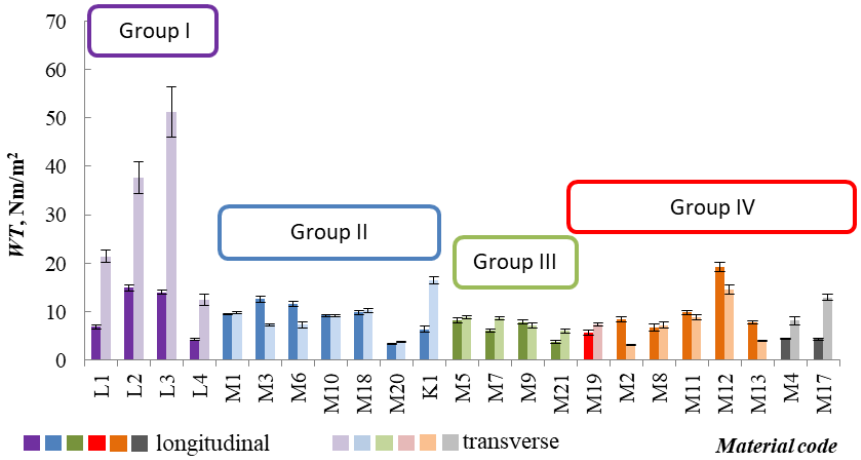

Figure 3.3. The difference between materials tensile energy *WT* (N·m/m^2) in the longitudinal and transverse directions

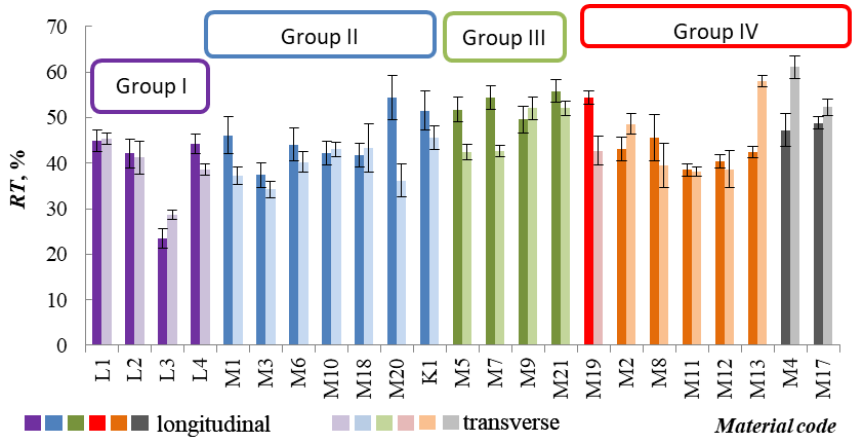

Figure 3.4. The difference between materials resilience *RT* (%) in the longitudinal and transverse directions

Resilience represents the recovery from tensile deformation. The higher the tensile resilience of a material, the better is its fabric handle (Kumari & Khurana, 2016). Figure 3.4 shows that all the investigated materials act in recovery more or less the same as their *RT* value in average equals to 44.6%. Still, several cases can be distinguished, e.g. the highest recovery in both longitudinal and transverse directions was found in two-layer sample M21 (55.84%; 52.03%) from Group III and one-layer sample M20 (54.41%; 55.84%) from Group II. Meanwhile, the highest recovery was found in corduroy fabric M4 from Group IV, but only in the transverse direction (61.08%). Figures 3.1 and 3.4 also show the tendency that resilience *RT* is in opposite relation with tensile strain *EMT*. For synthetic leathers, the correlation coefficient in the longitudinal direction is –0.79, in the transverse direction, it is –0.73; for one-layer materials, it is –0.91 (long.), 0.79 (trans.); for two-layer fused systems, it is –0.74 (long.) and –0.81 (trans.); for chenille fabrics, it reaches –0.74 (long., trans.).

3.1.2. Shear

The shear rigidity of a fabric depends on the mobility of threads at their intersection points, which depends on the weave, yarn diameter, and the surface characteristics of both the fiber and the yarn (Kumari & Khurana, 2016). Figure 3.5 shows that the highest shear rigidity *G* is found in all the synthetic leathers, especially in L4, where it reaches 18.75 N/m°. The lowest shear rigidity in the group of synthetic leathers was obtained for L3 (8.88 N/m°). It must be noted that a relatively high *G* value was found in knitted upholstery sample K1 at 5.12 N/m° and 7.24 N/m° in the longitudinal and transverse directions, respectively (Tables 3.1, 3.2).

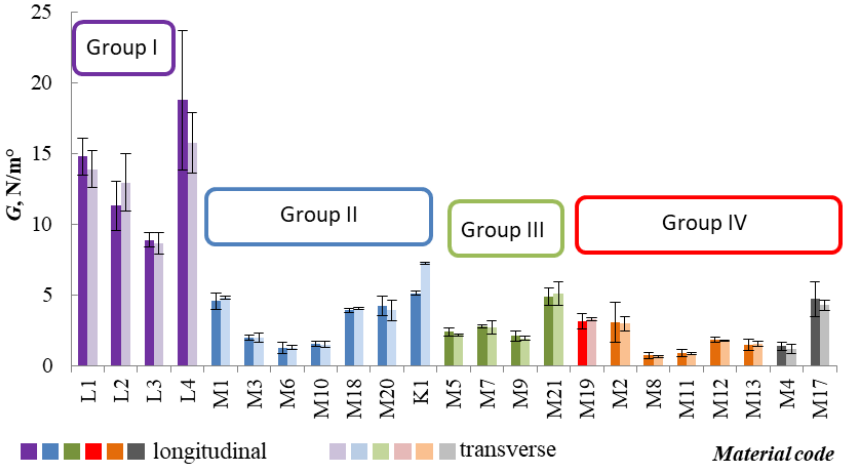

Figure 3.5. Histograms of shear rigidity *G* (N/m°) for the investigated upholstery materials in the longitudinal and transverse directions

It is known that the lower is the shear rigidity, the better is the fabric handle. Also, high shear rigidity limits the ability of plain materials and membranes to

obtain smooth spatial 3D shapes, which is very important in the production of soft furniture. From this standpoint, the most suitable materials for 3D-shaping are chenilles M8, M11, M13, one-layer materials M6, M10, and corduroy M4 (Fig. 3.5). Here, the lowest shear rigidity is found in chenille M8 (0.71 N/m°; 0.63 N/m°) and M11 (0.87 N/m°; 0.81 N/m°) samples. It must also be noted that shear rigidity *G* differs in the longitudinal and transverse directions. All the tested materials differ in respect to shear anisotropy G_{long}/G_{trans}. Anisotropic materials were knitted material K1 (0.71), synthetic leathers L4 (0.84), L2 (0.87) and fused corduroy M4 (0.87). Almost orthotropic materials were one-layer materials M3 (1.00), M6 (0.98), M10 (0.98) and M18 (0.97), synthetic leather L3 (0.97), and chenille M12 (0.97).

The shear hysteresis at 0.5° shows the highest *2HG* values for synthetic leathers, especially for L4 leather. The highest *2HG* value for one-layer materials is detected in knitted material K1 which is 87% higher in the longitudinal direction and 94% higher in the transverse direction compared to M6 material with the lowest *2HG* value (Fig. 3.6). The value of *2HG* for chenille material M2 is higher by about 85% compared to the lowest one (M8); corduroys may also largely differ – M17 value of *2HG* is higher by about 74% compared to M4. The differences of shear hysteresis at a large angle (5°) are more or less the same, an exception is one-layer material M1 whose value of *2HG5* is 56% higher in the longitudinal direction and 64% higher in the transverse direction compared to the value of angle 0.5°. It is evident that synthetic leathers are much more deformable compared to the remaining upholstery materials (Fig. 3.6).

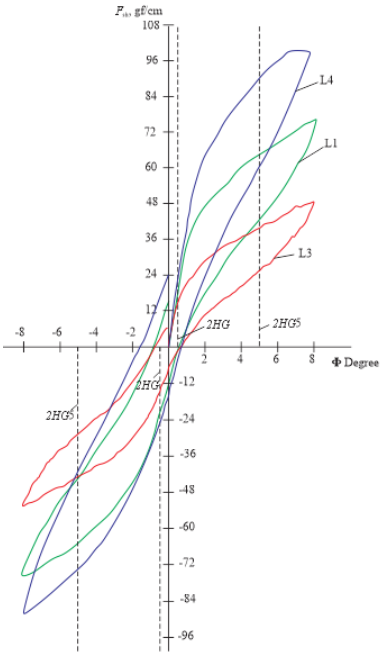

a

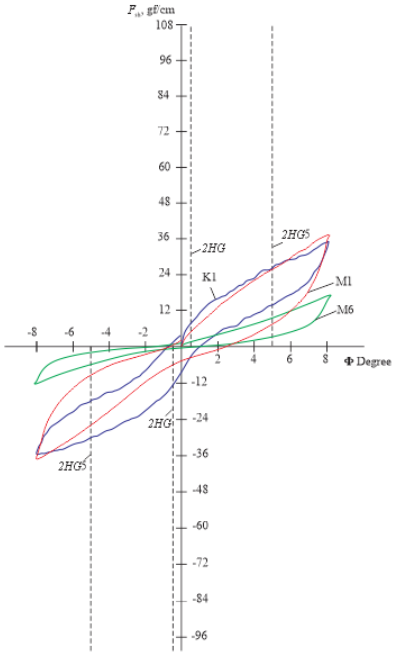

b

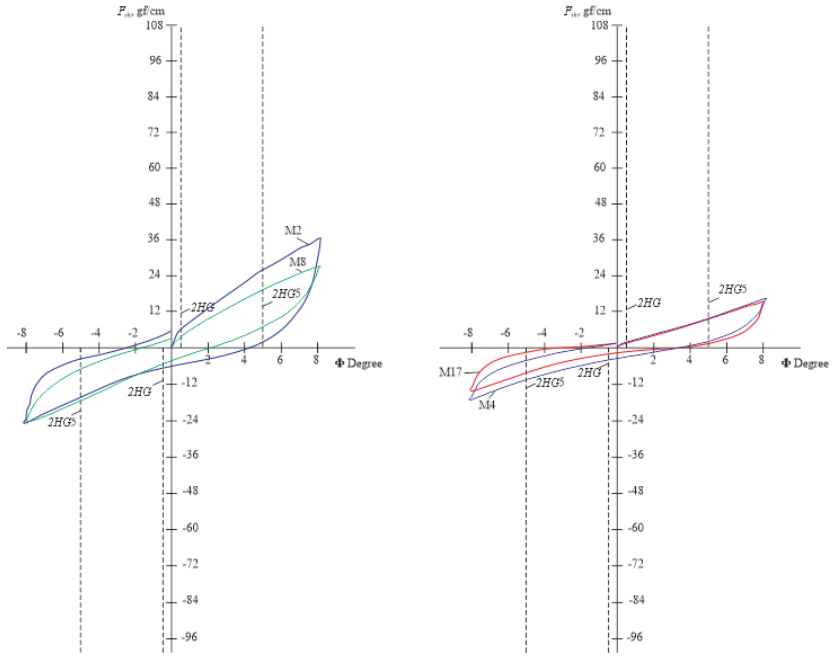

c d

Figure 3.6. Typical shear hysteresis of upholstery materials in the longitudinal direction for synthetic leathers L1, L3, L4 (a), one-layer materials M1, M6 (b), chenille materials M2, M8 (c) and corduroys M4, M17 (d)

3.1.3. Bending

The bending rigidity of a material depends on the bending rigidity of the constituent fiber and yarns from which the material is manufactured. The KES-F set of equipment is designed to test clothing, e.g. shirts, suits, dresses and their materials. The dimensions of specimens for the bending testing with KES-FB2 are 200 mm x 200 mm, but upholstery materials are much stiffer than clothing fabrics. Thus, according to other researches (Lomov, Verpoest, Barburski, & Laperre, 2003), (Bilbao, Soulat, Hivet, Launay, & Gasser, 2008), (Saceviciene, Strazdiene, Schacher, & Adolphe, 2012), during testing, the size of specimens was changed in order to make the sample suitable for testing. Unfortunately, the bending testing by KES-F failed when seeking to select the same sample dimensions for all the investigated upholstery materials. Other researchers in their investigations analyzed the mechanical parameters of 15 synthetic PU leathers by using the KES-F evaluation system, during which, the analysis of bending was excluded as the thickness of some samples was beyond the measurable scale (Roh, Oh, & Kim, 2013). Thus the decision was made to perform bending testing by using Pierce's method. The bending results obtained with Pierce's method are presented in Fig. 3.7.

It was established that some of the investigated upholstery materials are very stiff in the longitudinal direction, whereas others are stiff in the transverse direction.

Figure 3.7 shows that the difference between the directions for some materials is immense: bending rigidity B_P of chenille material M2 in the transverse direction is 85.3% higher than in the longitudinal direction. One-layer material M20 is stiffer in the longitudinal direction, and the difference is 83.6%; the same trend is obtained for corduroy material M17, of which, the difference between directions reaches 72.5%, one-layer material M10 (64.8%), two-layer materials M7 (62.6%) and M9 (68.7%), and chenille material M13 (63.2%). Two-layer materials M5 and M21 have no difference between the directions (B_P values vary within the error limits).

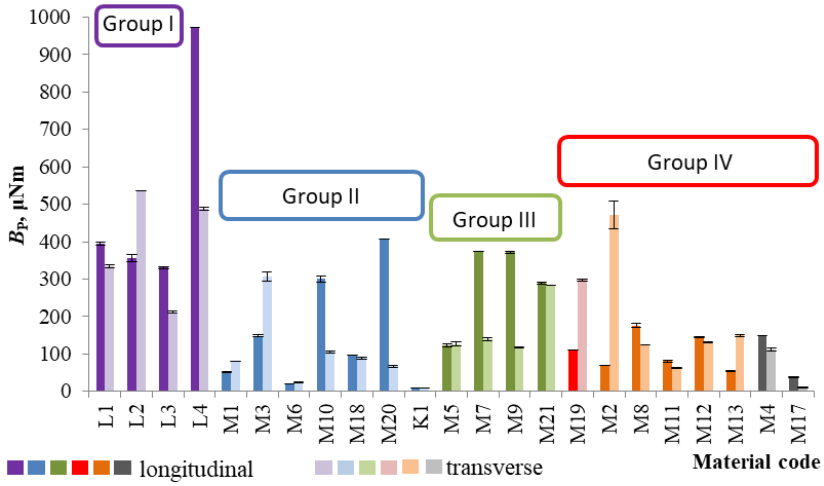

Figure 3.7. Bending rigidity B_P for the investigated upholstery materials determined by Pierce's method in the longitudinal and transverse directions

The obtained results have revealed that synthetic leathers as well as one-layer materials M3, M10, M20, two-layer materials M7, M9, M21, jacquard M19 and chenille material M2 are the stiffest in respect to the remaining upholstery materials. It must be mentioned that KES-FB2 testing for these particular materials was unsuitable. On the contrary, knitted material K1, one-layer materials M6, M1, M18, chenille M11 and corduroy M17 were the most flexible upholstery materials.

3.1.4. Compression

Compression is an important quality for soft furniture because, in many cases, it determines consumers' satisfaction and their buying decision. Compressibility expressed as the thickness difference between the uncompressed and the compressed state of the investigated materials is presented in Figure 3.8 and Table 3.3.

The highest compressibility is common in the thickest (T_0 = 3.56 mm) materials – corduroys M17 (45%) and M4 (42%). Compressible materials are also one-layer fabric M20 (40%) and knitted material K1 (40%). Meanwhile, synthetic leathers were the least compressible, i.e. they scored only 20%–31%. The thickest materials besides corduroy were jacquard and chenille, which belong to Group IV. Their thickness T_0 varied within the limits of 1.4–2.2 mm. The majority of the Group II

one-layer materials were the thinnest, especially plain woven fabric M6 (T_0 = 0.62 mm).

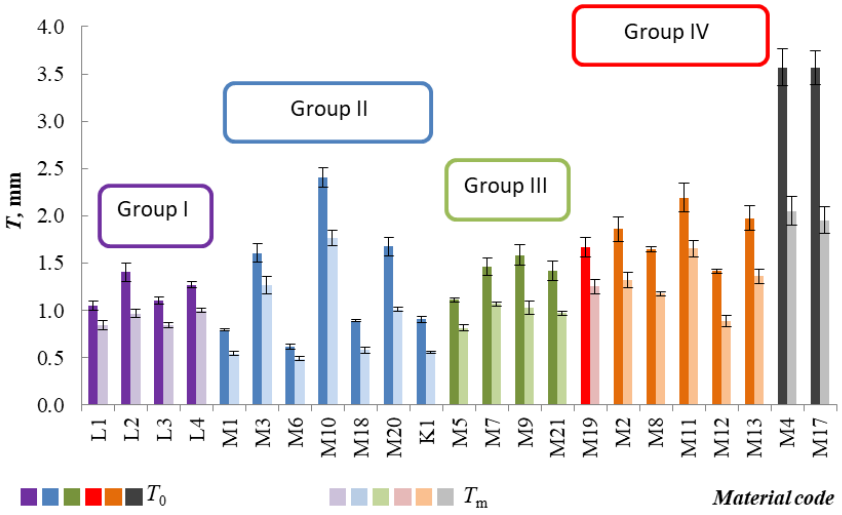

Figure 3.8. Histograms of thickness of uncompressed investigated upholstery materials (T_0) and the values after compression (T_m)

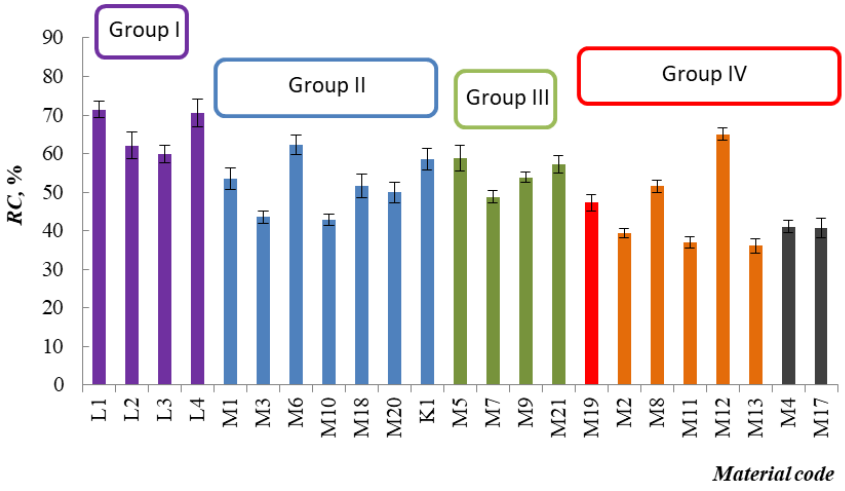

Figure 3.9. Histograms of compression resilience *RC* (%) for the investigated upholstery materials

Compression resilience *RC* describes the quality of materials and their performance in the course of exploitation. The best materials from this standpoint are synthetic leathers (Group I) because their compression resilience *RC* reaches on average 66%, whereas average compression resilience *RC* for Groups II and III are 54%. For Group IV (jacquard, chenille, corduroy), the average *RC* is the lowest at 45%, which means that the upholstery materials of the complex weave types are the

least able to recover to their initial shape although they are highly compressible (Fig. 3.9). This means that strong linear dependence exists between the compressibility expressed in percentage values and compression resilience *RC* which in the case of the investigated materials was as follows: for one layer materials, the correlation coefficient was r_c = –0.86 (*RC*–T_0) and r_c = –0.87 (*RC*–T_m), for two layer materials, it was slightly lower: r_c = –0.62 (*RC*–T_0) and r_c = –0.85 (*RC*–T_m), strong correlation was obtained for chenille fabrics r_c = –0.93 (*RC*–T_0) and r_c = –0.90 (*RC*–T_m). No correlation was found for synthetic leathers.

3.1.5. Surface

During the investigations, surface friction *MIU* (Fig. 3.10) and surface roughness *SMD* (Fig. 3.11) of the face sides of the upholstery materials was defined (Table 3.3).

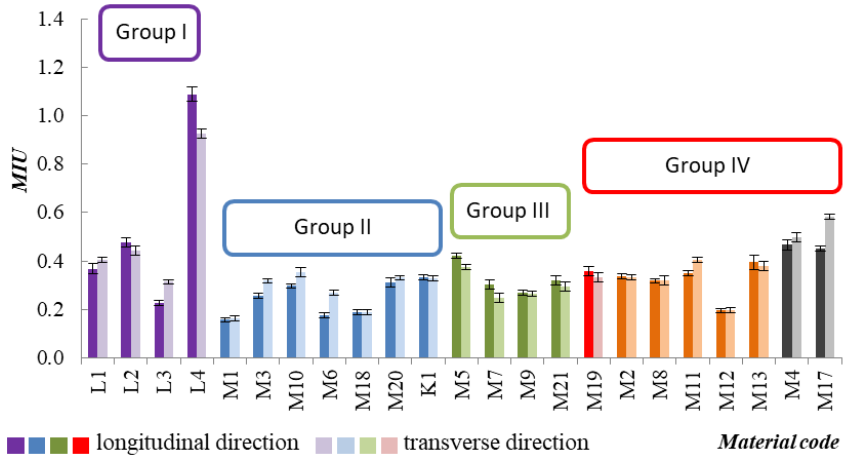

Figure 3.10. Histograms of coefficient of friction *MIU* for upholstery materials in the longitudinal and transverse directions

Surface roughness *SMD* of all the synthetic leathers is similar, and it does not show any difference in longitudinal and transverse directions. Only *SMD* of L3 leather is higher by 56% and 79%. For synthetic leathers, the differences appear in the case of surface friction *MIU*. L3 leather, whose surface roughness *SMD* was the highest (2.79; 2.61), has the lowest surface friction *MIU* in longitudinal (0.23) and transverse (0.31) directions. To the contrary, L4 leather, whose *SMD* was low (0.83; 1.15), has the highest *MIU* in longitudinal (1.10) and transverse (0.93) directions. It is higher by 58–67% compared to the surface friction of the other synthetic leathers.

Surface friction *MIU* of one-layer upholstery materials (Group II) differs in the longitudinal direction by 6%–16%; in the transverse direction, the difference is slightly higher, i.e. by 14%–40% (Fig. 3.10). This difference is not as significant as it is for surface roughness *SMD* (Fig. 3.11). Here, *SMD* difference between the longitudinal and transverse directions fluctuates between 4%–72%. It must be noted

that for most materials representing Group II, *SMD* in the longitudinal direction varies only by 9%, except for knitted material K1. Hence, in the transverse direction, *SMD* difference varies significantly between 31.5% and 81.9%. This is explained by the effect of the weave type and the different weaving threads and yarns applied in the warp and weft directions.

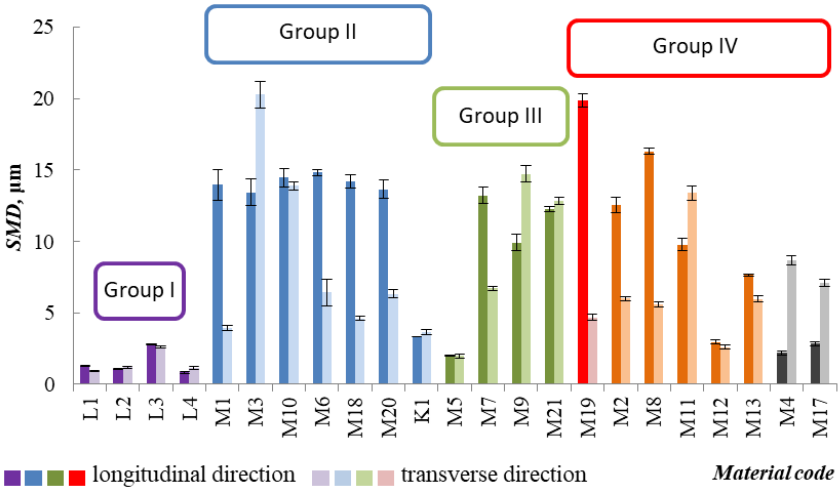

Figure 3.11. Histograms of surface roughness *SMD* (µm) for upholstery materials in the longitudinal and transverse directions

An example of this case can be sourced from upholstery material M6 *MIU* and *SMD* values which in the longitudinal and transverse directions are in opposite relationship. On the other hand, materials M5 and M7 can serve as an example that there is no relationship between surface friction *MIU* and surface roughness *SMD*. Material M5 features comparatively high friction *MIU* = 0.42, but its surface is not rough (*SMD* = 1.99), while the friction of material M7 is lower at 0.30, but its surface is much rougher at 13.23. This trend is especially evident in Group IV of upholstery materials denoted by complex weave types. Figure 3.12 (a, b) presents surface friction *MIU* and surface roughness *SMD* curves of jacquard M19 and Figure 3.12 (c, d) shows corduroy M4.

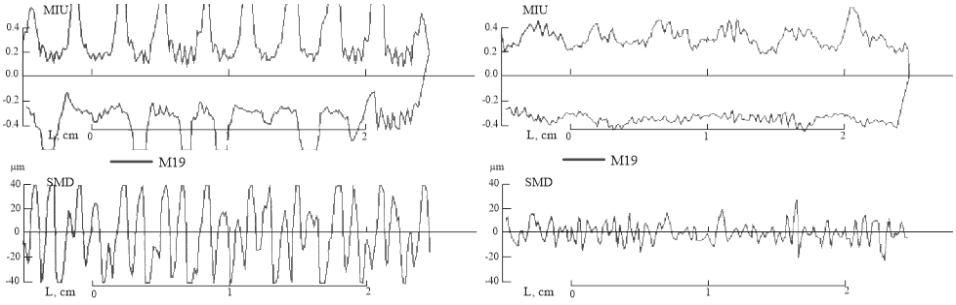

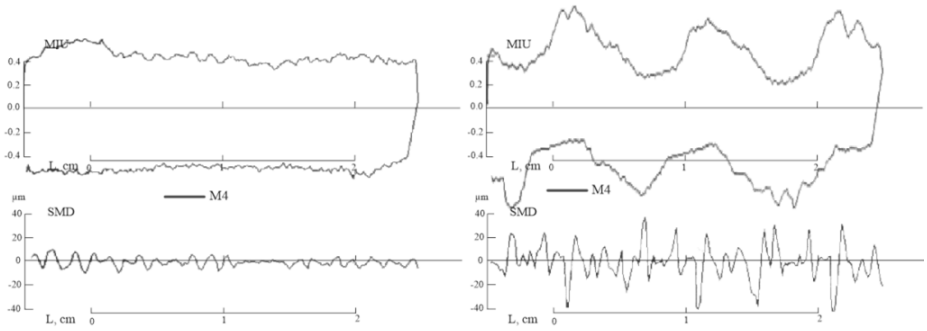

Figure 3.12. Surface coefficient of friction *MIU* and surface roughness *SMD* for jacquard material M19 and corduroy M4 in the longitudinal (a, c) and transverse (b, d) directions

It may be observed that the surface of jacquard M19 is very rough in the warp direction. Meanwhile, the surface roughness of corduroy M4 is greater in the weft direction, but surface friction *MIU* of both materials is more or less the same and varies within the limits of 6.2–7.5%. This means that, during the production of upholstered furniture with slippery surfaces, materials with complex weave types, e.g. jacquard or corduroy, special attention must be devoted to such materials.

KES-F characterization of the deformability for upholstery materials. Chapter summary. Among all the tested materials, special attention must be paid to synthetic leathers. Although they possess good consumer qualities, such as durability, abrasion resistance and easy care; however, in the manufacturing and, especially, design processes, e.g., digitized pattern making, they may cause problems in providing graceful three-dimensional shapes of soft furniture. From the standpoint of tensile strain *EMT* and shear rigidity *G*, synthetic leathers are highly extensible in the transverse direction (even by 400% compared to the longitudinal direction) and feature the highest shear rigidity. The latter point makes them problematic in obtaining spatial shapes during soft furniture production. It is known that upholstery materials are stiffer and have higher bending rigidity *B* compared to those used in the garment production. During compression testing, synthetic leathers were distinguished as the least compressible – only from 20% to 30% was scored. The thinnest were the one-layer materials from Group II, and the same level remained after compression.

3.2. Analysis of Creep and Relaxation Deformation Processes for Upholstery Furniture Manufacturers: Practical Application

For the covering of upholstery furniture parts, mostly, highly anisotropic flexible polymer materials of different fiber content are used – yet various structures and the deformation-relaxation behavior of these materials are very different. Therefore, while choosing a new fabric for the production of furniture, the values of pull-on ease (as applied before) are not suitable anymore as they are chosen without considering the mechanical properties of the fabric. While designing the upholstery

parts, the appropriate values of pull-on ease are applied when taking into account that it would be easy to fix the cover onto the furniture as it would precisely fit the surface of the furniture, even in cases of complicated shapes of furniture parts. The obtained shape of the cover should remain stable also in the course of the exploitation of the furniture; therefore, it is very important to investigate not only exploitation loadings but also to detect the caused relaxation behavior of the fabrics, that is, creep and deformation relaxation. The main task for solving real-life furniture upholstery issues is to define the relationship between the mechanical characteristics of upholstery fabrics and the values of pull-on ease by taking into account the relaxation behavior. The investigation allowed defining the coefficient of fabrics anisotropy, the deformation behavior of upholstery as well as its ease variation characteristics in respect of the furniture surface as well as the exploitation loadings impact.

For the testing, the loadings that typically act in the production processes and in the course of exploitation of upholstery furniture were chosen. Therefore, a decision was made to perform the uniaxial tension test up to 25 N, i.e. a low wearing level load according to the KES-F methodology and up to 100 N, i.e. the production level load applied for the upholstery pulling onto furniture. The latter results pertaining to rigidity modulus E_{m25} and E_{m100} as well as coefficients of anisotropy c_{a25} and c_{a100} are presented in Table 3.3.

The performed uniaxial tension (Table 3.4) and creep and relaxation deformation experiments (Table 3.5) showed the main differences between the longitudinal and transverse directions, and the obtained results allowed to identify the main direction (the stronger direction) of the fabric. The experimental curves of creep and relaxation deformation indicate major differences between the deformational behavior of different upholstery fabrics where synthetic leather L2 and knitted materials K1 and K2 as well as woven material M14 of twill weave 2/2 may be distinguished from the other investigated fabrics in the longitudinal direction (Fig. 3.13, a) and, especially, in the transverse direction (Fig. 3.13, b).

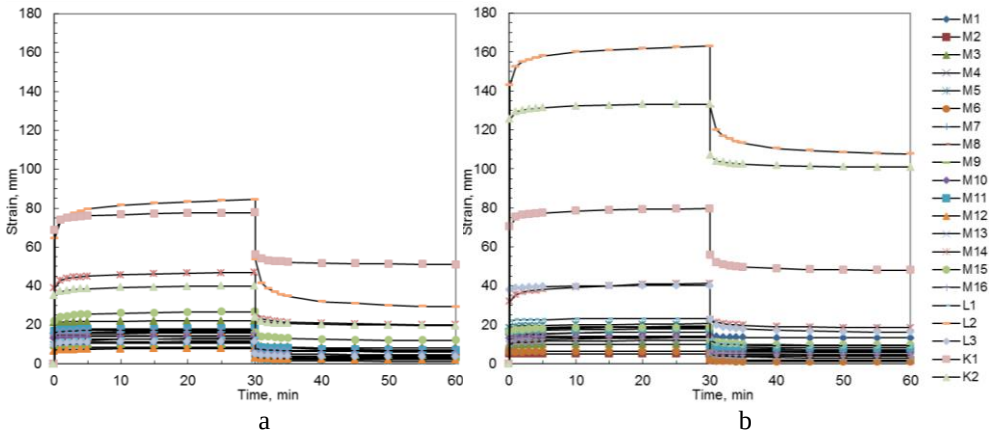

a b

Figure 3.13. Experimental curves of creep and relaxation deformation for upholstery materials with 100 N load in the longitudinal (a) and transverse (b) directions

Table 3.4. Mechanical characteristics of upholstery materials at break and at low loads of 100 N and 25 N

Material code	Strength parameters								Rigidity modulus E_m						Anisotropy coefficient c_a		
	Longitudinal direction		Transverse direction		Longitudinal direction		Transverse direction		E_{mmax}		E_{m100}		E_{m25}				
	F_{max}, N	ε_{max}, mm	F_{max}, N	ε_{max}, mm	ε_{100}, mm	ε_{25}, mm	ε_{100}, mm	ε_{25}, mm	Long	Trans	Long	Trans	Long	Trans	$c_{a\,max}$	$c_{a\,100}$	$c_{a\,25}$
M1	609.0	40.15	709.5	32.04	14.60	6.65	11.96	5.60	15.17	22.14	6.85	8.36	3.76	4.46	0.80	0.82	0.84
M2	1724.0	102.63	2042.5	44.20	11.50	6.13	3.60	1.90	16.80	46.21	8.70	27.78	4.08	13.16	0.43	0.31	0.31
M3	1650.0	89.25	1121.3	49.13	14.75	7.50	9.25	5.38	18.49	22.82	6.78	10.81	3.33	4.65	0.55	0.63	0.72
M4	1266.0	41.85	1341.0	66.00	3.15	1.20	11.93	6.98	30.25	20.32	31.75	8.39	20.83	3.58	0.63	0.26	0.17
M5	1656.0	94.40	1190.0	56.70	9.90	5.80	10.50	4.50	17.54	20.99	10.10	9.52	4.31	5.56	0.60	0.94	0.78
M6	1662.0	107.00	1562.0	72.23	13.38	5.00	6.90	3.30	15.53	21.63	7.48	14.49	5.00	7.58	0.68	0.52	0.66
M7	950.0	55.63	766.4	58.88	8.38	5.13	10.80	5.48	17.08	13.02	11.94	9.26	4.88	4.57	0.94	0.78	0.94
M8	1213.8	63.52	246.8	18.68	6.64	2.40	8.85	3.75	19.11	13.21	15.06	11.30	10.42	6.67	0.29	0.75	0.64
M9	1191.3	50.40	1205.0	61.75	8.00	4.70	11.38	6.13	23.64	19.51	12.50	8.79	5.32	4.08	0.82	0.70	0.77
M10	2287.5	77.13	1514.0	54.15	11.63	6.50	9.00	4.95	29.66	27.96	8.60	11.11	3.85	5.05	0.70	0.77	0.76
M11	1305.0	60.00	485.5	56.90	16.20	9.80	11.70	6.70	21.75	8.53	6.17	8.55	2.55	3.73	0.95	0.72	0.68
M12	1336.5	57.68	382.4	42.98	5.92	3.12	6.25	3.00	23.17	8.90	16.89	15.99	8.01	8.33	0.75	0.95	0.96
M13	1399.5	76.10	813.0	54.75	10.60	4.80	5.55	2.48	18.39	14.85	9.43	18.02	5.21	10.10	0.72	0.52	0.52
M14	400.0	116.88	310.0	65.55	30.00	11.50	18.98	9.15	3.42	4.73	3.33	5.27	2.17	2.73	0.56	0.63	0.80
M15	524.3	55.28	604.5	32.33	11.25	4.75	10.13	4.35	9.48	18.70	8.89	9.88	5.26	5.75	0.58	0.90	0.92
M16	1967.5	62.50	1858.0	57.30	14.00	8.20	11.60	7.00	31.48	32.43	7.14	8.62	3.05	3.43	0.92	0.83	0.85
L1	1091.3	54.60	347.2	35.93	8.50	3.00	22.13	11.25	19.99	9.66	11.76	4.52	8.33	2.22	0.66	0.38	0.27
L2	406.5	141.00	227.3	235.00	37.95	5.70	117.25	16.25	2.88	0.97	2.64	0.85	4.39	1.54	0.60	0.32	0.35
L3	619.5	34.35	679.5	79.84	6.83	3.60	38.08	25.20	18.03	8.51	14.65	2.63	6.94	0.99	0.43	0.18	0.14
K1	315.6	137.10	512.3	165.20	43.20	13.80	49.60	18.00	2.30	3.10	2.31	2.02	1.81	1.39	0.83	0.87	0.77
K2	570.0	94.10	365.2	201.00	26.90	11.80	110.00	61.30	6.06	1.82	3.71	0.91	2.10	0.40	0.47	0.24	0.19

Table 3.5. Constituent parts of creep and relaxation deformation (100 N load)

Code	ε_G, mm		ε_s, mm		ε_c, mm		ε_R, mm				ε_r, mm	
							ε_e, mm		ε_v, mm			
	Long	Trans	Long	Trans	Long	Trans	Long	Trans	Long	Trans	Long	Trans
M1	16.0	19.3	15.5	16.5	0.5	2.8	6.5	4.8	1.5	1.3	8.0	13.3
M2	16.8	5.0	15.5	5.0	1.3	0.0	10.8	3.0	1.3	0.3	4.8	1.8
M3	22.0	10.0	21.1	9.5	0.9	0.5	9.4	4.5	1.3	0.6	8.1	3.9
M4	8.0	16.3	7.0	14.5	1.0	1.8	4.5	7.8	0.8	2.3	2.8	6.3
M5	10.8	20.5	9.5	18.5	1.3	2.0	8.3	11.0	1.3	2.5	1.3	7.0
M6	14.5	6.3	13.5	6.0	1.0	0.3	10.5	4.8	0.3	0.5	3.8	1.0
M7	10.5	14.0	9.5	13.0	1.0	1.0	7.0	7.0	1.0	1.5	2.5	5.5
M8	12.8	16.0	11.0	13.5	1.8	2.5	7.8	5.5	2.3	1.5	2.8	9.0
M9	8.5	18.5	8.0	16.5	0.5	2.0	6.0	10.0	0.5	2.3	2.0	6.3
M10	14.0	13.8	13.3	13.0	0.8	0.8	7.0	6.8	1.0	1.0	6.0	6.0
M11	18.0	17.8	16.8	16.3	1.3	1.5	8.8	8.0	2.3	1.8	7.0	8.0
M12	7.9	13.3	6.6	10.4	1.3	2.9	3.1	6.1	1.0	2.1	2.1	4.0
M13	17.3	12.0	16.0	10.0	1.3	2.0	9.5	7.0	1.0	2.0	6.8	3.0
M14	47.0	41.3	39.0	32.0	8.0	9.3	20.5	18.8	6.5	4.0	20.0	18.5
M15	26.8	18.5	22.0	16.3	4.8	2.3	10.8	6.5	4.0	2.5	12.0	9.5
M16	15.7	13.7	14.7	13.0	1.0	0.7	9.8	8.1	1.3	0.8	4.7	4.8
L1	13.0	23.0	11.8	22.0	1.3	1.0	9.0	11.0	0.5	3.0	3.5	9.0
L2	84.5	158.0	64.5	143.0	20.0	15.0	31.0	39.0	24.3	19.8	29.3	99.3
L3	11.6	40.2	9.8	37.8	1.8	2.4	5.1	22.7	1.4	6.4	3.7	16.3
K1	77.7	79.5	68.6	70.3	9.1	9.2	56.2	55.9	5.2	8.0	51.0	47.9
K2	39.9	133.3	35.1	125.5	4.8	7.8	16.0	26.3	4.4	6.1	19.5	100.8

The most important criterion for evaluating the results of this experiment was the behavior of sudden deformation ε_s between the longitudinal and transverse directions. The obtained results revealed that the main direction (i.e. the stronger direction) of one-layer materials M3, M6, M10, M14, M16, chenille fabrics M2, M11, M13, M15 and synthetic leather L2 is the longitudinal direction while the transverse direction is inherently elastic (Table 3.5). The deformational behavior of the remaining materials is the opposite – the stronger direction is the transverse direction, while elasticity relates to the longitudinal direction. This is one of the parameters of the deformational behavior evaluation which must be taken into account when designing the product and applying the ease allowance, i.e. when identifying the stronger direction.

The investigated upholstery materials were classified into 7 groups according to the difference between the longitudinal and transverse directions in terms of sudden deformation ε_s. No ease allowance is needed for the upholstery fabrics with a difference between the directions of sudden deformation ε_s which did not exceed 2.5% (calculated from the initial length of the specimen). When the difference exceeds 2.5%, the cutting pattern for such materials has to be reduced by paying attention to the stronger direction.

What concerns the groups proposed to the manufacturers evaluating the difference of sudden deformation ε_s between the directions (Fig. 3.14), Group I involves upholstery materials (one-layer materials M1, M10, M16, chenille fabrics M8, M11, M12, two-layer material M7 and knitted material K1), of which the difference of sudden deformation ε_s between the longitudinal and transverse directions did not exceed 2.5%.

Group II includes one-layer material M14 and chenilles M13 and M15 with a higher (more than 2.5%) difference of sudden deformation ε_s between the directions. The cutting pattern for these materials has to be reduced to 2.5% in the longitudinal direction.

Group III covers upholstery materials (corduroy M4, two-layer materials M5, M9 and synthetic leather L1): the difference of ε_s between the directions consists of about –5%. In such a case, the cutting patterns for these materials have to be reduced in the transverse direction to 5%.

Group IV features one-layer materials M3, M6 and chenille fabric M2 whose difference is about 5%. Thus the cutting patterns should be reduced in the longitudinal direction to 5%.

Groups V–VII involve special (individual) cases when upholstery materials are particularly different in terms of their deformational behavior; they characteristically show a great deformability. The difference of ε_s between the directions is –14% for synthetic leather L3; therefore, the cutting pattern for this material has to be reduced in the transverse direction to 15%. Synthetic leather L2 is more deformable, and the difference reaches 39%; thus the cutting pattern has to be reduced in the longitudinal direction to 40%. The difference in knitted material K2 reaches even –45%; therefore, the reduction of the cutting pattern for such a material is 45% in the transverse direction.

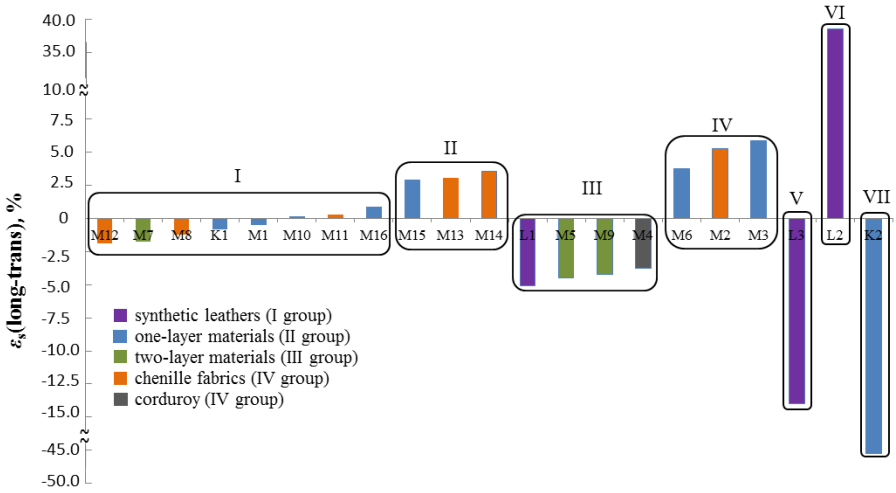

Figure 3.14. The groups composed in terms of the difference between the directions of ε_s

The classification of upholstery materials took place according to the difference between the longitudinal and transverse directions of sudden deformation, as determined by employing the uniaxial creep test when the constant load of 100 N was applied to the specimen. Anisotropy of sudden deformation c_{a25} (ε_s), i.e. the ratio of the longitudinal and transverse directions of sudden deformation as well as the anisotropy of tensile deformation c_a (*EMT*), i.e. the ratio of the longitudinal and transverse directions of tensile strain were calculated seeking to define the

correlation between ε_s and *EMT* at low loads of 25 N. It was discovered that sudden deformation ε_s at low loads (25 N) of the creep process is denoted by good correlation ($R^2 = 0.93$) with tensile deformation *EMT* obtained from the KES-F evaluation system. From this standpoint, it was interesting to analyze the correlation at higher loadings which are associated with the exploitation and upholstery covering loadings of 100 N. The results revealed that the correlation between tensile deformation *EMT* from the KES-F evaluation system and the anisotropy of ε_s from the uniaxial creep test for all the tested materials was low, at the level of $R^2 = 0.44$ (Fig. 3.15). Therefore, the decision was made to find the correlation in groups (synthetic leathers, one-layer materials, two-layer materials and materials of complex weave – chenille fabrics and corduroy). It was determined that tensile deformation *EMT* from the KES-F evaluation system is suitable for predicting the exploitation loadings of upholstery materials because strong correlations were obtained between the anisotropy of ε_s and the anisotropy of *EMT* at higher loadings of 100 N: for synthetic leathers, it was $R^2 = 0.95$, for one-layer materials, the value reached $R^2 = 0.83$, for two-layer materials, it equaled $R^2 = 0.90$, and for materials of complex weave, the value measured $R^2 = 0.74$.

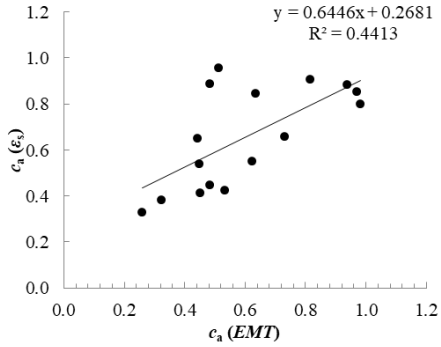

Figure 3.15. The correlation between the anisotropy of sudden deformation ε_s and the anisotropy of tensile deformation *EMT* (by KES-F) at higher loads of 100 N for the investigated upholstery materials: synthetic leathers, one-layer materials, two-layer materials, chenilles and corduroy

Analysis of creep and relaxation deformation processes for upholstery furniture manufacturers (practical application). Chapter summary. Simple tests, i.e. uniaxial tension till the breakage and creep and relaxation deformation with the load of 100 N were performed seeking to solve the practical problems of real-life furniture manufacturing concerning the investigation of the most frequently used upholstery materials. The offered simple testing method has proven that the difference between the longitudinal and the transverse directions for upholstery materials was determined by evaluating the main (the stronger) direction as well as the values of the differences, according to which, the fabrics were classified into the groups indicating the specific reduction and the direction to be reduced. It was found that the KES-F evaluation system which was developed and approved for the investigation and evaluation of the properties of thin fabrics of male suits is also

suitable for predicting the sudden deformation in the uniaxial creep test at higher loads of 100 N, which are considered as exploitation-level loads because strong dependence (R^2 = 0.86) between *EMT* and ε_s was detected.

These tests were conducted only at macro level in order to evaluate the deformational behavior of a large amount of upholstery fabrics and to offer a method as simple as possible for the manufacturers to apply. In further investigations, upholstery materials were explored by performing thorough and comprehensive analyses seeking to define the relations between the parameters of creep and relaxation deformation as well as uniaxial tension.

3.3. Creep and Relaxation Deformation of Upholstery Materials

After defining the uniaxial tension parameters for all the 27 samples, it was noticed that the deformation behavior of some fabrics is extremely similar. Therefore, the investigated samples were selected from the four groups established on the grounds of the KES-F testing results and by considering their anisotropy coefficient c_a, calculated at a tensile force equaling to 25 N (Table 3.4). In the further investigations of creep and relaxation deformation processes, only 3 representative samples (synthetic leather from Group I, one-layer material from Group II and chenille fabric from Group IV) from the KES-F groups and the additional sample of knitted materials (Group II) were used according to different levels of anisotropy: chenille sample M12 of low anisotropy ($0.9 < c_a < 1.0$); one-layer samples M3 and K1 of middle anisotropy ($0.5 < c_a < 0.9$), and synthetic leather sample L3 of high anisotropy ($c_a < 0.5$).

The characteristic force – strain – curves showed that the maximal breaking forces for the tested samples varied within the limits of 315 N÷1650 N (Fig. 3.16). Therefore, the decision was made to perform the uniaxial tension test up to 25 N, i.e. to use the low wearing level load according to the KES-F methodology and up to 100 N, i.e. the production level load applied for the upholstery pulling on furniture. In respect to these loadings, material rigidity modulus E_{m25} and E_{m100} and anisotropy coefficients c_{a25} and c_{a100} were calculated (Table 3.4).

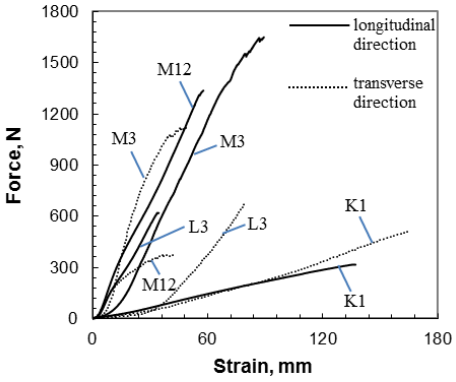

Figure 3.16. Typical force-strain curves for the selected upholstery materials in the longitudinal and transverse directions

The results of the uniaxial testing up to breaking (Table 3.4) showed that the highest levels of anisotropy were obtained for synthetic leather L3 (c_a = 0.43) as well as for one-layer fabric M3 (c_a = 0.55). The obtained results showed that, for both loading values, synthetic leather L3 features the highest elongation anisotropy. Meanwhile, the lowest values were scored by chenille fabric M12, which stood out with the highest rigidity modulus (E_{m25} ~ 8.0) in both – longitudinal and transverse – directions (Fig. 3.18). The lowest rigidity modulus was obtained for knitted fabric K1 (E_{m25} ~ 1.8) in the longitudinal direction and by synthetic leather L3 (E_{m25} ~ 1.0) in the transverse direction. The defined rigidity modulus is necessary for defining the relationship between the uniaxial tension and the creep process parameters at the same low loadings.

During the creep testing, sample general deformation ε_G and its components during the loading and after applying the load were defined. In terms of the loading duration, sudden deformation ε_s and creep deformation ε_c were defined from general deformation ε_G. Meanwhile, after unloading, reversible deformation ε_R, elastic deformation ε_e and viscoelastic deformation ε_v as well as residual deformation ε_r were determined. The values of deformation and its components for all the investigated fabrics are presented in Table 3.6.

Table 3.6. General deformation and its components at 25 N loading

Material code	General deformation ε_G, mm		Sudden deformation* ε_s, mm		Creep deformation ε_c, mm		Reversible deformation ε_R, mm				Residual deformation ε_r, mm	
							Elastic deformation** ε_e, mm		Viscoelastic deformation ε_v, mm			
	Long.	Trans.	Long.	Trans.	Long.	Trans.	Long.	Trans.	Long.	Trans.	Long.	Trans.
M3	9.5	4.2	9.3	4.1	0.2	0.1	4.9	1.6	0.1	0.6	4.5	2.0
M12	2.4	2.8	2.1	2.6	0.3	0.2	1.4	1.4	0.5	0.2	0.5	1.2
L3	4.1	30.1	3.8	27.3	0.3	2.8	2.0	14.8	0.5	5.5	1.6	9.8
K1	16.5	20.0	15.2	18.1	1.3	1.9	7.1	9.8	0.9	1.6	8.5	8.6

Note: * – immediately after loading; ** – immediately after unloading

For the samples of high anisotropy, e.g. L3, at 25 N loading or L3 and M3 at 100 N loading, the creep recovery behavior in the longitudinal and transverse directions after unloading stays proportional in all the constituent parts of the general deformation. For example, if general deformation ε_G of synthetic leather L3 (c_{a25} = 0.14) in the longitudinal direction is lower compared to the transverse direction (Table 3.6), the same tendency remains in the values of elastic ε_e and residual deformations. This phenomenon is important in predicting the tendencies of materials residual deformation ε_r when general deformation ε_G in the longitudinal and transverse directions is known. During the loading process, creep deformation does not have any relationship with anisotropy coefficient c_{a25}. Other dependencies between c_{a25} and constituent parts of the general deformation were not defined. Higher deformability in the transverse direction is mostly common in samples which feature low coefficients c_{a25}.

The conducted investigations showed that instantaneous rigidity modulus E_{m25} is more important than anisotropy coefficient c_{a25} in setting the dependencies

between uniaxial tension parameters and general deformation constituent parts (Table 3.4).

The obtained results (Fig. 3.17) proved that good correlations were traced between E_{m25} and general ε_G, sudden ε_s, reversible ε_R, residual ε_r and elastic ε_e deformations (R^2 = 0.79÷0.95). Medium correlation was obtained between instantaneous rigidity modulus E_{m25} and creep deformation ε_c (R^2 = 0.44÷0.74), and no correlation was found between viscoelastic deformation ε_v (R^2 = 0.04÷0.54).

Sudden deformation ε_s for different anisotropy samples ranges from 88% to 98%; creep deformation ε_c ranges from 2% to 13% of general deformation ε_G, respectively (Fig. 3.18). Reversible deformation ε_R after sample unloading comprises a major part of general deformation ε_G (48%÷79%), but only a minor part of residual deformation ε_r (21%÷52%). Reversible deformation in the major part is comprised of elastic deformation ε_e (from 73% to 98%), and in minor part of viscoelastic deformation ε_v (from 2% to 27%).

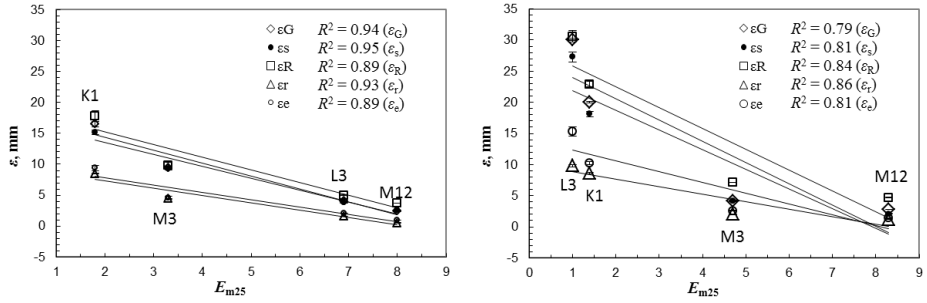

a b

Fig. 3.17. The dependence of rigidity modulus (at 25 N) upon general, sudden, reversible, residual and elastic deformations in the longitudinal (a) and transverse (b) directions

It was observed that for the materials characterized by high rigidity modulus E_{m25}, sudden deformation ε_s is small and, vice versa, e.g. for chenille fabric M12 (E_{m25} = 8.0), sudden deformation is ε_s = 2.1 mm, yet for knitted material K1 (E_{m25} = 1.8), sudden deformation is ε_s = 15.2 mm (Fig. 3.18).

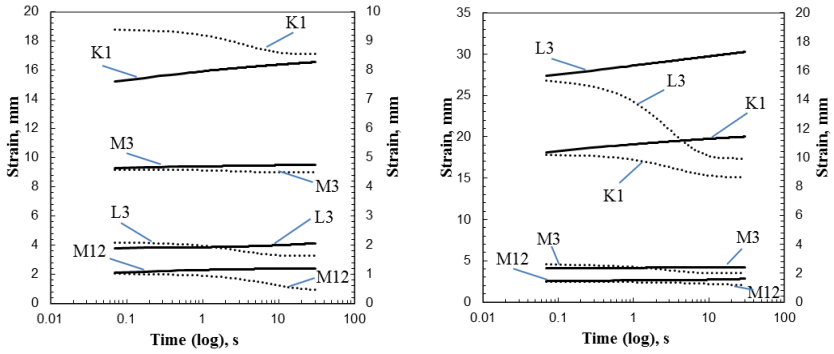

a b

Fig. 3.18. Creep (____) and deformation relaxation (.....) curves of the investigated materials loaded by 25 N in the longitudinal (a) and transverse directions (b)

The creep process is not dynamic, and its values ε_c are not high for materials which are characterized by high rigidity modulus E_{m25} and lower sudden deformation ε_s. It is the opposite: the creep process is sufficiently intensive ε_c, even at the final moments of its measurement, for the materials which are characterized by low rigidity modulus E_{m25} and high sudden deformation ε_s (Fig. 3.18).

Theoretical analysis was applied when modeling the creep and relaxation deformation processes for the investigated materials (M3, M12, L3 and K1) when using the power equation (2.19) for the creep deformation and exponent equation (2.20) for the relaxation deformation. The alteration of deformation for synthetic leather L3 and knitted material K1 experimental ε_{exp} (mm) and calculated ε_{cal} (mm) values, and the obtained relative error δ (%) are presented in Table 3.7. The diagrams of experimental ε_{exp} (mm) and calculated ε_{cal} (mm) values of creep deformation for the investigated materials are presented in Appendix 2, Figs. A2.1, A2.3. The obtained results showed that the calculated values used in the power equation (2.19) for the creep deformation agree well enough with the experimental values, even though the statistical random error reaches 5.05% in the middle of the deformation process part (Table 3.7). In general, the compliance of the experimental and theoretical (calculated) values of deformation depends on the curve equation; it depends on the intensity of deformation alteration as well. The greater discrepancy stems from the modeling relaxation deformation process when using exponent equation (2.20) because of a huge difference between the materials (Table 3.7). It is difficult to find the basic equation suitable for all the anisotropic materials to be modeled. The diagrams of experimental ε_{exp} and calculated ε_{cal} values of relaxation deformation for the investigated materials are presented in Appendix 2, Figs. A2.2, A2.4.

Table 3.7. The values of the experimental and calculated creep and relaxation deformation process of L3 and M12 materials when F = 25 N in the transverse direction

	Time, s	L3			M12		
		ε_{exp}, mm	ε_{cal}, mm	δ, %	ε_{exp}, mm	ε_{cal}, mm	δ, %
Creep	5	27.3	27.4	2.21	2.10	2.10	0.00
	300	29.4	29.4	0.00	2.35	2.36	2.56
	600	29.9	29.7	4.05	2.40	2.38	5.05
	900	29.9	29.9	0.00	2.40	2.39	2.52
	1200	30.1	30.1	0.00	2.40	2.40	0.00
	1500	30.1	30.2	2.00	2.40	2.40	0.00
	1800	30.1	30.3	4.00	2.40	2.41	2.51
Relaxation deformation	1805	15.3	15.3	0.00	1.00	1.01	6.01
	2100	10.8	11.0	11.08	0.80	0.76	30.96
	2400	10.5	10.1	23.45	0.60	0.62	19.80
	2700	10.0	10.0	0.00	0.50	0.54	46.45
	3000	9.9	9.9	0.00	0.50	0.51	11.96
	3300	9.8	9.9	6.13	0.50	0.49	12.20
	3600	9.8	9.9	6.13	0.50	0.48	24.64

Note: δ is the relative error, %

Figure 3.19 evidently shows the crossing point of two force–strain curves (L3 and K1) at the zone of higher loading values. This phenomenon is very important when the material behavior must be evaluated at a concrete level of the external loadings acting during the production or product exploitation. Comparative analysis between instantaneous rigidity modulus E_{m25} and E_{m100} showed (Table 3.4) that the rigidities of synthetic leather L3 and knitted material K1 changed significantly at the external loading of 50 N (Fig. 3.19, b).

Taking into account the fact that in the upholstery furniture production processes, upholstery materials are experiencing higher loadings than during the product exploitation, an external force of 100 N was selected for further research. Besides, such a level of the external force corresponds to the real loading which takes place during the upholstery material pull-on process in the upholstery furniture production. The investigation of the creep process with 100 N loading showed that sudden deformation ε_s of synthetic leather L3 in the transverse direction is smaller compared to sudden deformation ε_s of knitted material K1 (Table 3.5). Meanwhile, during the investigations with 25 N loading, the result was the opposite – sudden deformation ε_s of synthetic leather L3 in the transverse direction was 33.7% higher compared to sudden deformation ε_s of knitted material K1. The same tendency is valid for instantaneous rigidity modulus E_{m25} and E_{m100} (Table 3.4).

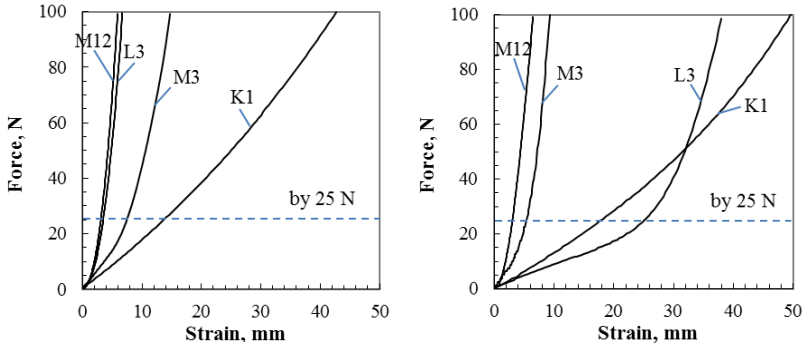

Fig. 3.19. Force–strain curves at 25 N and 100 N loading (*a* represents the longitudinal direction, *b* shows the transverse direction)

The results of the investigation with the 100 N loading showed that the deformational behavior of all the tested samples (except for knitted material K1) in the longitudinal and transverse directions after unloading remains proportional in all the constituent parts of general deformation ε_G. For example, if general deformation ε_G of synthetic leather L3 in the longitudinal direction is smaller compared to the transverse direction (Table 3.5), the same tendency remains for the values of other constituent deformations. For 100 N loading, as well as for 25 N loading, no correlation was found between the creeping process parameters and the coefficients of anisotropy.

The obtained results show that general deformation ε_G in the transverse direction for investigated materials M12, L3 and K1 is higher compared to the

longitudinal direction (the difference between the directions varies within the limits of 2%–71%); meanwhile, one-layer material M3 in the longitudinal direction after 1800 s stretched more than two times compared to the transverse direction. A particularly prominent difference of general deformation ε_G between the directions was obtained for synthetic leather L3 (the difference of the 25 N load reached even 86.4%, with 100 N it was at 71.1%), in the case when the anisotropy (when using 100 N) was the highest one.

It was noted that the higher is the rigidity modulus E_m for the investigated materials, the lower are the values of the deformation components, e.g. if rigidity modulus E_m for chenille material M12 is E_m = 16.89 (Table 3.4), the deformation components are ε_G = 7.9 (mm), ε_s = 6.6 (mm), ε_c = 1.3 (mm), ε_R = 5.8 (mm), ε_e = 4.8 (mm), ε_v = 1.0 (mm), ε_r = 2.1 (mm), respectively (Table 3.5). And, to the contrary, the lower is the rigidity modulus E_m for the investigated materials, the higher are the values of the deformation components.

Sudden deformation ε_s of the investigated materials ranges from 78% to 96% of general deformation ε_G (Fig. 3.20), creep deformation covers accordingly a smaller part of general deformation ε_G (4%–22%). Meanwhile, elastic deformation ε_e comprises a significant part (28%–61%) of the general deformation compared to viscoelastic deformation ε_v (6%–17%), and reversible deformation ε_R is higher than residual deformation ε_r. Figure 3.20 shows that synthetic leather L3 differs from the remaining samples because its deformations in different directions are not equal (the difference for sudden deformation ε_s is 74.1%). The dependence between instantaneous rigidity modulus E_{m100} and the constituent parts of deformation (ε_G, ε_s, ε_R, ε_r) in the case of 100 N loading is slightly weaker (R^2 = 0.70÷0.94 for the longitudinal direction and R^2 = 0.60÷0.81 for the transverse direction) compared to the dependence obtained at 25 N loading (Appendix 2, Fig. A2.9).

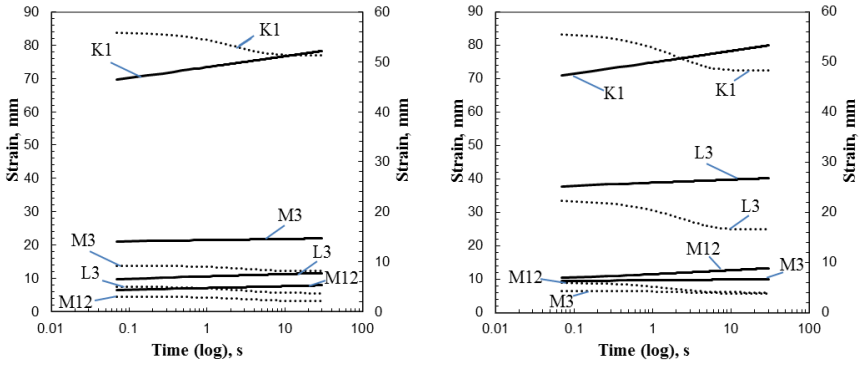

Fig. 3.20. Creep (——) and creep recovery (.....) curves of the investigated materials loaded with 100 N in the longitudinal (a) and in the transverse directions (b)

Table 3.8. Experimental and calculated values of the creep process and the relative errors for the investigated upholstery materials

Material code		**K1**													
Direction		Longitudinal direction							Transverse direction						
Time, s		0.01	0.1	1	10	100	1000	1800	0.01	0.1	1	10	100	1000	1800
ε_{exp}^{*}, mm		68.61	68.66	69.09	71.30	74.81	77.18	77.63	70.30	70.35	70.79	72.92	76.07	79.04	79.49
Maxwell-Thompson	ε_{cal}^{**}, mm	67.51	68.03	69.53	72.84	76.09	77.56	77.73	69.47	70.23	71.80	74.14	76.24	78.98	79.49
	δ, %	1.59	0.88	-0.93	-2.15	-1.71	-0.49	-0.11	1.18	0.18	-1.42	-1.67	-0.23	0.08	0.00
Kelvin-Voigt	ε_{cal}^{**}, mm	68.61	68.73	69.30	71.39	74.83	77.18	77.55	70.31	70.40	70.89	72.84	76.16	79.04	79.69
	δ, %	0.01	0.11	0.30	0.12	0.03	0.00	-0.11	0.01	0.07	0.14	-0.12	0.11	0.00	0.26
Material code		**L3**													
ε_{exp}^{*}, mm		9.80	9.80	9.83	10.05	10.74	11.41	11.55	37.83	37.84	37.93	38.33	39.13	40.01	40.19
Maxwell-Thompson	ε_{cal}^{**}, mm	9.54	9.60	9.77	10.29	11.10	11.52	11.57	37.44	37.60	37.92	38.57	39.61	40.16	40.22
	δ, %	2.61	2.08	0.62	-2.38	-3.34	-0.99	-0.22	1.03	0.65	0.03	-0.63	-1.23	-0.37	-0.08
Kelvin-Voigt	ε_{cal}^{**}, mm	9.80	9.81	9.85	10.06	10.74	11.41	11.47	37.83	37.83	37.84	38.09	39.04	40.01	40.24
	δ, %	0.00	0.05	0.18	0.11	-0.04	0.00	-0.69	0.00	-0.03	-0.25	-0.65	-0.24	0.00	0.13
Material code		**M3**													
ε_{exp}^{*}, mm		21.10	21.11	21.17	21.36	21.54	21.91	21.95	9.45	9.45	9.49	9.65	9.77	9.98	9.99
Maxwell-Thompson	ε_{cal}^{**}, mm	20.92	21.01	21.18	21.37	21.73	21.94	21.97	9.38	9.44	9.56	9.70	9.91	9.99	10.00
	δ, %	0.87	0.44	-0.04	-0.06	-0.86	-0.16	-0.06	0.71	0.16	-0.74	-0.54	-1.35	-0.06	-0.04
Kelvin-Voigt	ε_{cal}^{**}, mm	21.10	21.12	21.18	21.31	21.53	21.91	21.95	9.45	9.46	9.50	9.62	9.78	9.98	10.02
	δ, %	0.00	0.04	0.04	-0.23	-0.07	0.00	-0.01	0.01	0.06	0.13	-0.27	0.06	0.00	0.31
Material code		**M12**													
ε_{exp}^{*}, mm		6.55	6.56	6.60	6.79	7.17	7.78	7.85	10.40	10.40	10.45	10.80	11.81	13.00	13.30
Maxwell-Thompson	ε_{cal}^{**}, mm	6.34	6.42	6.58	6.89	7.52	7.84	7.87	10.06	10.15	10.41	10.93	12.38	13.25	13.36
	δ, %	3.16	2.03	0.36	-1.51	-4.81	-0.76	-0.23	3.30	2.41	0.39	-1.14	-4.80	-1.90	-0.42
Kelvin-Voigt	ε_{cal}^{**}, mm	6.55	6.56	6.62	6.79	7.20	7.78	7.88	10.40	10.41	10.47	10.80	11.88	13.00	13.21
	δ, %	0.01	0.12	0.22	-0.04	0.32	0.00	0.31	0.01	0.05	0.16	0.01	0.58	0.00	-0.68

ε_{exp}^{*} - experimental values of the creep process

ε_{cal}^{**} - calculated values of the creep process by Maxwell-Thompson and Kelvin-Voigt models

Table 3.9. Experimental and calculated values of the relaxation of the deformation process and the relative errors for the investigated upholstery materials

Material code		**K1**													
Direction		Longitudinal direction							Transverse direction						
Time, s		1800	1800	1801	1810	1900	2800	3600	1800	1800	1801	1810	1900	2800	3600
ε_{exp}^{*}, mm		56.20	56.19	56.10	55.41	53.24	51.32	51.00	55.90	55.88	55.71	54.44	51.09	48.33	47.86
Maxwell-Thompson	ε_{cal}^{**}, mm	56.87	56.70	56.23	55.18	52.39	51.07	50.94	56.88	56.55	55.74	54.36	49.94	47.72	47.77
	δ, %	1.20	0.91	0.23	-0.41	-1.60	-0.50	-0.11	1.75	1.20	0.06	-0.15	-2.25	-1.26	-0.19
Kelvin-Voigt	ε_{cal}^{**}, mm	56.20	56.17	56.01	55.41	53.24	51.09	50.77	55.90	55.91	55.87	54.44	51.09	48.22	47.75
	δ, %	0.00	0.03	0.17	0.00	0.00	0.45	0.46	-0.01	-0.06	-0.30	0.00	0.00	0.22	0.23
Material code		**L3**													
ε_{exp}^{*}, mm		5.06	5.05	5.04	4.94	4.39	3.74	3.67	22.67	22.66	22.55	21.68	19.05	16.63	16.19
Maxwell-Thompson	ε_{cal}^{**}, mm	5.20	5.17	5.11	4.95	4.07	3.69	3.66	22.87	22.72	22.16	21.07	17.85	16.27	16.11
	δ, %	2.80	2.37	1.34	0.20	-7.37	-1.43	-0.40	0.88	0.27	-1.69	-2.82	-6.27	-2.15	-0.50
Kelvin-Voigt	ε_{cal}^{**}, mm	5.06	5.05	5.03	4.94	4.39	3.85	3.78	22.67	22.66	22.57	21.68	19.05	16.49	16.05
	δ, %	0.01	0.07	0.37	0.00	0.00	-2.76	-2.80	-0.01	-0.03	-0.13	0.00	0.00	0.84	0.87
Material code		**M3**													
ε_{exp}^{*}, mm		9.30	9.30	9.29	9.22	8.77	8.12	8.04	4.45	4.45	4.45	4.40	4.15	3.87	3.85
Maxwell-Thompson	ε_{cal}^{**}, mm	9.46	9.44	9.39	9.23	8.43	8.06	8.03	4.51	4.50	4.47	4.43	4.02	3.85	3.84
	δ, %	1.67	1.50	1.05	0.17	-3.88	-0.78	-0.21	1.34	1.11	0.62	0.59	-3.07	-0.58	-0.16
Kelvin-Voigt	ε_{cal}^{**}, mm	9.30	9.30	9.30	9.22	8.77	8.29	8.21	4.45	4.45	4.44	4.40	4.15	3.91	3.88
	δ, %	0.00	-0.01	-0.04	0.00	0.00	-2.00	-2.01	0.00	0.04	0.24	0.00	0.00	-0.86	-0.86
Material code		**M12**													
ε_{exp}^{*}, mm		3.07	3.07	3.06	3.00	2.64	2.17	2.12	6.06	6.05	6.03	5.80	4.82	4.05	3.99
Maxwell-Thompson	ε_{cal}^{**}, mm	3.17	3.16	3.11	2.87	2.36	2.13	2.10	6.20	6.15	6.02	5.79	4.50	4.00	3.97
	δ, %	3.47	3.03	1.44	-4.35	-10.72	-1.91	-0.53	2.39	1.59	-0.09	-0.15	-6.59	-1.22	-0.35
Kelvin-Voigt	ε_{cal}^{**}, mm	3.07	3.07	3.07	3.00	2.64	2.28	2.23	6.06	6.06	6.05	5.80	4.82	4.05	3.99
	δ, %	0.00	-0.05	-0.24	0.00	0.00	-4.97	-5.07	-0.01	-0.07	-0.34	0.00	0.00	0.00	0.03

ε_{exp}^{*} - experimental values of the relaxation of the deformation process

ε_{cal}^{**} - calculated values of the relaxation of the deformation process by Maxwell-Thompson and Kelvin-Voigt models

The modeling of the creep and relaxation deformation when using the 100 N load was performed with the classical mechanical models, i.e. the Maxwell-Thompson system of equations (2.21, 2.22) and the mechanical model composed of Kelvin-Voigt elements (2.23, 2.24). Relaxation deformation is calculated according to the regular spectrum of duration, and the values of relaxation duration differ between each other by one row, i.e. $\tau_1 = 0.1$, $\tau_2 = 1$, $\tau_3 = 10$, $\tau_4 = 100$, $\tau_5 = 1000$. The experimental values and the values calculated by classical models as well as relative error δ (%) are presented in Table 3.8 (modeling the creep deformation) and Table 3.9 (modeling the relaxation deformation). The system of equations by Maxwell-Thompson is more suitable for modeling the creep deformation for the investigated sample of upholstery materials (Tables 3.8, 3.9). It was observed that the experimental values of creep and relaxation deformation correspond to the theoretical values of deformations when using the mechanical model as developed by Kelvin-Voigt. Unfortunately, this model does not agree with the end-of-the-relaxation deformation (elastic deformation) due to the highest relative errors (Tables 3.8, 3.9).

It was observed that the system of equations by Maxwell-Thompson provides experimental values of the creep deformation of one-layer fabric M3 whereas experimental values of the relaxation deformation are obtained for knitted material K1 (Appendix 2, Figs. A2.5, A2.7). No such peculiarities were defined when using mechanical model by Kelvin-Voigt.

The highest mismatch was detected at $\tau_4 = 100$ s when modeling the experimental values of the creep and relaxation deformation by employing the Maxwell-Thompson system of equations. In some cases, relative error δ reaches 10.72% (Tables 3.8, 3.9). When comparing the two classical models with each other, the mechanical model by Kelvin-Voigt matches more the experimental values of the creep and relaxation deformation for the tested upholstery materials than the mechanical model by the Maxwell-Thompson system of equations (Appendix 2, Figs. A2.5–2.8).

Creep and relaxation deformation of upholstery materials. Chapter summary. Creep and relaxation investigation results allow stating that upholstery materials for upholstery furniture production can be classified after defining their sudden deformation ε_s in the longitudinal and transverse directions, and their anisotropy coefficient c_{a100} is defined at 100 N external loading. The case of high anisotropy coefficient c_{a100} shows that the investigated material must be assigned to the list of problematic cases of furniture upholstery construction. Even more, the deformational behavior in the longitudinal and transverse directions after unloading remains proportional in all the constituent parts of the general deformation: should sudden deformation ε_s be bigger in the transverse direction, then, elastic ε_e, viscoelastic ε_v and residual ε_r deformations will be bigger in the same direction, as well. The other important piece of information is provided by sudden deformation ε_s which allows checking a material's stretch ability in different directions. On the basis of sudden deformation ε_s, producers of upholstery furniture can foresee the

values of general, creep, elastic, viscoelastic and residual deformations because strong dependencies were defined between them and sudden deformation ε_s.

The performed investigations revealed that upholstery fabrics experience higher loadings during their exploitation. Therefore, the loading of 100 N is recommended for upholstery furniture producers because it is related to upholstery tension forces during the 'pull-on' process. It is possible to predict the deformation behavior of upholstery fabrics because E_{m25} and E_{m100} values obtained from uniaxial tension up to the exploitation level forces (25 N and 100 N) have a strong correlation with general ε_G, sudden ε_s, reversible ε_R and residual ε_r deformations defined at analogous loadings ($R^2 = 0.60 \div 0.95$). Upholstery materials can be classified according to E_{m100} determined in the longitudinal and transverse directions and K_{100} calculated from the results of uniaxial tension at loadings characteristic for the upholstery production process, i.e. 100 N.

The classical mechanical model, i.e. the Maxwell-Thompson system of equations, matches better the experimental values of creep deformation of different anisotropic materials than the experimental values of relaxation deformation. The mechanical model exploring the duration of relaxation by employing the Kelvin-Voigt system is more suitable for matching the experimental values of creep and relaxation deformation processes for all the investigated upholstery materials than the system of equations by Maxwell-Thompson.

3.4. The Effect of Fusing Materials Structure upon the Variations of Flexible Multilayer Systems Spatial Shape

There is no available information concerning the effect of pre-tension upon the biaxial behavior of fused multilayer textile systems which are often used in the interior product and upholstery furniture production. The testing method which is presented in this research is aimed at solving this problem. Its basis comes from our previous investigation of furniture upholstery behavior under *in situ* conditions (Zubauskiene, Strazdiene, Urbelis, & Saceviciene, 2012) which was not convenient from the standpoint of the specimen preparation and the reliability of the obtained testing results.

The previous investigation was not very precise because the testing was performed by using the whole upholstery covering, yet the distribution of tension forces and strains acts not only on the top of the pouffe, which is hanged by a hook, but also act on the lateral sides involving all the covering during the hanging process. Furthermore, differences also stem from the amount of material that was used in sewing the entire covering (including the accuracy of the cutting and sewing processes) and the different tension used in the upholstering process (including the human factor). What concerns all the inaccuracies and weaknesses, a new method was created in order to evaluate the effect of the precise pre-tension level upon biaxial punching processes. A special device was constructed (Fig. 2.12) which had the specimens pre-tensioned by 0.0%, 1.2% and 2.1%.

The aim of this chapter is to evaluate the effect of two perpendicular pre-tension directions and the levels of pre-tension upon fused two-layer textile system

performance behavior under biaxial punching. During the first stage of investigation, uniaxial behavior of M fabric and its two-layer fused systems was analyzed. Their strength and extension characteristics are presented in Table 3.10. Uniaxial testing results show that high elongation anisotropy is observed in basic cotton material M and the woven interlinings as well as in low elongation anisotropy for non-woven and knitted interlinings. It must be noted that tension characteristics after fusing two-layered systems with all the investigated interlinings (woven, non-woven and knitted) became highly anisotropic and very close. Uniaxial strength F_{max} varied from 21.39% to 21.91%; breaking elongation ε_{max} ranged from 7.27% to 17.53%.

The results showed that the strength parameters and the tensile behavior of the tested interlinings (woven, knitted and non-woven) differ significantly. The weakest point is non-woven interlining. Its breaking strength is less by 80.5%–91.5% compared to the remaining samples. Two woven interlinings W1 and W2 differ only in terms of adhesive density, i.e. 52 and 76 dots/cm^2, which affects their strength parameters because the maximal breaking force of W1 interlining is 34.2%–48.4% lower in both directions compared to W2. The same can be noted for breaking elongation which is smaller for W1 by 18.2%–30.9% compared to W2. The different behavior during uniaxial tension was detected in knitted interlinings. In this case, the weaker was the sample with the higher density of adhesive dots, i.e. W5 interlining, because its surface density was only 36 g/m^2. It must be noted that high elongation anisotropy is observed in basic cotton fabric and woven interlinings, but anisotropy coefficient c_a for knitted interlinings W4 and W5 is not so significant and equals to 0.73–0.80. Meantime, the anisotropy coefficient after fusing became meaningful for all the tested systems (0.24–0.31), even for those systems which were composed of W4 and W5 interlinings (Table 3.10).

Table 3.10. Strength characteristics of the investigated two-layered systems and their separate components

Material code	Thick-ness, mm	Surface density, g/m^2	Strength parameters				Coefficient of anisotropy c_a
			warp/course		weft/wale		
			F_{max}, N	ε_{max}, %	F_{max}, N	ε_{max}, %	
W1	0.30	44	46.70	7.90	42.60	24.38	0.32
W2	0.31	53	71.00	11.44	82.60	29.81	0.38
W3	0.26	50	8.30	22.20	9.20	31.15	0.71
W4	0.39	50	82.00	41.05	97.30	29.85	0.73
W5	0.16	36	92.30	31.91	75.00	40.13	0.80
M	0.31	136	235.80	4.51	177.60	18.10	0.25
MW1	0.54	181	358.40	5.64	189.20	18.30	0.31
MW2	0.59	184	403.50	5.50	242.30	19.00	0.29
MW3	0.57	178	367.60	5.35	190.60	18.40	0.29
MW4	0.61	184	379.60	5.44	203.20	20.10	0.27
MW5	0.52	168	317.20	5.23	196.60	22.19	0.24

The uniaxial tensile behavior of fused interlinings is essentially different due to their structure (woven, knitted or non-woven) when tension is induced in the

longitudinal direction (Fig. 3.21, a). For the transverse direction, this difference is not so evident, except for non-woven interlining W3 (Fig. 3.21, b).

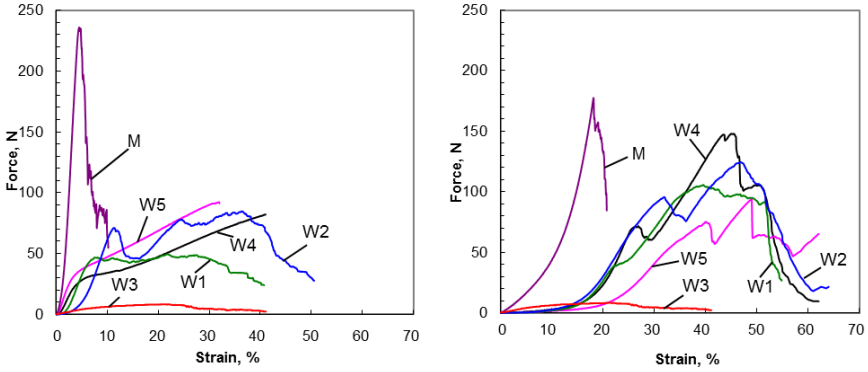

a b

Figure 3.21. Typical force-strain curves of cotton fabric M and interlinings in the longitudinal (a) and transverse (b) directions

Figure 3.21 shows that woven interlining W2 strengthens basic material M in the longitudinal and transverse directions most of all. Meanwhile, knitted interlining W5 makes M fabric the most deformable in the main directions. It must be noted that the tensile behavior of all the tested interlinings differs essentially, but this difference disappears in terms of their fused systems. The effect of fusing is evident from the standpoint of the maximal force and the maximal elongation, which in the longitudinal direction of a two-layer system becomes higher for the breaking force by 25.7–41.6% and for the breaking elongation by 13.6–20.0% compared to the uniaxial strength parameters of M cotton fabric. A slightly lower increase was obtained in the transverse direction: 6.1–26.7% and 1.1–18.4%, respectfully. The changes in the tensile behavior of a two-layer system which can be observed from the tension curves are also meaningful (Fig. 3.22). The initial part of the curves is equal; it shows the negligible effect of the structure (woven, knitted or non-woven) of the fused interlining, i.e. their elasticity modulus expressed via $tg\alpha$ is very close and equals to 11.5.

In the transverse direction, the same phenomenon is observed, except for the two zones where the characteristic elasticity modulus (initial $tg\alpha = 0.48$ and strength $tg\alpha = 2.72$) can be distinguished. Besides, in the transverse direction, several peaks of the maximal force appear which are related to the strength characteristics of fused interlining. Often, the second or the third strength peak is higher than the first, which corresponds to the maximal breaking force of a two-layer system interlining.

Meanwhile, an interesting view can be observed while analyzing the further tension process where the systems with woven interlinings show a different behavior. The results of the uniaxial tension in the transverse direction are the same as in the longitudinal direction – they show that the strength characteristics of single non-woven interlining are very low and significantly differ from basic material M (Fig. 3.22, a). Nevertheless, the strength and extension characteristics of a two-layer

system comprised of those two materials were shown to be the same as those of the other investigated systems. Two-layer systems with woven interlinings feature the second breaking point which is higher if compared to the first point (system MW1). The same phenomenon takes place in the case of knitted interlinings and their systems. The difference is that the third breaking point appears (system MW4), which is higher compared to the first and to the second one.

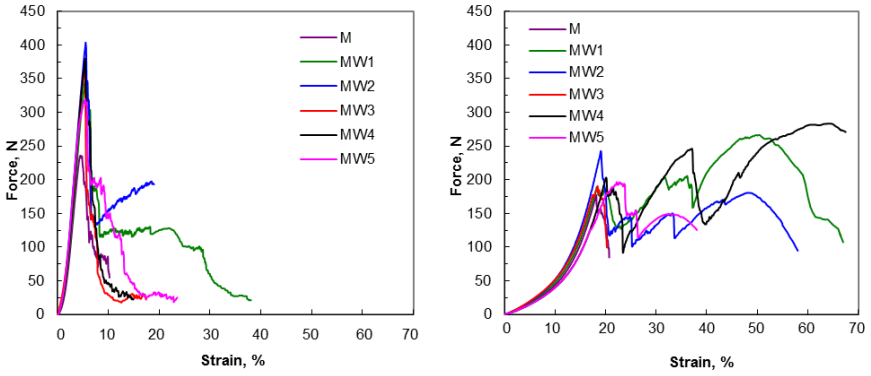

Figure 3.22. Typical tension curves of fused systems in the longitudinal (a) and transverse (b) directions

It must be noted that the uniaxial behavior of separate materials differed significantly, but, after fusing, the strength parameters became closer to the parameters of basic material M (Table 3.10). In the case of a two-layered system with non-woven interlining, the breaking force and elongation is slightly higher than those of basic material M. The same can be observed with woven interlinings and their systems, where breaking characteristics of woven interlining W2 are higher compared to W1. It can be explained by the significant difference in the density of adhesive dots per cm^2 of those two interlinings, while their surface density (g/m^2) and yarn density (cm^{-1}) differed negligibly (Table 2.3).

The analysis of the tension process of fused systems up to the first breaking point allows to state that the strength and extension characteristics for all the systems differ insignificantly (Fig. 3.22). The breaking character of a specimen pre-tensioned in the transverse direction does not differ significantly from the ones pre-tensioned in the longitudinal direction. In this case, the strongest is also basic material M which breaks at comparatively small elongations (Table 3.10). The weakest is non-woven interlining W3. Meanwhile, the breaking characteristics of woven and knitted interlinings in the transverse direction are higher by 20–75% compared to the longitudinal direction. When analyzing the tension curves up to 20% of elongation, we can see that the breaking character of the systems is very similar. The second and the third breaking points appear after the first, and they are higher. The first peak point is related with the breaking of basic material M, while the second is related with the breaking of the interlining material, and the third peak concurs with the breaking of the last threads.

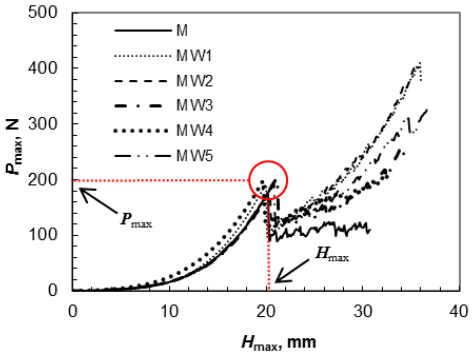

Fig. 3.23. Punching curves of non-tensioned base fabric M and its fused two-layer systems

During the second stage of investigation, the punching behavior of non-tensioned two-layer systems was analyzed. Figure 3.23 shows that there is no significant difference in the behavior of all the investigated systems up to the first breaking point. Punching height H_{max} varied from 0.99% to 4.55%, while punching force P_{max}, N increased from 3.28% to 17.15% with respect to the punching strength and height of base fabric M. These results confirm the remarks made by (Kovacevic, Ujevic, & Brnada, 2010) that the fabric which has the highest bursting strength also has the lowest anisotropy. In our case, the anisotropy coefficients of all the fused systems are very close, thus their bursting strengths are very close as well. Twill 2/2 weave is characterized as having the equal length of yarn floats along the warp and weft directions, which creates a homogeneous structure leading to a higher fabric elasticity in the case of bagging deformation (Doustar, Shaikhzadeh, & Maroufi, 2010). The twill 2/2 structure deforms easier and recovers from bagging deformation faster than the other weave types (Doustar, Shaikhzadeh, & Maroufi, 2010). Attention can be pointed to system MW4 with knitted interlining and system MW1 with woven interlining punching heights H_{max}, mm of which are lower compared to the other fused systems. The same phenomenon was observed for uniaxial breaking in both directions (Fig. 3.22). The results of the uniaxial and biaxial tension of base fabric M and its systems formed with woven, knitted and non-woven interlinings allow summarizing that the behavior of two-layer fused systems in both types of tension up to the first breaking point becomes very close even though the interlinings of a different structure were used. Significant differences appear in the further process because the second breaking point reveals that the variation of the second breaking results becomes very wide.

The punching properties (punching force P_{max}, N and punching height H_{max}, mm) of the fused systems vary unevenly in terms of the changing pre-tension level (Fig. 3.24). There is no main tendency applicable to all the investigated systems pre-tensioned in the longitudinal direction. Individual cases are specific to basic material M and the fused system with knitted interlining MW4 whose punching force P_{max} and punching height H_{max} decrease when pre-tensioned from 0.0% to 1.2% and increase when pre-tensioned from 1.2% to 2.1%. Fused system MW2 with the woven interlining decreases with the increase of the pre-tension level, but due to the

value of the relative error it can be stated that the punching properties vary within the range of errors with the increase of the pre-tension level. It means that the pre-tension level does not influence the punching properties for fused system MW2 with the woven interlining in the longitudinal direction. To the contrary, systems MW1, MW3 and MW5 increase with the pre-tension level increase (Fig. 3.24). In general, the punching properties of fused systems of different structures vary unevenly with the increase of the pre-tension level in the longitudinal direction.

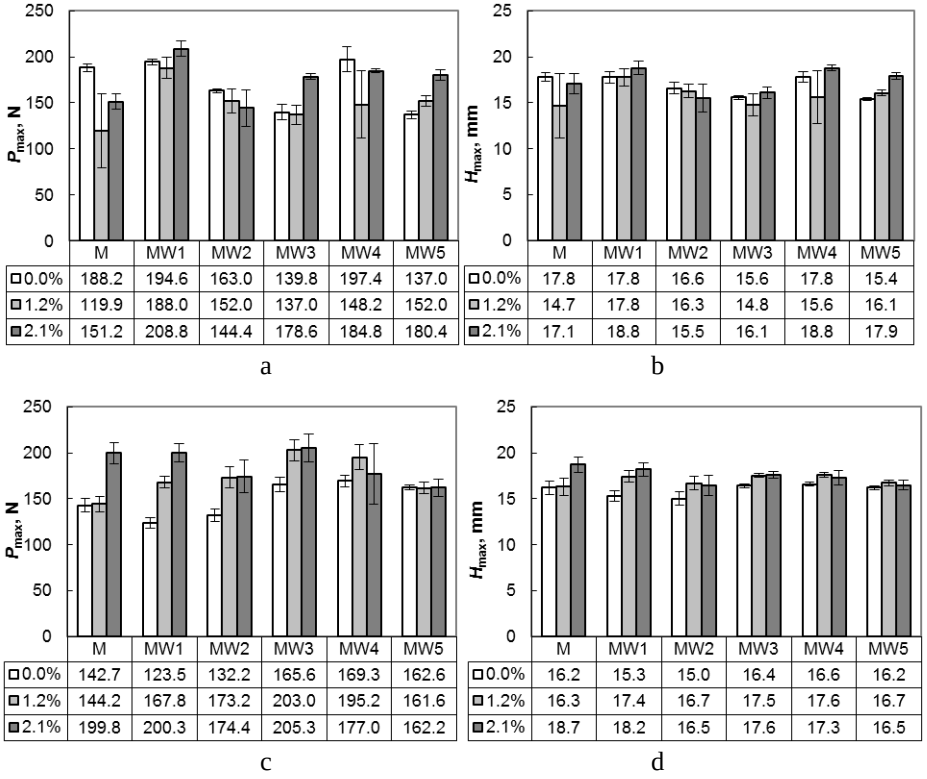

a

	M	MW1	MW2	MW3	MW4	MW5
0.0%	188.2	194.6	163.0	139.8	197.4	137.0
1.2%	119.9	188.0	152.0	137.0	148.2	152.0
2.1%	151.2	208.8	144.4	178.6	184.8	180.4

b

	M	MW1	MW2	MW3	MW4	MW5
0.0%	17.8	17.8	16.6	15.6	17.8	15.4
1.2%	14.7	17.8	16.3	14.8	15.6	16.1
2.1%	17.1	18.8	15.5	16.1	18.8	17.9

c

	M	MW1	MW2	MW3	MW4	MW5
0.0%	142.7	123.5	132.2	165.6	169.3	162.6
1.2%	144.2	167.8	173.2	203.0	195.2	161.6
2.1%	199.8	200.3	174.4	205.3	177.0	162.2

d

	M	MW1	MW2	MW3	MW4	MW5
0.0%	16.2	15.3	15.0	16.4	16.6	16.2
1.2%	16.3	17.4	16.7	17.5	17.6	16.7
2.1%	18.7	18.2	16.5	17.6	17.3	16.5

Fig. 3.24. Histograms of biaxial punching *P-H* for fused systems and basic material M pre-tensioned by 0.0%, 1.2% and 2.1% in the longitudinal (a, b) and transverse directions (c, d)

During the third stage of the investigations, punching characteristics of fused two-layer systems were analyzed by taking into account the initial pre-tension level of the samples: 0.0%, 1.2% and 2.1% in the longitudinal direction (all the punched specimens are presented in Appendix 3, Fig. A3.1). The first level of pre-tension (1.2%) showed evident differences compared to the biaxial deformation of unstrained specimens because the breaking force and breaking deformation became higher in the transverse direction. It was of interest to observe that for the systems with woven interlinings which were pre-tensioned by 2.1% and deformed with a punch, the third peak of the maximal force was observed during the breaking process. Meanwhile, the behavior of the other systems was different, and they did not exhibit such peaks.

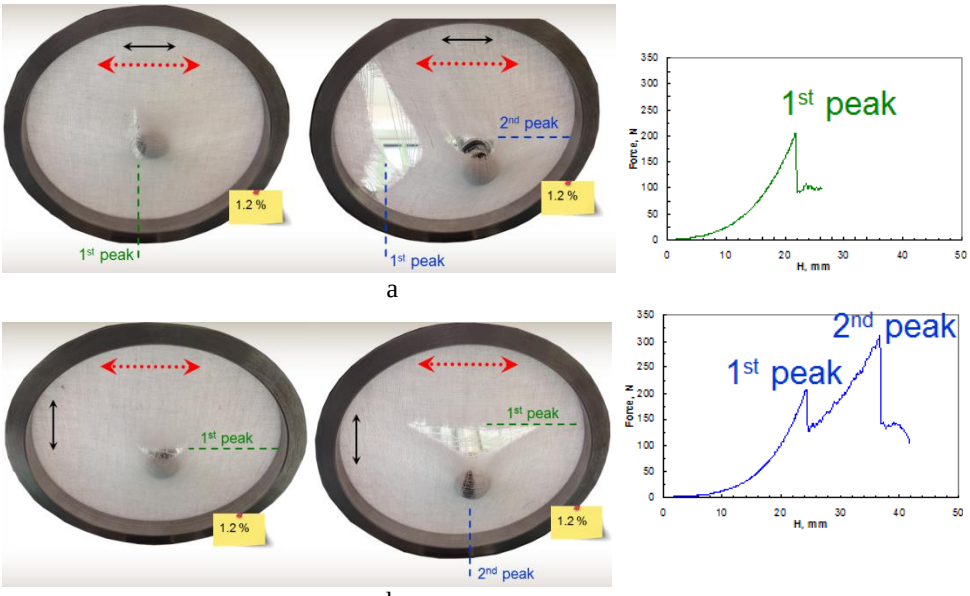

Figure 3.25. Biaxial tension for specimens pre-tensioned by 1.2% in the longitudinal (a) and transverse (b) directions where the black arrows indicate the direction of the specimen whereas the red dashed arrows indicate the pre-tension direction

It can be observed that in the longitudinal pre-tension, the threads of the stronger longitudinal direction break first, after which, the punching process does not stop due to the friction between the punch and the material (Fig. 3.25). Because of this, the punching load translocates onto the weaker and more deformable transverse direction, which becomes the main load-carrying direction (Fig. 3.26). Thus the second breaking takes place here. The most important role here is played by the friction between the specimen and the punch. Only because of that, the torn specimen does not slip from the surface of the punch, and the punching process proceeds.

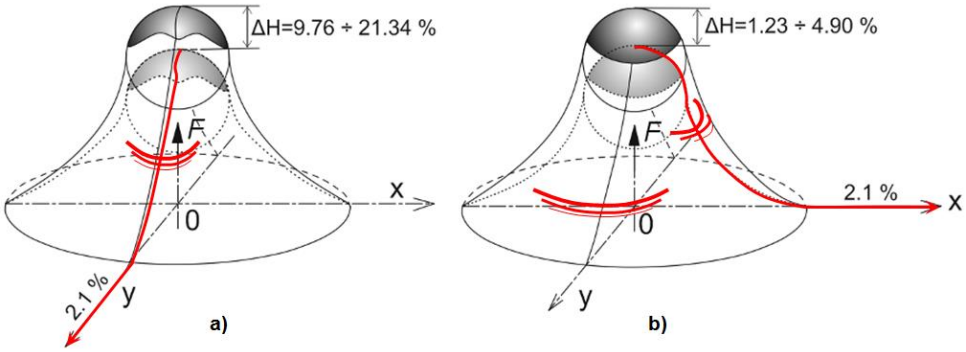

Figure 3.26. Biaxial punching of the specimen pre-tensioned by 2.1% in the longitudinal (a) and transverse (b) directions

While analyzing the breaking characteristics for the case of transverse pre-tension, it was of interest to observe that, irrespective of the pre-tension in the transverse direction, the first breaking manifested in the longitudinal direction in this case as well. The rest of the process was going as in the previously described case of the longitudinal pre-tension. It means that at low levels of pre-tension, e.g. 2.1%, it is possible to control the height of punching (deformation) but not to change the location of the critical stresses.

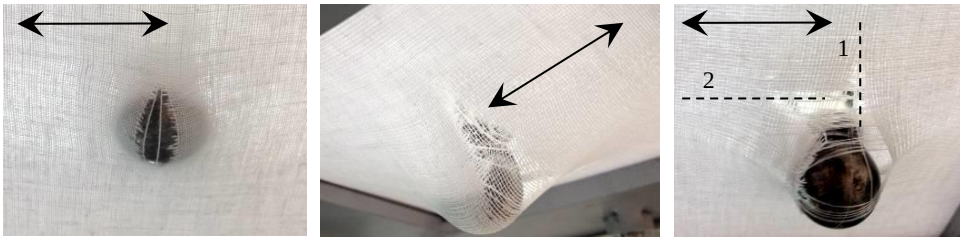

a b c

Figure 3.27. Typical crack propagation types in two-layer systems during biaxial deformation: a) the breaking type related to Peak I of the force/strain curve; b) the breaking type related to Peak II; c) the breaking type related to Peak III (1 – breaking of threads in the longitudinal direction; 2 – breaking of threads in the transverse direction)

The investigations of the punching strength parameters of a two-layer system show that the initial pre-tension of the tested samples affects the deformational behavior of the fused systems. System breaking character depends upon the location of the breaking crack (Fig. 3.27). Three types of breaking character can be distinguished:

1. Two layers of a fused system composed of a basic fabric and interlining are punched simultaneously, and the breaking crack orientates in one – the weaker one, i.e. the transverse – direction (Fig. 3.27, a). In this case, the treads of the stronger longitudinal direction break. It is common for single fabric M and two-layer system MW3 with non-woven interlining;
2. The most frequent is the case when the first crack appears in basic cotton fabric M and is followed by interlining breaking (Fig. 3.27, b). This mostly occurs in the systems with woven and knitted interlinings (Fig. 3.26), whose tension curves usually have two peaks of maximal forces. The first peak is related to the basic fabric breaking, while the second is connected to the interlining breaking;
3. The third case is obtained (Fig. 3.27, c) when basic fabric M breaks in one direction (the first peak); after that, the break occurs in the second perpendicular direction (the second peak), and only after that, the interlining breaks (the third peak). This typically happens in system MW1 with woven interlining (Fig. 3.28, b).

Further analysis was performed for the basic material and its system with each type of interlining (woven, knitted and non-woven) separately (Fig. 3.28). For all the cases of single fabrics M uniaxial pre-tension, the crack during the punching process firstly appeared in the transverse direction, i.e. warp threads were broken. When pre-tension was increased in the longitudinal direction, the maximal punching force and

height decreased by 19.7–36.3% and 3.9–17.4%, respectively. The effect of pre-tension in the transverse direction was only seen for the value of 2.1% pre-tension. In this case, the maximal punching force and height were higher by 28.6% and 13.4% compared to the relevant characteristics of the non-tensioned specimen. The same trends of crack propagation were observed for the system with non-woven fabric MW3.

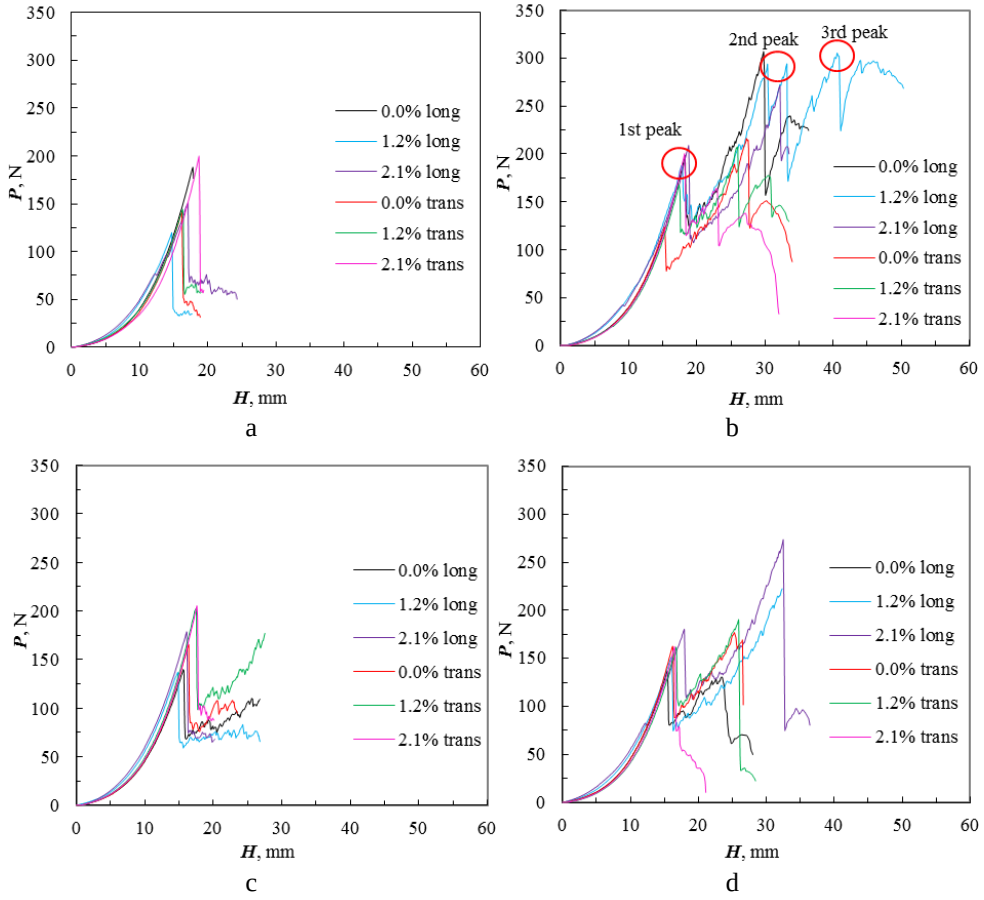

Figure 3.28. Breaking curves of biaxial tension for specimens pre-tensioned in the longitudinal and transverse directions by 0.0%, 1.2% and 2.1% for the investigated base fabric M (a) and its systems: MW1 (b), MW3 (c), MW5 (d)

A different character of force/strain curves commonly occurs in two-layer systems with woven and knitted components. Systems with knitted interlining, e.g. MW5, may have two (Fig. 3.28, d), while systems with woven interlinings, e.g. MW1, may have even three peaks of the maximal force (Fig. 3.28, b). Also, the final peak is often higher if compared to the first. This can be explained by the fact that, at first, warp threads of base cotton fabrics are broken. After that, first cracks appear in

interlining, and the highest force – the third peak of maximal force – is needed to break separate threads of interlining.

The obtained results of biaxial punching for certain systems (i.e. woven systems MW1 and MW2) immediately after the punching showed evident residual deformations which are located in the areas where materials experience the highest deformations, and thus puckering appears (Appendix 3, Fig. A3.1). Comprehensive analysis can be done in the future with the objective to evaluate the deformability of the material after detecting the accurate duration of particular time intervals.

The effect of fusing materials structure upon the variations of flexible multilayer system spatial shape. Chapter summary. The breaking behavior of woven, knitted and non-woven interlinings largely differs. Also, different effects upon the deformational behavior of base fabric M are evident. In general, fabric M, when fused with certain interlining, becomes stronger during uniaxial tension by 25.7–41.6% in the longitudinal direction and by 6.1–26.7% in the transverse direction. Also, it becomes more deformable, specifically, by 13.6–20.0% in the longitudinal and by 1.1–18.4% in the transverse direction. The results of the investigations showed that the initial uniaxial pre-tension in the two main directions exerts a significant effect upon the spatial deformational behavior and strength parameters of fused two-layer systems. Fusing interlinings of different structures have different effects upon the total breaking process of fused systems which may have one, two or even three peaks of the maximal force. The systems of the latter type are those with woven interlinings and are the strongest during biaxial deformation. Similar effects are exhibited by knitted interlinings.

3.5. Analysis of the Pre-Tension Level upon the Biaxial Behavior of Fused Systems

In our previous investigations (Chapter 3.4), the specimens were fixed in a square shaped frame (Fig. 2.12) when seeking to define the effect of different pre-tension levels, i.e. 0.0%, 1.2% and 2.1%. According to other researches (Chen, McGregor, Harper, Endruweit, & Warrior, 2016) or (Nishi & Hirashima, 2013), it is evident that the stress concentration distributes unevenly in such a square-shaped frame. Additional experiments have to be conducted with a round-shaped frame in order to avoid additional stresses which appear in the corners of a square-shaped frame during the punching process. The results of the experiments with a differently shaped frame were obtained by using the same fused systems and compared with each other (Fig. 3.29). It is evident that biaxial punching properties depend on the different shape of the frame.

Fig. 3.29 shows that biaxial punching forces for fused system MW1 in the longitudinal direction vary insignificantly with the different initial pre-tension levels while the shape of the frame makes essential difference for the punching heights: when using a square-shaped frame, the initial pre-tension level does not affect the results of biaxial punching height H_{max}, while the use of the round-shaped frame leads to a decrease of the results of biaxial punching height with the increase of the initial pre-tension level.

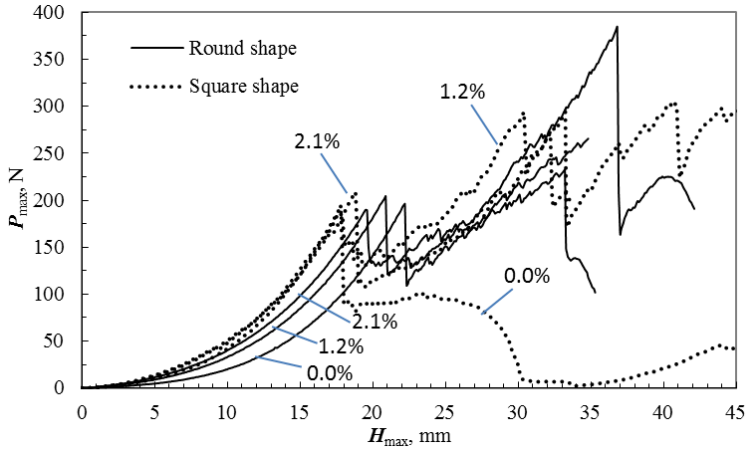

	H_{max}, mm			P_{max}, N		
	0.0 %	1.2 %	2.1 %	0.0 %	1.2 %	2.1 %
Round shape	22.04	20.76	19.45	193.0	200.8	188.8
Square shape	17.63	17.76	18.64	188.6	188.0	204.4

Fig. 3.29. Biaxial punching curves obtained when using a different shape of frame pre-tensioned by 0.0%, 1.2% and by 2.1%

During the next stage of investigation, the effect of the pre-tension direction and its level upon punching strength P_{max} and punching height H_{max} of the tested two-layer samples was analyzed by using a flat circular (round) shape frame. In the case of longitudinal pre-tension, punching height H_{max} of the first breaking point decreased from 10.29% to 21.50% when pre-tension was increased from 0.0% up to 2.1% (Fig. 3.30).

Different results were obtained for pre-tension in the transverse direction. The main difference is that the decrease of the punching height during breaking is not as high as in the case of the longitudinal pre-tension – it changed from 3.75% to 13.17%. Coefficient of variation v of the biaxial punching process for investigated basic material M and fused systems MW1–MW5 pre-tensioned by 0.0%, 1.2% and 2.1% when using a flat circular (round) shape frame in the longitudinal and transverse directions did not exceed 8.2%.

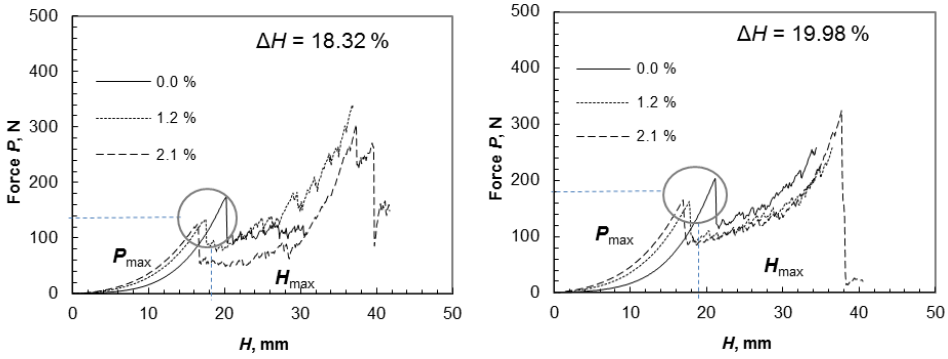

a b

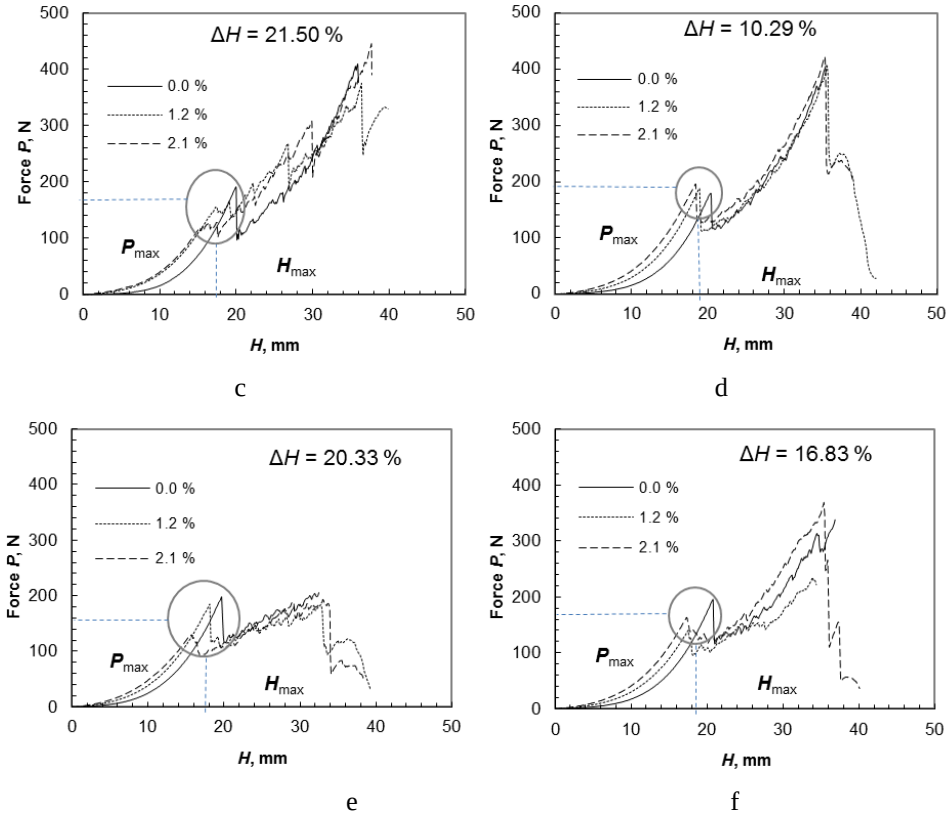

Fig. 3.30. Punching curves of 0.0%, 1.2% and 2.1% pre-tensioned samples in the longitudinal direction for base fabric M (a) and its systems: MW3 (b), MW1 (c), MW2 (d), MW4 (e), MW5 (f), where ΔH describes the change of punching height H_{max} of the first break between non-tensioned and pre-tensioned samples

The effect of initial pre-tension becomes evident when the difference between the tested systems deformability in the longitudinal and transverse directions is compared (Fig. 3.31). Punching height H_{max} of the first break of base material M and of all its fused systems decreases when the initial pre-tension is increased from 0.0% to 2.1% in the longitudinal direction (Fig. 3.31, a). The variation coefficient of all the fusing interlinings and their systems did not exceed 5.87%, except for W2 and W4 interlinings which varied within the limits of 8.06%–23.97%.

It can be seen that the deformability of MW2 system fused with woven interlining W2 is the lowest because its punching height H_{max} at all the levels of pre-tension starting with 0.0% and ending at 2.1% changes only by 10.29%. It can be explained by the fact that the strength properties of this system in uniaxial tension are also the highest among the tested ones (Table 3.10). Meanwhile, in the transverse pre-tension, only the behavior of base material M can be distinguished. For fused two-layer systems, the effect of pre-tension is insignificant and is smaller if compared to all the longitudinal pre-tension levels by 39% (Fig. 3.31, b). The

effect of the initial pre-tension level upon deformability of each tested fused system and base material M is illustrated in Figure 3.31. The last step of analysis was to define the dependence between the level of initial pre-tension and the total deformability of all the investigated fused systems. For this purpose, complex criterion *S* of total deformability was used (2.26).

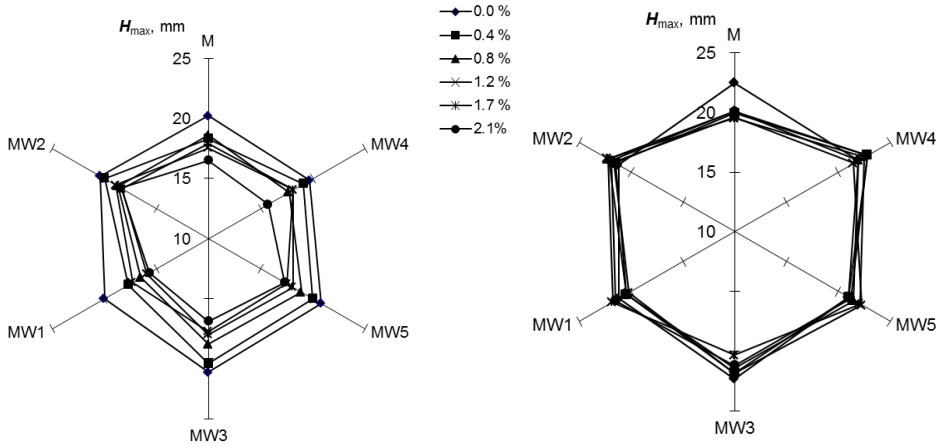

Fig. 3.31. The effect of initial pre-tension upon the changes of punching height H_{max} (mm) in the longitudinal (a) and transverse (b) directions

Figure 3.32 (a) shows the dependencies between the criterion of total deformability S_1 which was defined on the basis of the changes of punching height H_{max} and the levels of initial pre-tension in the longitudinal and transverse directions.

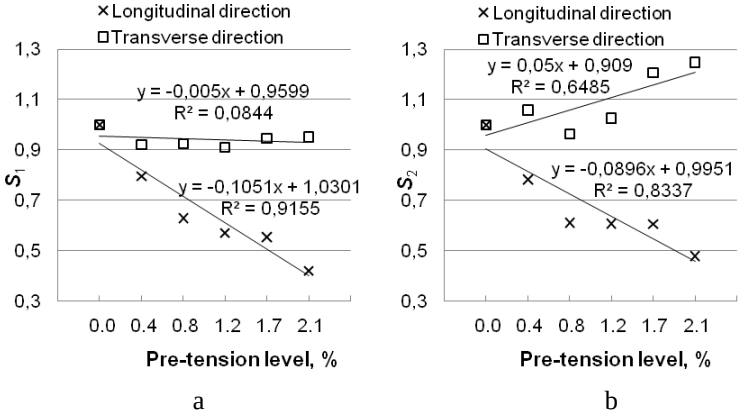

Fig. 3.32. The changes of total deformability criterion S_1 (a) and total strength criterion S_2 (b) in respect to the levels of initial pre-tensions in the longitudinal and transverse directions

Figure 3.32 (b) illustrates the same dependencies of total strength criterion S_2 which was defined on the basis of the changes of punching force P_{max}. It is evident

that the most significant effect of pre-tension is experienced in the longitudinal direction. The decrease of the tested systems deformability can be described as linear dependence (R^2 = 0.834÷0.916). Different results are obtained for transverse pre-tension. It does not exert any effect on total deformability criterion S_1 (R^2 = 0.084). Meanwhile, total strength criterion S_2 slightly increases (R^2 = 0.649) with the increase of pre-tension from 0.0% up to 2.1%.

The investigations performed by other researchers showed that there is no significant difference between uniaxial and biaxial deformations of woven, non-woven and knitted systems (Kovacevic, Ujevic, & Brnada, 2010). Meanwhile, the novelty of this work is the investigation of the pre-tension effect of differently composed systems which revealed the difference between the pre-tension direction, e.g. when the initial pre-tension was increased from 0.0% to 2.1% breaking height H_{max} decreased by 47.88% in the longitudinal direction and by 28.51% in the transverse direction.

Analysis of the pre-tension level upon the biaxial behavior. Chapter summary. A method to evaluate the effect of the pre-tension direction and level upon the biaxial behavior of two-layer materials was developed. After fusing the uniaxial behavior of two-layer systems up till the first break became very close for the investigated materials (F_{max} varied between 21.39% and 21.91%, ε_{max} varied between 7.27% and 17.53%), even though fusing interlinings of different structure (woven, non-woven and knitted) and characteristics were used. The same can be said about the biaxial punching of the same two-layer systems whose behavior became even closer (P_{max} varied between 3.28% and 17.15%, H_{max} varied between 0.99% and 4.55%). Breaking height H_{max} of the two-layer textile system decreased by 47.88% when the initial pre-tension was increased from 0.0% to 2.1% in the longitudinal direction. Meanwhile, this decrease measured 28.51% when the same initial pre-tension was applied in the transverse direction. What concerns the breaking character of two-layer systems, it was observed that for fusing interlinings which had several breaking maximums in uniaxial tension, the same trend remained in their fused systems uniaxial tension even though the base material of the fused system had only one very evident and prominent breaking point. Moreover, the same tendency becomes evident in the process of biaxial loading, e.g. punching.

3.6. The Effect of Friction in the Punch-to-Specimen Contact Zone upon Punching Behavior

During the investigation, punching was performed from both sides of the specimens thus referring to the fact that the products made of synthetic leather, e.g. upholstery furniture, car seats, etc. experience external normal loading from both sides during production and, especially, during their performance and utilization. Figure 3.33 presents typical punching curves *P/H* (punching force/punching height) of synthetic leathers L5 and L6 when punched from both sides with r_1, r_2 and r_3 punches without the application of any lubricant. It was obtained that maximal punching force P_{max} depends upon punch radius r_1, r_2, r_3 (Fig. 3.35).

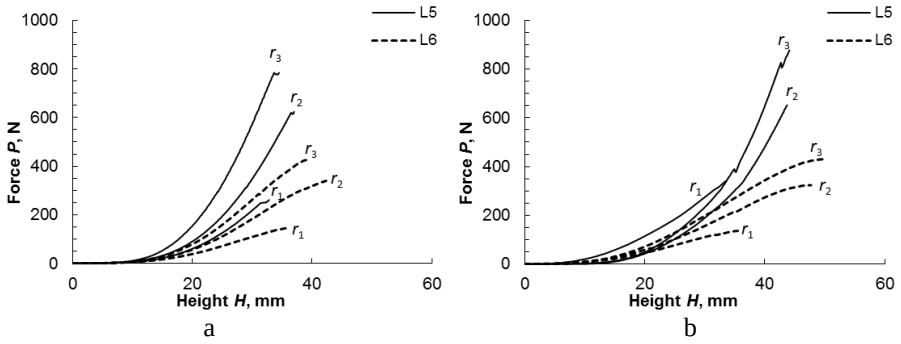

Fig. 3.33. Punching curves of synthetic leathers L5 and L6 when punched with r_1, r_2 and r_3 punches without application of lubricants from face vinyl side (a) and reverse textile side (b)

These results confirm the tendencies obtained by other researches (Zhang, Sahraei, & Wang, 2016), whose investigations were performed with PE, three-layer, ceramic-coated and non-woven materials. Also, the obtained results confirm the same relationships obtained for knitted materials (Strazdiene, Gutauskas, Papreckiene, & Williams, 1997), which showed that punching strength characteristics were dependent upon the size of the punch, i.e. punching force P_{max} increased whereas punching height H_{max} decreased with the increase of ratio *r/R*. In the work of (Strazdiene, Gutauskas, Papreckiene, & Williams, 1997), the decision was made to apply universal ratio *r/R* for comparative analysis of the effect of the punch-to-material contact area. From this standpoint, all the three investigations (including the current research) confirm the same trend of P_{max} in respect to ratio *r/R*. In the current research, P_{max} increased on average by 2.72 times for non-perforated leather L5 and on average 2.90 times for perforated leather L6 when the punch radius increased from r_1 = 9.0 mm (r_1/R = 0.15) to r_3 = 31.0 mm (r_3/R = 0.52), (Fig. 3.34).

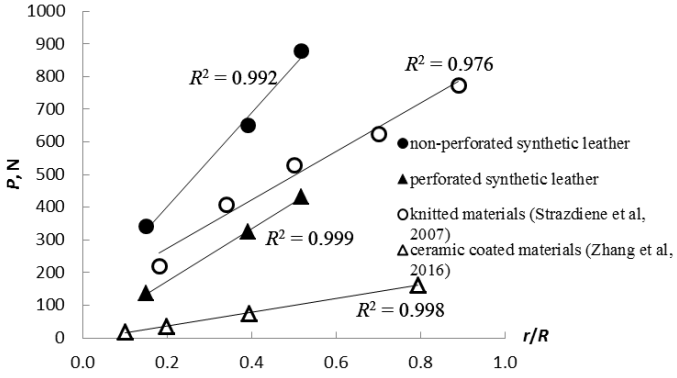

Fig. 3.34. The dependencies of maximal punching forces P_{max} upon ratio *r/R* for knitted materials (Strazdiene, Gutauskas, Papreckiene, & Williams, 1997), ceramic-coated materials (Zhang, Sahraei, & Wang, 2016) and non-perforated and perforated synthetic leathers (current research)

Comparative analysis of the obtained results showed that synthetic leather L5 is nearly twice as strong but less deformable compared to perforated leather L6 due to the increased stress concentration undergone by round perforated holes (Fig. 3.33 and Fig. 3.35).

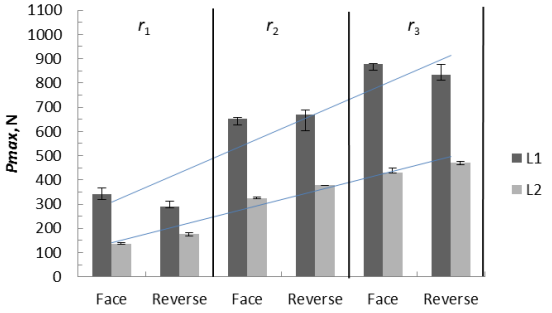

Fig. 3.35. The effect of the punch size upon maximal punching force P_{max} for synthetic leathers L5 and L6 when punched from the face (vinyl) side and the reverse (textile) side without application of lubricants

The differences between the maximal punching forces of L5 when punched with r_1, r_2 and r_3 punches from the reverse and face sides were negligible and varied within the limits of the standard error. Meanwhile, the same differences for perforated leather L6 were more evident. P_{max}, when punched form the reverse textile side, was higher by 8.4%–23.2% compared to the face side (Fig. 3.35). It should be noted that no evident trends were estrablished for punching heights H_{max} of non-perforated L5 and perforated L6 leathers.

In order to analyze the effect of friction in the contact zone, punch-to-leather upon the punching strength characteristics, four different lubricants L_A, L_B, L_C and L_D were applied. The punching results after their application are presented in Figures 3.36 and 3.37 (coefficient of variation v of the punching results for investigated leathers L5 and L6 using different lubricants did not exceed 9.19%). These results confirm the same linear dependencies between maximal punching strength P_{max} and radius r/R: for L_A lubricant R^2 = 0.996–1.000; for L_B lubricant R^2 = 0.981–1.000; for lubricant L_C R^2 = 0.977–0.999 and for lubricant L_D R^2 = 0.979–1.000. For all the four types of lubricants, non-perforated leather L5 was nearly twice as strong if compared to perforated leather L6, and P_{max} was higher when punched from the reverse textile side on average by 8.4%–36.3% compared to the face vinyl side (Fig. 3.36).

It must be noted that for all four L_A, L_B, L_C and L_D lubricants, similar tendencies were detected in respect to maximal punching height H_{max}, differently from the case when no lubricant was applied. The average values of maximal deformation H_{max} are higher for perforated leather L6 compared to L5 by 6.3%–20.65%, and they increase with the increase of the punch size. Especially, linear dependence between H_{max} and ratio r/R (R^2 = 0.883–0.935 for L6) is evident when leather samples are punched from the reverse textile side. Almost in all the cases, H_{max} was higher on average by 4.6%–17.7% when punched from the reverse side than from the face side (Fig. 3.37).

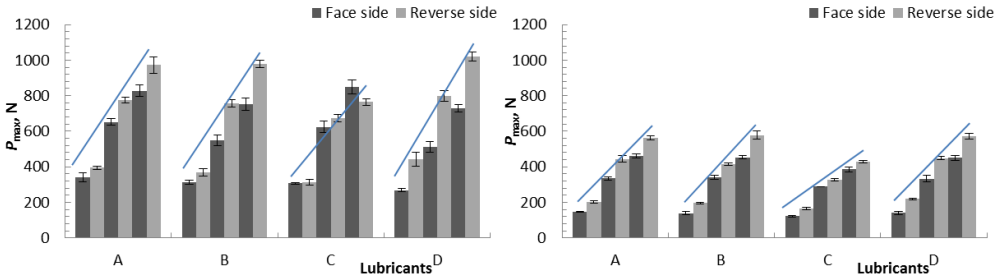

a b

Fig. 3.36. Maximal punching force P_{max} of synthetic leathers L5 (a) and L6 (b) when punched from the face and reverse sides with punches r_1, r_2 and r_3 after the application of L_A, L_B, L_C and L_D lubricants

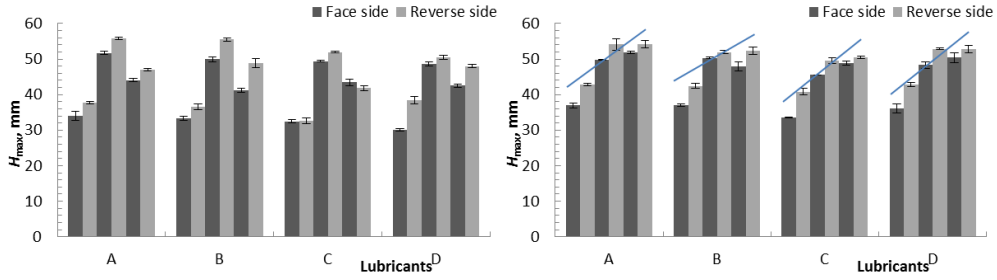

a b

Fig. 3.37. Maximal punching height H_{max} of synthetic leathers L5 (a) and L6 (b) when punched from the face and reverse sides with punches r_1, r_2 and r_3 after the application of L_A, L_B, L_C and L_D lubricants

A comprehensive analysis of the effect of the applied lubricants in respect to the punching characteristics of the samples without lubricants revealed that lubricant L_A (pure water) did not have any effect on maximal punching force P_{max} of non-perforated leather L5 when punched from the face side (Fig. 3.38 and Fig. 3.39). It varied within the limits of standard error, whilst it increased by 23% when punched from the reverse side, i.e. the textile background. Maximal punching force P_{max} of perforated leather L6 after the application of lubricant L_A slightly increased: from the face side on average by 6%; from the reverse side on average by 17%.

Lubricant L_B (cleaner *Smash* leather treatment *Arexons*) showed a more evident effect compared to pure water. It must be noted that P_{max} after the application of lubricant L_B from non-perforated leather L5 face (vinyl) side decreased on average by 13% but increased on average by 19% when the same lubricant was applied from the textile (reverse) side. Even more, these trends of the increase and decrease become more significant with the increase of the punch radius. In the case of perforated leather L6, P_{max} increased from both the face (4%) and reverse (14%) sides (Fig. 3.38 and Fig. 3.39). Pure silicone lubricant L_C decreased the strength of non-perforated leather L5 by 6% when punching from the face side but had almost no effect when punching from the reverse side. It also decreased the strength of perforated leather L6 by 11% when punching from the face side, and it

was the only lubricant which decreased (by 10.8%) the strength of perforated leather L6 from the reverse side. The most significant effect can be observed with lubricant L_D (commercial leather cleaner and conditioner *Turtle Wax Professional*). Maximal punching force P_{max} of non-perforated leather L5 when punching from the face side decreased by 20% and increased by 31% when punching from the textile (reverse) side. In the case of perforated L6 leather, it decreased by 3% and increased by 21%, respectively. Thus it is evident that lubricants L_A, L_B and L_D have a more significant effect upon P_{max} when they are applied from the textile (reverse) side in respect to the case when no lubricant was applied, i.e. P_{max} decreases when samples are punched from the vinyl side and increases when they are punched from the textile side. The punching behavior of the samples is different when pure silicone is applied – P_{max} slightly decreases in all the cases.

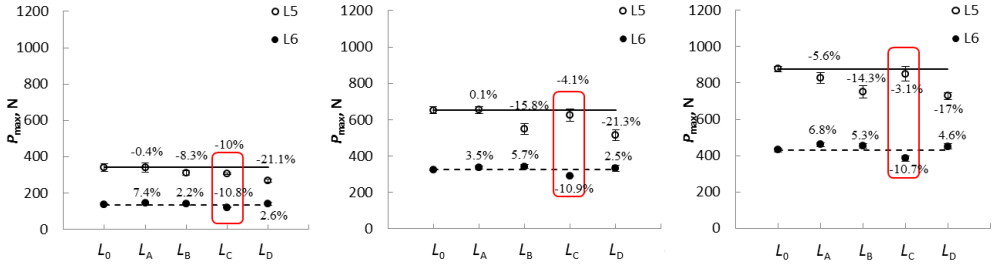

Fig. 3.38. Maximal punching force P_{max} of synthetic leathers L5 and L6 when punched from the face side with punches r_1 (a), r_2 (b) and r_3 (c) after the application of L_A, L_B, L_C and L_D lubricants

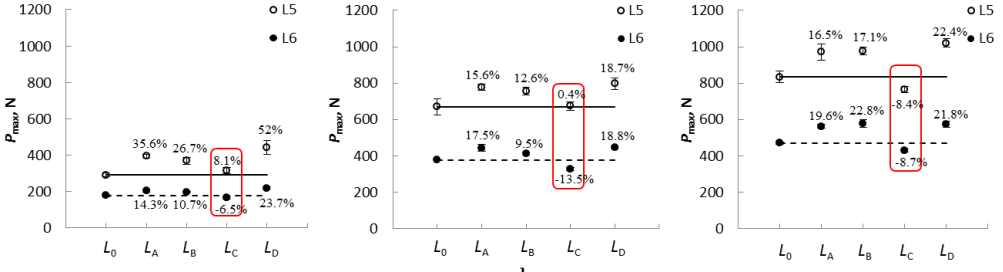

Fig. 3.39. Maximal punching force P_{max} of synthetic leathers L5 and L6 when punched from the reverse side with punches r_1 (a), r_2 (b) and r_3 (c) after the application of L_A, L_B, L_C and L_D lubricants

The obtained results confirm the findings of (Strazdiene, Daukantiene, & Gutauskas, 2001) that the use of different lubricants punching force P and height H for non-perforated synthetic leather L5 when punching from the vinyl side is lower compared to the specimens without the application of lubricants. Meanwhile, the punching characteristics of the lubricated specimens when punching from the reverse (textile) side are higher than the ones without lubrication. This investigation also supplements the findings of (Strazdiene, Daukantiene, & Gutauskas, 2001) of perforated leather when punching from the face and reverse sides with punches r_1,

r_2, r_3 after the application of L_A, L_B and L_D lubricants, punching force P and height H are higher in all the cases compared to the specimens without lubricant application. The only exception is silicone lubricant L_C which decreases the punching characteristics.

Table 3.11. Friction characteristics of non-perforated L5 and perforated L6 synthetic leathers

Material	Direction	Face side				Reverse side			
		F_S	μ_S	F_D	μ_D	F_S	μ_S	F_D	μ_D
without lubricant L_0									
L5	Long	1.79	0.91	1.26	0.65	0.44	0.23	0.47	0.24
	Trans	1.33	0.68	0.95	0.48	0.45	0.23	0.50	0.26
L6	Long	0.99	0.50	0.53	0.27	0.62	0.32	0.49	0.25
	Trans	1.36	0.69	1.00	0.51	0.50	0.26	0.40	0.20
lubricant L_A									
L5	Long	0.99	0.51	0.74	0.38	0.62	0.32	0.64	0.33
	Trans	1.02	0.52	0.84	0.43	0.70	0.36	0.78	0.40
L6	Long	0.90	0.46	0.70	0.36	0.59	0.30	0.63	0.32
	Trans	1.00	0.51	0.84	0.43	0.58	0.30	0.59	0.30
lubricant L_B									
L5	Long	1.02	0.52	0.92	0.47	0.50	0.25	0.54	0.28
	Trans	0.93	0.47	0.77	0.39	0.79	0.40	0.82	0.42
L6	Long	0.72	0.37	0.49	0.25	0.46	0.23	0.46	0.24
	Trans	0.79	0.40	0.61	0.31	0.66	0.34	0.68	0.35
lubricant L_C									
L5	Long	1.22	0.62	0.74	0.38	0.26	0.13	0.23	0.12
	Trans	1.20	0.61	0.57	0.29	0.66	0.34	0.67	0.34
L6	Long	0.90	0.46	0.57	0.29	0.37	0.19	0.33	0.17
	Trans	0.55	0.28	0.48	0.25	0.43	0.22	0.35	0.18
lubricant L_D									
L5	Long	1.15	0.59	0.58	0.30	0.38	0.20	0.42	0.22
	Trans	1.19	0.61	0.55	0.28	0.51	0.26	0.51	0.26
L6	Long	0.85	0.43	0.52	0.27	0.41	0.21	0.41	0.21
	Trans	0.86	0.44	0.27	0.24	0.51	0.26	0.49	0.25

It can be seen that all the four lubricants show a different effect upon the punching behavior of investigated leathers L5 and L6 from the face vinyl side as well as from the reverse textile side. Thus the effect of friction in the punch-to-specimen contact zone was investigated during the next research stage. The results of static F_S and dynamic F_D friction forces as well as static μ_S and dynamic μ_D friction coefficients are presented in Table 3.11 (coefficient of variation v of friction did not exceed 5.54%). It can be seen that the static friction parameters compared to the dynamic parameters are evidently higher from the face (vinyl) side. In certain cases, this difference reaches as high as 68.6%. However, from the reverse (textile) side, the friction process is smoother, and this difference does not exist or varies within the limits of standard errors.

The differences of friction parameters between L5 and L6 leathers were analyzed from two standpoints: (1) in respect to the longitudinal and transverse directions and (2) in respect to the face and reverse sides. In all the cases of applying lubricants, friction characteristics from the face side of non-perforated leather L5 were higher compared to perforated leather L6. Here, the case without lubricant can be exceptional, because the difference in the longitudinal direction was very significant, i.e. 44.7%–58.5% compared to the remaining cases. Meanwhile, the difference in the transverse direction became the opposite as the friction parameters of perforated leather L6 became higher on average by 1.5%–6.3%. The friction characteristics from the reverse side maintain the same trends for all the lubricants although the difference between L5 and L6 leathers is a bit lower, except for the cases when no lubricant or industrial silicone – L_C lubricant – is applied. The friction characteristics of L6 leather's reverse side in opposition to the values of the face side in the longitudinal direction were higher even by 41.0% and 46.2%, respectively. An assumption can be made that the four applied lubricants L_A, L_B, L_C and L_D make the values of static μ_S and dynamic μ_D friction coefficients lower (from the face side), e.g. by 27.69–53.85% in L5 leather's longitudinal direction and by 15.69–59.42% in L6 leather's transverse direction.

During the punching process, the part of the specimen which is in contact with the punch obtains its shape (Fig. 2.14). The remaining part of the specimen from the point where it loses its touch with the punch up to the clamp obtains the shape of a concaved curve. Earlier investigations have proved that the specimen tearing line is always located at the top of the formed shell, i.e. in the place where the specimen loses its touch with the punch (Strazdiene, Gutauskas, Papreckiene, & Williams, 1997) and found that it can extend along the whole perimeter (Fig. 3.40, a) or can be localized in one place (Fig. 3.40, b).

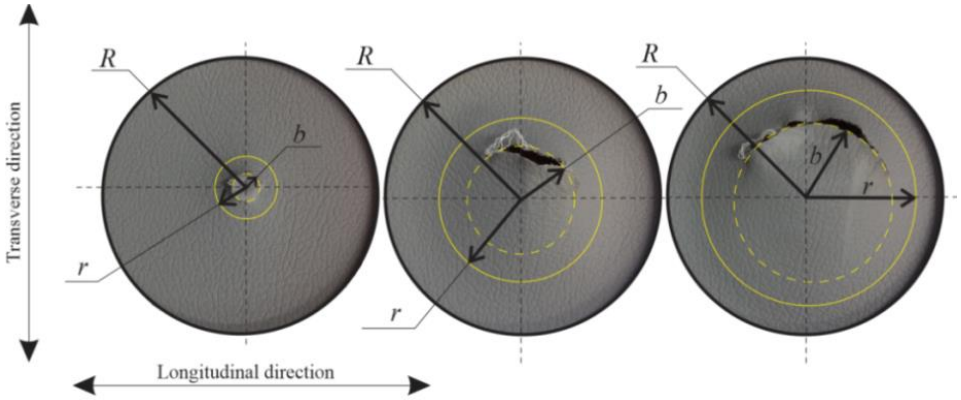

Figure 3.40. Examples of synthetic leather L5 tearing lines when punched from the face side with punches r_1 (a), r_2 (b) and r_3 (c)

The results obtained during the testing performed with non-perforated L5 and perforated L6 synthetic leathers did not contradict these findings (Fig. 3.40). On the one hand, the position of the tearing line depends on the fact whether the sample was

punched from the face (vinyl) or from the reverse (textile) side. On the other hand, it depends on the size of the punch, i.e. the bigger was the punch in use, the further from the centre the tearing line was located and the bigger was the area *S*, mm^2 of the punch-to-leather contact zone during tearing. In most of the cases, the tearing line is perpendicular to the transverse direction of the tested specimens (Strazdiene, Gutauskas, Papreckiene, & Williams, 1997).

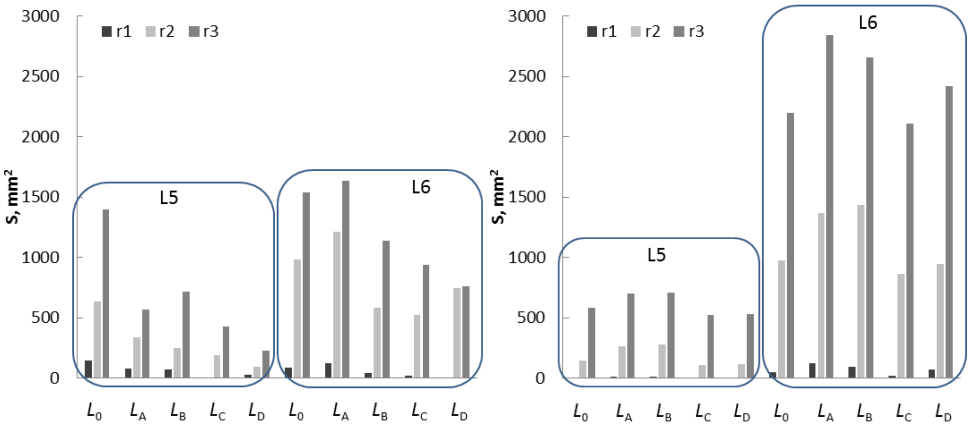

Figure 3.41. Areas S of punch-to-leather contact zones during the tearing of non-perforated L5 and perforated L6 leathers when punching with punches r_1, r_2 and r_3 without any lubricant (L_0) and with all the lubricants (L_A – L_D) from the face (a) and the reverse (b) sides

Areas *S* of the punch-to-leather contact during the tearing were defined according to the scheme presented in Figure 2.14. The results of the calculations are presented in Figure 3.41. It can be seen that bigger contact areas *S* during the tearing occur in perforated leather L6 for all the types of lubricants when punched both from the face and the reverse sides. A comparison of the face and the reverse sides shows that bigger areas belong to the reverse (textile) side; it is especially evident in the case of perforated leather L6. The effect of L_A, L_B, L_C and L_D lubricants was more evident when they were applied from the face (vinyl) side (Fig. 3.41, a). After their application, areas *S* of the punch-to-leather contact zones during the tearing of L5 and L6 leathers decreased by 25.9–61.2% in the case of L_A and L_B lubricants and by 24.1–96.5% in the case of L_C and L_D lubricants. This trend was not observed when leather samples were punched from the reverse (textile) side as area *S* became bigger if compared to those cases when no lubricant was applied (Fig. 3.41, b).

The aim of this research is to define the effect of friction in the contact zone punch-to-material upon the character of tearing and the strength of non-perforated and perforated synthetic leathers under biaxial punching. Thus it was defined that for both – non-perforated L5 and perforated L6 – leathers, there is no difference in the dependencies between areas *S* and static μ_S and dynamic μ_D friction coefficients in longitudinal and transverse directions (Table 3.12). Meanwhile, clear difference exists between μ_S and μ_D coefficients. Determination coefficient R^2 of μ_D

dependence is higher, and for non-perforated leather L5, it varies within the limits of 0.65÷0.98, while for perforated leather L6 within the limits of 0.29÷0.87.

Table 3.12. The dependencies (determination coefficients R^2) between area S, mm^2 of the punch-to-leather contact during tearing, and static μ_S and dynamic μ_D friction coefficients in the longitudinal and transverse directions

Material code	Punch size	Longitudinal direction				Transverse direction			
		Face side		Reverse side		Face side		Reverse side	
		μ_S	μ_D	μ_S	μ_D	μ_S	μ_D	μ_S	μ_D
L5	r_1	0.40	0.78	0.70	0.68	0.03	0.91	0.50	0.71
	r_2	0.60	0.85	0.69	0.71	0.16	0.82	0.50	0.69
	r_3	0.63	0.98	0.72	0.73	0.13	0.74	0.44	0.65
L6	r_1	0.19	0.44	0.15	0.70	0.44	0.78	0.70	0.76
	r_2	0.28	0.51	0.10	0.51	0.53	0.60	0.90	0.87
	r_3	0.20	0.29	0.08	0.62	0.49	0.87	0.68	0.79

It must be noted that punching is a biaxial process during which friction acts simultaneously in both – longitudinal and transverse – directions. Taking this into account together with the research results of other investigators (Fontaine, Marsiquet, & Renner, 2006) or (Ezazshahabi, Latifi, & Tehran, 2015), a decision was made to use the averaged values of these coefficients in two main directions. The results of the dependencies (determination coefficients R^2) between area S of the punch-to-leather contact during tearing and the averaged values of static μ_{SA} and dynamic μ_{DA} friction coefficients are presented in Table 3.13.

Table 3.13. The dependencies (determination coefficients R^2) between area S, mm^2 of punch-to-leather contact during tearing and averaged values of static μ_{SA} and dynamic μ_{DA} friction coefficients

	L5				L6			
	Face side		Reverse side		Face side		Reverse side	
	μ_{SA}	μ_{DA}	μ_{SA}	μ_{DA}	μ_{SA}	μ_{DA}	μ_{SA}	μ_{DA}
r_1	0.25	0.92	0.94	0.97	0.45	0.94	0.54	0.94
r_2	0.45	0.93	0.94	0.98	0.56	0.79	0.55	0.90
r_3	0.45	0.97	0.91	0.96	0.49	0.94	0.43	0.92

These results confirm the obvious difference in the effect of static μ_{SA} and dynamic μ_{DA} friction coefficients. Determination coefficient R^2 of μ_{DA} dependence is significantly higher (Fig. 3.42). For non-perforated leather L5, it varies within the limits of 0.79÷0.98, while for perforated leather L6, it varies across the wider limits of 0.25÷0.94. It is important to mention that these dependencies are valid for individual punches r_1, r_2 and r_3. The same dependence among the research results of all the three punches is weaker: R^2 does not reach 0.50.

Further investigations have revealed that linear dependencies exist between maximal punching force P_{max} and punch-to-leather contact areas S during tearing (Fig. 3.43).

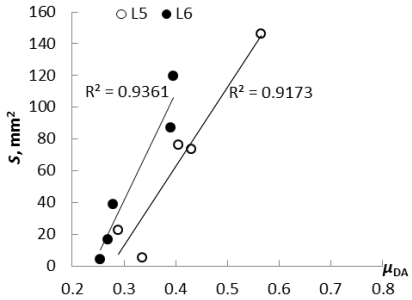

Figure 3.42. The dependencies between area S of the punch-to-leather contact zone during tearing and dynamic μ_{DA} friction coefficients of non-perforated L5 and perforated L6 synthetic leathers when they were punched with r_1 punch

In the case of non-perforated leather L5 for all the three punch sizes and both – face and reverse – sides, they are as follows: without lubricant (L_0), $R^2 = 0.615$, for lubricant L_A, $R^2 = 0.869$, for lubricant L_B, $R^2 = 0.772$, for lubricant L_C, $R^2 = 0.737$, and for lubricant L_D, $R^2 = 0.753$. In the case of perforated leather L6, these dependencies are even stronger: without lubricant (L_0), $R^2 = 0.919$, for lubricant L_A, $R^2 = 0.923$, for lubricant L_B, $R^2 = 0.891$, for lubricant L_C, $R^2 = 0.819$ and for lubricant L_D, $R^2 = 0.807$.

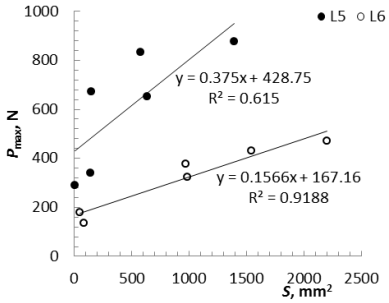

Figure 3.43. Dependencies between area S of the punch-to-leather contact zone during tearing and P_{max} when no lubricant was applied from the face and reverse sides of non-perforated L5 and perforated L6 synthetic leathers

The effect of friction in the punch-to-specimen contact zone upon punching behavior. Chapter summary. The results of our investigations have confirmed the dependence between maximal punching force P_{max} and radius r of the punch for non-perforated and perforated synthetic leathers. P_{max} increased on average by 2.72 times for non-perforated leather L5 and on average by 2.90 times for perforated leather L6 when the punch radius increased from $r_1 = 9.0$ mm ($r_1/R = 0.15$) to $r_3 = 31.0$ mm ($r_3/R = 0.52$). The same trend is observable in the cases when different levels of friction act in the punch-to-specimen contact zone or when the specimens are punched from the face (vinyl) or from the reverse (textiles) side. Comparative analysis has shown that non-perforated leather is nearly twice as strong but less deformable compared to perforated leather due to the increased stress

concentration around the perforated holes. The surfaces of synthetic leathers from the face and the reverse sides differ because they have a textile background coated with a vinyl layer. Thus the punching characteristics from both sides are different not only taking into account the size of the punch but also regarding the contact friction.

It was also detected that for non-perforated and perforated synthetic leathers, dependencies exist between area S of the punch-to-leather contact zone during the tearing, and that averaged static μ_{SA} and dynamic μ_{DA} friction coefficients, i.e. the tearing area, increase with the increase of friction. An especially strong relationship was obtained in the case of dynamic friction μ_{DA}. It must be noted that static friction parameters compared to dynamic friction are evidently higher from the face (vinyl) side. In certain cases, this difference reaches even 68.6%. However, from the reverse textile side, the friction process is smoother, and this difference does not exist – or else it varies within the limits of standard errors.

4. Conclusions

1. It is not reasonable to take into account only the strength properties of upholstery materials during furniture development because, during the exploitation of furniture, its materials are exposed to lower level external loads. Therefore, the deformation of these materials significantly differs from their behavior during breaking, i.e. in the cases of maximal loading. Our investigation has shown that standard strength parameters of furniture upholstery may even be opposite to the corresponding parameters at low level loading, e.g. deformation ε of knitted fabric K1 while getting extended up to the breaking point was 79.33%, whereas deformation *EMT* at low loads (25 N) was 6.56%, but the deformations of artificial leather L3 were the opposite: deformation ε was 39.60%, while deformation *EMT* was 21.33%.

2. The KES-F evaluation system, which was developed and approved for the investigation and evaluation of the properties of thin costume fabrics at low loads (25 N), is suitable for predicting the behavior of upholstery materials which are different in terms of structure and composition at exploitation level loads (100 N) because strong correlation between tensile deformation *EMT* (determined by KES-F) and sudden deformation ε_s (determined from the creep test) was found, specifically for synthetic leathers $R^2 = 0.95$, one-layer materials $R^2 = 0.83$, two-layer materials $R^2 = 0.90$, and for materials of complex weave $R^2 = 0.74$.

3. A relationship was established between the instantaneous rigidity modulus of the uniaxial tensile test and creep and relaxation deformations, which allows to predict the deformational behavior of furniture upholstery because its instantaneous rigidity modulus (E_m) at low loads (25 N and 100 N) shows a strong correlation ($R^2 = 0.64 \div 0.95$) with the general ε_G, sudden ε_s, reversible ε_R and residual ε_r deformations determined at the same loads.

4. A novel research method was developed in order to determine the influence of pre-tension upon the biaxial behavior of upholstery. It was defined that uniaxial

pre-tension in different directions has a significant effect upon the spatial behavior and strength properties of two-layer textile systems. Fusing interlinings which have different structures affect differently the overall bursting process of two-layer systems which are characterized by one, two or even three breaking peaks. A two-layer system with the woven interlining has three breaking peaks: the first breaking peak P_{1max} occurs at 188 N, deformation height H_{1max} is 17.8 mm; the second peak P_{2max} is observed at 294 N, H_{2max} is 30.4 mm; the third peak P_{3max} is visible at 304 N, H_{3max} is 40.7 mm. The strength of a two-layer system with knitted interlining is lower, and it has two breaking peaks: the first breaking peak P_{1max} is at 152 N, deformation height H_{1max} is 16.1 mm; the second peak P_{2max} is observed at 223 N, H_{2max} is 32.3 mm.

5. After fusing the uniaxial behavior of two-layer systems until the first break, it is very close for the investigated materials (F_{max} varies between 21.39% and 21.91%, ε_{max} varies between 7.27% and 17.53%) even though the fusing interlinings of different structures (woven, non-woven and knitted) and characteristics are used. The same can be said about biaxial punching of the same two-layer systems whose behavior becomes even closer (P_{max} varies between 3.28% and 17.15%, H_{max} varies between 0.99% and 4.55%). Breaking height H_{max} of a two-layer textile system decreases by 47.88% when the initial pre-tension is increased from 0.0% to 2.1% in the longitudinal direction. Meanwhile, this decrease becomes lower by 28.51% when the same initial pre-tension is applied in the transverse direction.

6. What concerns the breaking character of two-layer systems, it was observed that fusing interlinings which featured several breaking maximums in uniaxial tension maintained the same trend in their fused systems uniaxial tension even though the base material of the fused system had only one very prominent breaking point. Moreover, the same trend is evident in the process of biaxial loading, e.g. punching.

7. The results of our investigation have confirmed the dependence between maximal punching force P_{max} and radius r of the punch for non-perforated and perforated synthetic leathers. P_{max} increased on average by 2.72 times for non-perforated leather L5 and on average by 2.90 times for perforated leather L6 when the punch radius increased from r_1 = 9.0 mm (r_1/R = 0.15) to r_3 = 31.0 mm (r_3/R = 0.52). The same trend is also observed in the cases when different levels of friction act in the punch-to-specimen contact zone or when the specimens are punched from the face (vinyl) or from the reverse (textiles) side. Comparative analysis has demonstrated that non-perforated leather is nearly twice as strong but less deformable compared to perforated leather due to the increased stress concentration around the perforated holes. The surfaces of synthetic leathers from the face and reverse sides differ because they are made of a textile background coated with a vinyl layer. Thus the punching characteristics from both sides are different not only when taking into account the size of the punch but also in respect to contact friction.

8. For non-perforated and perforated synthetic leathers, dependencies exist between area S of the punch-to-leather contact zone during tearing and the averaged dynamic μ_{DA} friction coefficients, i.e. the tearing area increases with the increase of

friction. It must be noted that static friction parameters compared to the dynamic parameters are evidently higher from the face (vinyl) side. In certain cases, this difference reaches as high as 68.6%. However, from the reverse (textile) side, the friction process is smoother, and this difference does not exist or varies within the limits of standard errors.

5. References

1. ABBAS, A. (2017, January 23). *Guide to Upholstery Fibers: Characteristics of Plant Based, Animal, and Synthetic Fibers*. Retrieved April 10, 2017, from About.com Corporation The Spruce Web site: http://www.thespruce.com
2. ABID, K., DHOUIB, S., & SAKLI, F. (2011). Mechanical Modelling of Materials Coated with Nanocomposite. In: *Journal of the Textile Institute, Vol. 102, Issue 2*, 157–163.
3. AHMAD, F., CHOI, H.S., & PARK, M.K. (2015). A Review: Natural Fiber Composites Selection in View of Mechanical, Light Weight, and Economic Properties. In: *Macromolecular Materials and Engineering, Vol. 300, Issue 1*, 10–24.
4. AKGUN, M., BECERIR, B., ALPAY, H.R., KARAASLAN, S., & EKE, A. (2010). Investigation of the Effect of Yarn Locations on Color Properties of Polyester Automotive Upholstery Woven Fabrics after Abrasion. *Textile Research Journal, Vol. 80 (14)*, 1422–1431.
5. ANCUTIENE, K., & STRAZDIENE, E. (2010). Investigation of Fused Textile Systems Resilience Properties. *Scienticif Journal of Riga Technical University/Material Science and Applied Chemistry, Vol. 21*, 45-50.
6. ANCUTIENE, K., STRAZDIENE, E., & NESTEROVA, A. (2010). The Relationship Between Fabrics Bending Rigidity Parameters Defined bu KES-F and FAST Equipment. In: *Materials Science (Medžiagotyra), Vol. 16, No. 4*, 346–352.
7. APURBA, D., ABHIJIT, M., & SUKUMAR, R. (2016). Prediction of Fabric Hand Characteristics Using Extraction Principle. In: *Indian Journal of Fibre & Textile Research, Vol. 41*, 33–39.
8. *ARE Perforated Leather Seats Better*. (2014). Retrieved April 12, 2016, from Leather Seats and Trims. Prestige Sunroofs Web Site: http://prestigesunroofs.com.au
9. ARNALD, J. (2014, March 21). *About Corduroy Fabric, Corduroy Blazer Men*. Retrieved April 12, 2017, from LinkedIn Corporation: https://www.slideshare.net
10. ASAYESH, A., & JEDDI ALI, A.A. (2010). Modeling the Creep Behavior of Plain Woven Fabrics Constructed from Textured Polyester Yarn. in: *Textile Research Journal, Vol. 80, No. 7*, 642–650.
11. *AUTOMOTIVE Interior*. (2010–2016). Retrieved September 22, 2016, from Seiren Co. Ltd: http://www.seiren.com
12. *BACKING or Back Coatings*. (2017). Retrieved April 13, 2017, from Duralee: https://www.duralee.com
13. BAGHAEI, B., SHANBEH, M., & GHAREAGHAJI, A.A. (2010). Effect of Tensile Fatigue Cyclic Loads on Bagging Deformation of Elastic Woven Fabrics. In: *Indian Journal of Fibre & Textile Research, Vol. 35*, 298–302.

14. BAHADIR, S.K., KALAOGLU, F., JEVSNIK, S., ERYURUK, S.H., & SARICAM, C. (2015). Use of Artificial Neural Networks for Modelling the Drape Behaviour of Woolen Fabrics Treated with Dry Finishing Processes. In: *Fibers & Textiles in Eastern Europe, Vol. 23, No. 2 (110)*, 90–99.
15. *BALDINIAI audiniai ir jų klasifikavimas*. (2011). Retrieved April 10, 2017, from Audimpeksas, UAB website: http://www.audiniai.lt
16. BEKAMPIENE, P., DOMSKIENE, J., & SIRVAITIENE, A. (2011). The Effect of Pre-tension on Deformation Behaviour of Natural Fabrics Reinforced Composite. In: *Materials Science (Medžiagotyra), Vol. 17, No. 1*, 56–61.
17. BERTAUX, E., LEWANDOWSKI, M., & DERLER, S. (2007). Relationship between Friction and Tactile Properties for Woven and Knitted Fabrics. In: *Textile Research Journal, Vol. 77, Issue 6*, 387–396.
18. BILBAO, E.D., SOULAT, D., HIVET, G., LAUNAY, J., & GASSER, A. (2008). Bending Test of Composites Reinforcements. In: *International Journal Materials Forming*, 835–838.
19. BILISIK, K., & YOLACAN, G. (2009). Abrasion Properties of Upholstery Flocked Fabrics. In: *Textile Research Journal Vol.79 (17)*, 1625–1632.
20. BISHOP, D.P. (1996). Fabrics: Sensory and Mechanical Properties. In: *Textile Progress, Vol. 29, No. 3*, 62.
21. BRANKE, D., KASTNER, M., POHL, M., & ULBRICHT, V. (2014). Modeling of the Effective Viscoelastic Material Behavior of Textile Reinforced Composites Using a Multi-Scale Approach. In: *Proceedings in Applied Mathematics and Mechanics, Vol. 14*, 547–548.
22. BRIDGENS, B., GOSLING, P., JOU, G.T., & HSU, X.Y. (2012). Inter-Laboratory Comparison of Biaxial Tests for Architectural textiles. In: *The Journal of the Textile Institute, Vol 103, Issue 7*, 706–718.
23. CALIN, M.A., KHENOUSSI, N., SCHACHER, L., ADOLPHE, D., MANEA, L.R., GRADINARU, I., *et al*. (2013). Morphological and Broadband Dielectric Spectroscopy Approaches on PA6 – CNT Nanofibres. In: *Material Plastice, Vol. 50, No. 4*, 257–263.
24. CEVEN, E.K., & OZDEMIR, O. (2006). Evaluation of Chenille Yarn Abrasion Behavior with Abrasion Tests and Image Analysis. In: *Textile Research Journal, Vol.76 (4)*, 315–321.
25. CHEN, J., CHEN, W., & ZHANG, D. (2013). Experimental Study on Uniaxial and Biaxial Tensile Properties of Coated Fabric for Airship Envelopes. In: *Journal of Reinforced Plastics and Composites, Vol.33 (7)*, 630–647.
26. CHEN, S., MCGREGOR, O.L., HARPER, L.T., ENDRUWEIT, A., & WARRIOR, N.A. (2016). Defect Formation During Preforming of a Bi-Axial Non-Crimp Fabric with a Pillar Stitch Pattern. In: *Composites Part A: Applied Science and Manufacturing*, 91, ISSN 1359-835X, 156–167.
27. *CHENILLE Fabric*. (2017, April 8). Retrieved April 12, 2017, from The Wikimedia Foundation, Inc.: http://en.wikipedia.org
28. COSTA, S.M., AGUIAR, A., LUZ, S.M., PESSOA, A., & COSTA, S.A. (2015). Sugarcane Straw and Its Cellulosic Fraction as Raw Materials for Obtainment of Textile Fibers and Other Bioproducts. In: *Polysaccharides*, 513–533.

29. DAS, A., KOTHARI, V.K., KUMAR, A., & MEHTA, M.S. (2005). Study on Anisotropic Creep Behavior of Nonwoven Geotextiles. In: *Fibers and Polymers, Vol. 6, No. 4*, 313–317.
30. DAUKANTIENE, V., & GUTAUSKAS, M.V. (2001). The Influence of Specimen Geometry and Loacl Defects on Polyethylene Membrane Behaviour in Punch Deformation Process. In: *Polymer Testing 20*, 579–583.
31. DE BOOS, A., & TESTER, D. (1989). A System for Fabric Objective Measurement and Its Application in Fabric and Garment Manufacture. *Geelong: CSIRO Division of Wool Technology*, 42.
32. DEGIRMENCI, Z., & CELIK, N. (2013). The Effects of Selected Improving Methods on Wrinkle Resistance of Warp Knitted and Laminated Car Seat Cover Fabric. In: *Journal of Industrial Textiles, Vol.44 (2)*, 245–256.
33. DERLER, S., SCHRADE, U., & GERHARDT, L.C. (2007). Tribology of Human Skin and Mechanical Skin Equivalents in Contact with Textiles. In: *Wear 263*, 1112–1116.
34. *DIFFERENT Grades of Vinyl Upholstery Fabric*. (2016). Retrieved April 10, 2017, from Luxafoamnorth.com Corporation Web site: https://medium.com
35. DOBRICH, O., GEREKE, T., & CHERIF, C. (2016). Modeling the Mechanical Properties of Textile-Reinforced Composites With a Near Micro-Scale Approach. In: *Composite Structures, Vol. 135*, 1–7.
36. DOBRICH, O., GEREKE, T., CHERIF, C., & KRZYWINSKI, S. (2013). Analysis and Finite Element Simulation of the Draping Process of Multilayer Knit Structures and the Effect of a Localized Fixation. In: *Advanced Composite Materials, Vol. 22, Issue 3*, 175–189.
37. DONG, Y., KONG, J., MU, C., & LU, X. (2015). Materials Design towards Sport Textiles with Low-friction and Moisture-wicking Dual Functions. In: *Materials and Design 88*, 82–87.
38. DOUSTAR, K., SHAIKHZADEH, N.S., & MAROUFI, M. (2010). The Effect of Fabric Design and Weft Density on Bagging Behavior of Cotton Woven Fabrics. In: *The Journal of the Textile Institute, Vol. 101, Issue 2*, 135–142.
39. ESCARPITA, D.A., CARDENAS, D., ELIZALDE, H., RAMIREZ, R., & PROBST, O. (2012). Biaxial Tensile Strength Characterization of Textile Composite Materials. In: *Composites and Their Properties, InTech*, 83–106.
40. EZAZSHAHABI, N., LATIFI, M., & TEHRAN, M.A. (2015). Analysis of Frictional Behavior of Woven Fabrics by a Multi-directional Tactile Sensing Mechanism. In: *Journal of Engineered Fibers and Fabrics, Vol. 10, Issue 3*, 129–135.
41. *FANCY Weaves*. (2012). Retrieved April 12, 2017, from LinkedIn Corporation : https://www.slideshare.net
42. FARUKH, F., DEMIRCI, E., SABUNCUOGLU, B., ACAR, M., POURDEYHIMI, B., & SILBERSCHMIDT, V.V. (2013). Characterisation and Numerical Modelling of Complex Deformation Behaviour in Thermally Bonded Nonwovens. In: *Computational Materials Science, Vol. 71*, 165–171.
43. *FEKIWEBSTUDIO*. (2014–2016). Retrieved October 13, 2016, from Narum Web site: http://www.narum.hu
44. *FLOCKING (texture)*. (2017). Retrieved April 12, 2017, from Wikimedia Foundation, Inc.: https://en.wikipedia.org

45. FONTAINE, S., MARSIQUET, C., & RENNER, M. (2006). Adhesion, Roughness and Friction Characterization on Time-Dependent Materials: Example with Fibrous Structures. In: *SEM Annual Conference and Exposition on Experimental and Applied Mechanics, Vol. 4*, 1948–1953.
46. FUNG, W. (2000). Textiles in Transportation. In FUNG, W. *Handbook of Technical Textiles* (pp. 490–524). Cambridge, UK: Woodhead Publishing Limited.
47. FUNG, W. (2002). *Coated and Laminated Textiles*. Cambridge, UK: Woodhead Publishing Limited.
48. FUNG, W., & HARDCASTLE, M. (2000). *Textiles in Automotive Engineering*. Cambridge, UK: Woodhead Publishing Limited.
49. GAO, X., CHEN, H., & SUN, S. (2015). Analysis of the Creep Properties of Nonwoven Fabric with Mechanical Models. In: *Fibers & Textiles in Eastern Europe, Vol. 109, No. 1*, 72–76.
50. GAO, X., SUN, Y., MENG, Z., & SUN, Z. (2012). Analytical Approach of Creep Behavior of Carpet Yarn. In: *Journal of Applied Polymer Science, Vol. 124, Issue 2*, 1160–1167.
51. *GARDNER Business Media*. (2012). Retrieved November 09, 2016, from Automotive Design & Production website: http://www.adandp.media
52. GERHARDT, L.C., LOTTENBACH, R., ROSSI, R.M., & DERLER, S. (2013). Tribological Investigation of a Functional Medical Textile with Lubricating Drug-delivery Finishing. In: *Colloids and Surfaces, Biointerfaces*.
53. *GLOBE News Wire*. (2016). Retrieved November 09, 2016, from Lectra launches DesignConcept Furniture V3R1, its 2D/3D design, costing and virtual prototyping solution: https://globenewswire.com
54. *GUIDE to Upholstery Fabrics*. (2017). Retrieved April 10, 2017, from Meredith Corporation website: http://www.bhg.com
55. GUPTA, P., MAHESHWARI, P., & KUMARI, S. (2016). *Evaluation and Performance Criteria of Monofilament Yarn in Automotive Seating System*. SAE Technical Paper.
56. GUTAUSKAS, M.V., PAPRECKIENE, L., MASTEIKAITE, V., DAUKANTIENE, V., & STRAZDIENE, E. (2000). Behavior Evaluation and Prognosis of Textile and Polymer Material Shells. In: *International Journal of Clothing Science and Technology, Vol. 12, Issue 6*, 14–16.
57. HADA, J.S., & GARG, Y. (2015). Seat Upholestery/ Fabrics used in Automobiles. In: *Man-Made Textiles in India, Vol. 43, Issue 2*, 51–55.
58. HASANI, H., ZADEH, S.H., & BEHTAJ, S. (2012). Bagging Behavior of Different Fabric Structures Knitted From Blended Yarns Using Image Processing. In: *Journal of Engineering Fibers and Fabrics, Vol. 7, Issue 3*, 8–15.
59. HUFENBACH, W.A., MADER, E., ULBRICHT, V., BRANKE, D., KASTNER, M., & POHL, M. (2013). Experimental and Numerical Investigation of the Long-Term Behaviour of Modified Textile-Reinforced Polypropylene. In: *Proceedings of he 19th International Conference on Composite Materials*, 1-10.
60. JABBAR, M., & SHAKER, K. (2016). Textile Raw Materials. In: *Physical Sciences Rewiews, Vol. 1, Issue 7*.

61. JAFARI, S., & GHANE, M. (2016). An Analytical Approach for the Recovery Behavior of Cut Pile Carpet After Static Loading by Mechanical Models. In: *Fibers and Polymers, Vol. 17, Issue 4*, 651–655.
62. JAMES, D. (2001). *Upholstery. A Complete Course.* East Sussex: Guild of Master Craftsman Publications Ltd.
63. JAOUACHI, B. (2013). Study of Knitting Factors Contribution on Residual Bagged Fabric Behaviour. In: *Journal of the Textile Institute, Vol. 104, Issue 10*, 1132–1140.
64. JAWALE, S.N., & PATIL, U.J. (2011). Yarn Friction and Its Importance, Theory, Factors, Measurement. In: *The Indian Textile Journal*.
65. JEZEK, G. (2015). *What is Vinyl*. Retrieved September 25, 2016, from What is Vinyl website: http://www.whatisvinyl.com
66. JOAO, L.S., CARVALHO, R., & FANGUEIRO, R. (2016). A Study on the Durability Properties of Textile Membranes for Architectural Purposes. In: *Procedia Engineering, Vol. 155*, 230–237.
67. JONES, W.G., SMALL, J.D., WALTON, J.H., BALDWIN, A.F., & MIKAELIAN, Z. (2013). *Patent No. US20130117940 A1*. United States of America.
68. JUNG, I.H., LEE, S.B., KIM, J.J., RYU, H.N., & KO, H.S. (2016). Modeling the Non-Elastic Stretch Deformation of Cloth Based on Creep Analysis. In: *Textile Research Journal, Vol. 86, Issue 3*, 245–255.
69. JUODSNUKYTE, D., GUTAUSKAS, M.V., & CEPONONIENE, E. (2006). Mechanical Stability of Fabrics for Military Clothing. In: *Materials Science (Medžiagotyra), Vol. 12, No. 3*, 243–246.
70. KADOLE, P.V., GOTIPAMUL, R.L., DHANABALAN, V., & SALONI, S. (2013). A Review of Jacquard Fabrics. In: *The Indian Textile Journal*.
71. KADOLPH, S.J. (2009). The Use of Knitted, Woven and Nonwoven Fabrics in Interior Textiles. In ROWE, T. *Interior Textiles. Design and Developments* (pp. 47–89). USA: Woodhead Publishing Limited and CRC Press LLC.
72. KAN, C.W., LEUNG, M.H., & MONGKHOLRATTANASIT, R. (2016). Using KES-F System for Determining the Bending Properties of Paper Towels. In: *Applied Mechanics and Materials, Vol. 848, Chapter 2*, 170–173.
73. KIM, Y.K. (2011). Flocked Fabrics and Structures. In Gong, R.H. *Specialist Yarn and Fabric Structures – Developments and Applications* (p. 301). Philadelphia: Woodhead Publishing Limited.
74. KINGE, A.P., LANDAGE, S.M., & WASIF, A.I. (2013). Nonwoven for Artificial Leather. In: *International Journal of Advanced Research in Engineering and Applied Sciences, Vol. 2, No. 2*, 18–33.
75. KISILAK, D. (1999). New Method of Evaluating Spherical Fabric Deformation. In: *Textile Research Journal, Vol. 69*, 908–913.
76. KLEVAITYTE, R., & MASTEIKAITE, V. (2008). Anisotropy of Woven Fabric Deformation After Stretching. In: *Fibres and Textiles in Eastern Europe, Vol. 16, No. 4*, 52–56.
77. KOC, S.K., MECIT, D., BOYACI, B., ORNEK, M., & HOCKENBERGER, A. (2016). Effects of Filament Cross Section on the Performance of Automotive Upholstery Fabrics. In: *Journal of Industrial Textiles*, , 1–15.

78. KOOCHAKZAEI, A., AHMADI, H., & ACHACHLUEI, M.M. (2016). An Experimental Comparative Study on Silicone Oil and Polyethylene Glycol as Dry Leather Treatments. In: *JALCA, Vol. 111, No. 10*, 377–382.
79. KOVACEVIC, S., UJEVIC, D., & BRNADA, S. (2010). Coated Textile Materials. *Woven Fabric Engineering*, InTech, DOI: 10.5772/10468, 241–255.
80. KRUGER, M., REINHARDT, H.W., & FICHTLSCHERER, M. (2001). Bond Behaviour of Textile Reinforcement in Reinforced and Prestressed Concrete. In: *Otto-Graf-Journal, Vol. 12*, 33–50.
81. KUMAR, R.S. (2014). *Textiles for Industrial Applications.* CRC Press, Taylor & Francis Group.
82. KUMARI, A., & KHURANA, K. (2016). Regenerated Cellulose-Based Denim Fabric for Tropical Regions: An Analytical Study on Making Denim Comfortable. In: *Journal of Textiles*, 1–10.
83. *LEATHER CLASSICS*. (2016). Retrieved April 10, 2017, from Goodrich Global Pte. Ltd.: http://www.goodrichglobal.com
84. *LEATHER SEATS and Trims, Are Perforated Leather Seats Better*. (2014). Retrieved June 15, 2016, from Prestige Sunroofs website: http://prestigesunroofs.com.au
85. LENGYEL, B.C., FAUR, N., NES, C.S., & CERNESCU, A. (2016). Analytic Study Regarding Yarn Geometry of Two Synthetic Materials Used in Furniture and Automotive Industry. In: *Solid State Phenomena, Vol. 254*, 116–119.
86. LIU, C.K., LATONA, N.P., LEE, J., & COOKE, P.H. (2009). Microscopic Observations of Leather Looseness and Its Effects on Mechanical Properties. In: *Journal of the American Leather Chemists Association, Vol. 104, No. 7*, 230–236.
87. LOMOV, S.V., VERPOEST, I., BARBURSKI, M., & LAPERRE, J. (2003). Carbon Composites Based On Multiaxial Stitched Preforms. Part 2. KES-F Characterisation of the Deformability of the Preforms at Low Loads. In: *Composites, Part A: 34*, 359–370.
88. MADKAIKAR, M. (2012, December 14). *Fabric study*. Retrieved April 12, 2017, from LinkedIn Corporation : https://www.slideshare.net
89. MAKINEN, M., & MEINANDER, H. (2005). *Influence of Physical Parameters on Fabric Hand.*
90. MALLETT, M. (2000). *Basic Tribal and Village Weaves*. Retrieved April 11, 2017, from Marla Mallett Web site: http://marlamallett.com
91. MAMI, A., NAJOUA, B., MELLOUKI, I., & YACOUBI, N. (2017). Determination of Thermal Characterisation by Photopyroelectric Technique: Application on Textile. *Nondestructive Testing and Evaluation, 32:1*, 103–111.
92. MANEA, L.R., SCARLET, R., AMARIEI, N., NECHITA, E., & SANDU, I.G. (2015). Study on Behaviour of Polymer Solutions in Electrospinning Technology. In: *Revista de Chimie 66, No.4*, 542.
93. MANEA, L.R., STANESCU, I., NECHITA, E., & AGOP, M. (2015). Some Fractal Logical Elements in Nanostructures. In: *Journal of Computational and Theoretical Nanoscience, Vol.12, No.11*, 4373–4376.
94. MATUKONIS, A., PALAIMA, J., & VITKAUSKAS, A. (1989). Tekstilės medžiagotyra. In Matukonis, A., Palaima, J. & Vitkauskas, A. *Tekstilės medžiagotyra* (p. 308). Kaunas: Mokslas.

95. MCKOY, K. (2015). *Tapestry*. Retrieved April 15, 2017, from Science 189, Course Hero, Inc.: https://www.coursehero.com
96. MCMAHON, M. (2017). *What Is Velour?* Retrieved April 12, 2017, from A Conjecture Corporation: http://www.wisegeek.com
97. MCMULLAN, A., & MEALMAN, M. (2001). An Investigation of Automotive Seat Fabric Sound Absorption. In: *SAE Technical Paper, doi: 10.4271/2001-01-1454*, 1–6.
98. *MOQUETTE*. (2017). Retrieved April 20, 2017, from Wikimedia Foundation, Inc.: https://en.wikipedia.org
99. MOSES, J.J., & VENKATARAMAN, V.K. (2014). Study of Mechanical and Surface Properties on some Chemical Treated Cotton Fabric by KES-F, SEM and FTIR Analysis. In: *Journal of Textile Science & Engineering*, 1–7.
100. MOURID, A.E., GANESAN, R., & LEVESQUE, M. (2013). Comparison between Analytical and Numerical Predictions for the Linearly Viscoelastic Behavior of Textile Composites. In: *Mechanics of Materials, Vol. 58*, 69–83.
101. NACHBAUER, W., MOSSNER, M., ROHM, S., SCHINDELWIG, K., & HASLER, M. (2016). Kinetic Friction od Sport Fabrics on Snow. *Lubricants, Vol. 4, Issue 7*, 1–8.
102. NASHY, E.-S. H., ESSA, M.M., & HUSSAIN, A.I. (2012). Synthesis and Application of Methyl Methacrylate/Butyl Acrylate Copolymer Nanoemulsions as Efficient Retanning and Lubricating Agents for Chrome-Tanned Leather. In: *Journal of Applied Polymer Science, Vol. 124*, 3293–3301.
103. NIELSEN, K.J. (2007). *Interior Textiles: Fabrics, Application, and Historic Style.* John Wiley & Sons.
104. NIKKI. (2014). *Characteristics of Vinyl Fabric*. Retrieved April 10, 2017, from Blog at WordPress.com : http://sailrite.wordpress.com
105. NISHI, M., & HIRASHIMA, T. (2013). Approach for Dry Textile Composite Forming Simulation. *The 19th International Conference on Composite Materials (ICCM-19)*, 7486–7493.
106. OZDEMIR, H., & YAVUZKASAP, D. (2012). The Effects of Yarn and Fabric Structural Parameters on the Seam Slippage, Abrasion and Pilling Properties of Double Woven Upholstery Fabrics. In: *Industria Textila, Vol. 63 (6)*, 307–314.
107. OZDEMIR, H., & MERT, E. (2013). The Effect of Fabric Structural Parameters on the Tensile, Bursting and Impact Strengths of Cellular Woven Fabrics. In: *The Journal of the Textile Institute, Vol. 104, Issue 3*, 330–338.
108. OZDEMIR, O., & CEVEN, E.K. (2004). Influence of Chenille Yarn Manufacturing Parameters on Yarn and Upholstery Fabric Abrasion Resistance. In: *Textile Research Journal, Vol.74 (6)*, 515–520.
109. PAI LUNG MACHINERY MILL CO., LTD., Taiwan. Corduroy Fabric. Inventors: PAI, T.H. Int. Cl: D04B 7/12, Appl. No. 11/898,466. US patent US 7503192 B1. (2009). Retrieved April 20, 2017, from website: http://www.google.com/patents/US7503192
110. PAMUK, G., & CEKEN, F. (2008). Comparatıve Study of the Abrasion Resistance of Automobile Seat Covers. In: *Fibres & Textiles in Eastern Europe, Vol. 16, No. 4 (69)*, 57–61.

111. PASAYEV, N., KORKMAZ, M., & BASPINAR, D. (2011). Investigation of the Techniques Decreasing the Seam Slippage in Chenille Fabrics (Part II). In: *Textile Research Journal, Vol.81 (20)*, 2075–2081.

112. PATIL, P.G., & NACHANE, R.P. (2009). Study of Inverse Creep in Textile Yarns. *Journal of Engineered Fibers and Fabrics, Vol. 4, Issue 4*, 42–49.

113. PELED, A., COHEN, Z., PASDER, Y., ROYE, A., & GRIES, T. (2008). Influences of Textile Characteristics on the Tensile Properties of Warp Knitted Cement Based Composites. In: *Cement & Concrete Composites, Vol. 30 (3)*, 174–183.

114. PHILLIPP, M. (2014). Reduced Textile Friction for Cotton, Synthetics and Blends: GLIDER by HeiQ. *Textile Intelligence Inside*, 1–3.

115. POPELY, R. (2012). *What's the Difference between Perforated Leather and Regular Leather*. Retrieved April 26, 2016, from I'm Just Wondering website: http://ask.cars.com

116. PRESTON, J. (2016). *Man-Made Fibre*. Retrieved April 20, 2017, from Encyclopædia Britannica, Inc.: https://www.britannica.com

117. RAJ, S., & SREENIVASAN, S. (2009). Total Wear Comfort Index as an Objective Parameter for Characterization of Overall Wearability of Cotton Fabrics. In: *Journal of Engineered Fibers and Fabrics, Vol. 4, No. 4*, 29–41.

118. RENAUD, J., VERNET, N., RUIZ, E., & LEBEL, L.L. (2016). Creep Compaction Behavior of 3D Carbon Interlock Fabrics with Lubrication and Temperature. In: *Composites: Part A, Vol. 86*, 87–96.

119. ROCHER, J.E., ALLAOUI, S., HIVET, G., & BLOND, E. (2013). Experimental Testing of Two Three-Dimensional (3D)-Non Crimp Fabrics of Commingled Yarns. In: *13th Autex World Textile Conference*, 1–6.

120. ROH, E.K., OH, K.W., & KIM, S.H. (2013). Classification of Syntetic Polyurethane Leather by Mechanical Properties according to Consumers' Preference for Fashion Items. In: *Fibers and Polymers, Vol. 14, No. 10*, 1731–1738.

121. ROTARU, G.M., PILLE, D., LEHMEIER, F.K., STAMPFLI, R., SCHEEL-SAILER, A., ROSSI, R.M., *et al*. (2013). Friction between Human Skin and Medical Textiles for Decubitus Prevention. In: *Tribology International, Vol. 65*, 91–96.

122. SACEVICIENE, V., STRAZDIENE, E., SCHACHER, L., & ADOLPHE, D. (2012). Mechanical Properties of Multilayered Textiles at Low Loading. In: *Proceedings in 12th World Textile Conference Autex*, 1227–1230.

123. SACEVICIENE, V., STRAZDIENE, E., VILUMSONE, A., & BALTINA, I. (2012). Analysis of Multilayer Materials Behaviour under Biaxial Deformation. In: *Proceedings of the 17th International Conference Mechanika*, 260–266.

124. SAVA, C., & ICHIM, M. (2015). Yarns and Woven Fabrics Made from Cotton and Cottonised Flax Blends for Upholstery Applications. In: *Fibres & Textiles in Eastern Europe, Vol. 113, No. 5*, 30–34.

125. SCARBOROUGH, S.E., FREDRICKSON, T., CADOGAN, D.P., & BAIRD, G. (2008). Creep Testing of High Performance Materials for Inflatable Structures. In: *Material and Process Engineering, Vol. 11, No. 4*, 171–193.

126. SCHAEFFER, C. (2003). Sew any Fabric: a Quick Refernce to Fabrics from A to Z. In: *Krause Publications Craft. ISBN 1-4402-2033-6*, p. 37.

127. SCHWARZ, I.G., KOVACEVIC, S., & KOS, I. (2015). Physical-Mechanical Properties of Automotive Textile Materials. In: *Journal of Industrial Textiles, Vol. 45, Issue 3*, 323–337.
128. *SELECTING Fabric for Upholstery*. (2009). Retrieved April 13, 2017, from Kravet Inc.: http://kravet.typepad.com
129. SHANTHI, R., & ISWARIYA, M.G. (2013). *Nonwovens for Home Textiles*. Retrieved April 20, 2017, from Rodman Media: http://www.nonwovens-industry.com
130. SIYUAN, G., YONGGANG, C., & AIYING, W. (2013). Design and Development of Warp-Knitted Velour Fabric for Automobile. *Techical Textiles, No. 4*.
131. *SILK Fabrics for Upholstery*. (2014). Retrieved April 10, 2017, from JRB Silk Fabrics, LLC: http://www.jrbsilks.com
132. SINGHA, K. (2012). A Review on Coating & Lamination in Textiles: Processes. in: *American Journal of Polymer Science, Vol. 2, No. 3*, 39–49.
133. SLOT, A., WEERD, J., ROOS, M., BAIKER, M., STOEL, R.D., & ZUIDBERG, M.C. (2017). Tracers as Invisible Evidence — the Transfer and Persistence of Flock Fibres During a Car Exchange. In: *Forensic Science International, Vol. 275*, 178–186.
134. *SPECIFICATION Guidelines.* (2016). Retrieved September 20, 2016, from The Fabric Project Web Site: http://fabricproject.com
135. *SPINNEYBECK.* (2016). Retrieved 10 13, 2016, from Spinneybeck Web site: http://www.spinneybeck.com
136. STANYS, S., ADOMAVIČIŪTĖ, E., & JONAITIENĖ, V. (2012). *Neaustinės medžiagos I dalis.* Kaunas: Technologija.
137. STRAZDIENE, E., & GUTAUSKAS, M.V. (2001). The Peculiarities of Textile Behavior in Biaxial Punch Deformation. In: *International Journal of Clothing Science and Technology Vol. 3/4, Issue 13*, 176–185.
138. STRAZDIENE, E., & GUTAUSKAS, M.V. (2003a). Behavior of Stretchable Textiles with Spatial Loading. *Textile Research Journal, Vol. 73, Issue 6*, 530–534.
139. STRAZDIENE, E., & GUTAUSKAS, M.V. (2003b). The Evaluation of Fused Knitted Systems Stability. In: *International Journal of Clothing Science and Technology, Vol. 15, Issue 3*, 204–210.
140. STRAZDIENE, E., DAUKANTIENE, V., & GUTAUSKAS, M.V. (2001). Friction Factor in Polyethylene Membrane Punch Deformation. In: *Polymer Testing 20*, 191–197.
141. STRAZDIENE, E., DAUKANTIENE, V., & GUTAUSKAS, M.V. (2003). Bagging of Thin Polymer Materials: Geometry, Resistance and Application. In: *Materials Science (Medžiagotyra), Vol. 9, No. 3*, 262–266.
142. STRAZDIENE, E., GUTAUSKAS, M.V., PAPRECKIENE, L., & WILLIAMS, J.T. (1997). The Behaviour of Textile Membranes in Punch Deformation Process. In: *Materials Science (Medžiagotyra), Vol. 2, Issue 5*, 50–54.
143. SURESHKUMAR, P. S., THANIKAIVELAN, P., PHEBE, K., KALIAPPA, K., JAGADEESWARAN, R., & CHANDRASEKARAN, B. (2012). Investigations on Structural, Mechanical, and Thermal Properties of Pineapple Leaf Fiber-Based Fabrics and Cow Softy Leathers: An Approach toward Making Amalgamated Leather Products. In: *Journal of Natural Fibers, Vol. 9, Issue 1*, 37–50.

144. TAKUYA, S., TSUNEAKI, Y., SOO, K.I., & YUJI, E. (2010). Frictional Properties of Electrospun Polyurethane Nanofiber Web. In: *Tribology Online, Vol. 5, Issue 6*, 262–265.
145. TANG, X., ZHANG, X., ZHUANG, X., ZHANG, H., & YAN, X. (2017). Acoustical Analysis of Corduroy Fabric for Sound Absorption: Experiments and Simulations. *Journal of Industrial Textiles*, 1–20.
146. TASRON, D.N., THURSTON, T.J., & CERRE, M.J. (2015). Frictional Behaviour of Running Sock Textiles Against Plantar Skin. In: *Procedia Engineering, Vol. 112*, 110–115.
147. *TECHNICAL MANUAL Chapter 2: Yarns – Chenille*. (2013). Retrieved April 10, 2017, from Fabrics Unravelled: http://www.fabricsunravelled.co.za
148. *TECHNICAL TEXTILE Laminates and Interlinings for Upholstery*. (2014). Retrieved April 13, 2017, from Konus Konex: http://konuskonex.com
149. THOMAS, P., & THOMAS, G. (2006). *Velvet in Fashion 2005–2006*. Retrieved April 12, 2017, from Fashion-era.com : http://www.fashion-era.com
150. TIJUNELIENE, L., STRAZDIENE, E., & GUTAUSKAS, M.V. (1999). The Behavior of Polythylene Membrane Due to Punch Deformation Process. In: *Polymer Testing, Vol. 18, Issue 8*, 635–640.
151. TOKMAK, O., BERKALP, O.B., & GERSAK, J. (2010). Investigation of the Mechanics and Performance of Woven Fabrics Using Objective Evaluation Techniques. Part I: The Relationship Between FAST, KES-F and Cusick's Drape-Meter Parameters. In: *Fibers & Textiles in Eastern Europe, Vol. 18, No. 2 (79)*, 55–59.
152. TSAKNAKI, V., FERNAEUS, Y., & SCHAUB, M. (2014). Leather as a Material for Crafting Interactive and Physical Artifacts. In: *Research Gate, Vol. 05*.
153. TURK, M., EHRMANN, A., & MAHLTIG, B. (2014). Water-, Oil-, and Soil-Repellent Treatment of Textiles, Artificial Leather, and Leather. In: *Journal of the Textile Institute, Vol. 106, Issue 6*, 1–10.
154. UJEVIC, D., KOVACEVIC, S., WADSWORTH, L.C., SCHWARZ, I., & SAJATOVIC, B.B. (2009). Analysis of Artificial Leather with Textile Fabric on the Backside. In: *Journal of Textile and Apparel, Technology and Management, Vol. 6, Issue 2*, 1–9.
155. ULKU, S., ORTEK, H.G., & OMEROGLU, S. (2003). The Effect of Chenille Yarn Properties on the Abrasion Resistance of Upholstery Fabrics. In: *Fibers & Textiles in Eastern Europe, Vol. 11, No. 3 (42)*, 38–41.
156. *UNDERSTANDING Upholstery: From Fabric to Frame*. (2017). Retrieved April 10, 2017, from Hayneedle Inc.: http://www.hayneedle.com
157. *UPHOLSTERY Cover Fabrics and Leathers*. (2017). Retrieved April 10, 2017, from The Furniture Industry Research Association – part of the Exova Group: http://www.fira.co.uk
158. URBELIS, V., PETRAUSKAS, A., & VITKAUSKAS, A. (2005). Creep and Creep Recovery of Textile Fabrics and Their Fused Systems. In: *Materials Science (Medžiagotyra), Vol. 11, No. 2*, 162–168.
159. VANCLOOSTER, K., ESHGHYAR, A., & LOMOV, S.V. (2011). Biaxial Extension of Knitted Steel Fibre Fabrics. In: *The 14th International ESAFO)RM Conference on Material Forming*, 907–912.

160. VANLEEUW, B., CARVELLI, V., BARBURSKI, M., LOMOV, S.V., & VAN VUURE, A.W. (2015). Quasi-unidirectional Flax Composite Reinforcement: Deformability and Complex Shape Forming. In: *Composites Science and Technology (110)*, 76–86.
161. VILHENA, L., & RAMALHO, A. (2016). Friction of Human Skin against Different Fabrics for Medical Use. In: *Lubricants, Vol. 4, Issue 6*, 1-10.
162. WANG, G., CHEN, F., CHENG, H., & LI, X. (2012). Interactive Effect Between Warp and Weft of a Woven Ramie Fabric under Biaxial Loadings. In: *The Journal of the Textile Institute, Vol. 103, Issue 3*, 283–291.
163. *WHAT Is the Difference between Velvet and Velour*. (2017). Retrieved April 12, 2017, from IAC Publishing, LLC: https://www.reference.com
164. WINTERS, S. (2012). *Drapery Fabric for Upholstery*. Retrieved April 14, 2017, from Stephen Winters: http://www.upholsteryresource.com
165. WU, F.F., ZHANG, G.A., & WU, X.F. (2012). Extrinsic Size Effects on Performance of Zr-Based Metallic Glass Under Biaxial Loading. In: *Journal of Material Science, Vol. 47*, 2213–2217.
166. YANG, R.H., WU, W.M., WAN, Y.Q., WANG, H.B., GAO, W.D., XIE, C.P., *et al.* (2012). Effect of Filament Pre-Tension on the Performance of Solo-Sirofil Composite Yarn. In: *Indian Journal of Fibre & Textile Research, Vol. 37*, 378–380.
167. YEUNG, K.W., LI, Y., ZHANG, X., & YAO, M. (2002). Evaluating and Predicting Fabric Bagging with Image Processing. In: *Textile Research Journal, Vol. 72*, 693–700.
168. YIN, H., PENG, X., DU, T., & GUO, Z. (2014). Draping of Plain Woven Carbon Fabrics Over a Double-Curvature Mold. In: *Composites Science and Technology, Vol. 92*, 64–69.
169. ZHANG, X., SAHRAEI, E., & WANG, K. (2016). Deformation and Failure Characteristics of Four Types of Lithium-Ion Battery Separators. In: *Journal of Power Sources 327*, 693–701.
170. ZUBAUSKIENE, D., STRAZDIENE, E., URBELIS, V., & SACEVICIENE, V. (2012). The Investigation of Soft Furniture Upholstery Deformational Behaviour. In: *Material Science (Medžiagotyra), Vol. 18, No. 4*, 367–372.
171. АРОНОВА, Е.И., & СОЛОВЬЕВ, А.Н. (1971). Испытание трикотажных полотен на многоостное растяжение до разрыва. *Механические свойства и износостойкость текстильных материалов: VII Всесоюзная научная конференция по текстильному материаловедению*, (pp. 221–224). Вильнюс – Каунас.
172. КОБЛЯКОВ, А.И. (1973). Структура и механические свойства трикотажа. *Легкая индустрия*, 190–191.

List of Research and Other Publications of Dissertation Topic, Conference Participation

Articles published in journals included in scientific international databases

Indexed in the "Clarivate Analytics Web of Science" with Impact Factor

1. **ZUBAUSKIENĖ, Donata**; STRAZDIENĖ, Eugenija; URBELIS, Virginijus; SACEVIČIENĖ, Virginija. (2012). The Investigation of Soft Furniture Upholstery Deformational Behaviour. *Materials Science = Medžiagotyra*. Kaunas University of Technology, Academy of Sciences of Lithuania. Kaunas: Technologija, 2012, vol. 18, no. 4, pp. 367–372. ISSN 1392-1320. doi: DOI:org/10.5755/j01.ms.18.4.3099 [INSPEC; Science Citation Index Expanded (Web of Science)] IF: 0.522; AIF: 3.264; IF/AIF: 0.160; Q4 (2012, SCIE)] [Contribution: 0.250]
2. **ZUBAUSKIENĖ, Donata**; STRAZDIENĖ, Eugenija; URBELIS, Virginijus. (2015). Analysis of Pre-Tension Level upon Biaxial Behaviour of Fused Systems. *Materials Science = Medžiagotyra*. Kaunas University of Technology, Academy of Sciences of Lithuania. Kaunas: KTU, 2015, vol. 21, no. 2, pp. 276–281. ISSN 1392-1320. doi: 10.5755/j01.mm.21.2.5788 [Scopus; INSPEC; Science Citation Index Expanded (Web of Science)] [IF: 0.428; AIF: 3.984; IF/AIF: 0.107; Q4 (2015, SCIE)] [Contribution: 0.334]
3. **ZUBAUSKIENĖ, Donata**; STRAZDIENĖ, Eugenija. (2017). Effect of Friction in the Punch-to-Specimen Contact Zone Upon the Punching Behaviour of Synthetic Leathers. *Fibres and Textiles in Eastern Europe*. Lodz: Institute of Biopolymers and Chemical Fibres, 2017, vol. 25, iss. 3, pp. 121-128. ISSN 1230-3666. 2017, vol. 25, No. 3, pp. 121–128. ISSN 1230-3666. doi: 10.5604/12303666.1237248 [Scopus; Science Citation Index Expanded (Web of Science)] [IF: 0.626; AIF: 1.655; IF/AIF: 0.378; Q2 (2016, SCIE)] [Contribution: 0.500]

[Contribution in the publications group: 1.084]

Articles published in journals belonging to scientific international databases

Indexed in the "Clarivate Analytics Web of Science" without Impact Factor

1. **ZUBAUSKIENĖ, Donata**; STRAZDIENĖ, Eugenija; URBELIS, Virginijus. (2012). The Investigation of Relaxation Behaviour of Flexible Polymer Materials. In: *Mechanika 2012: proceedings of the 17th international conference, 12, 13 April 2012, Kaunas University of Technology, Lithuania*. Kaunas University of Technology, Lithuanian Academy of Science, IFTOMM National Committee of Lithuania, Baltic Association of Mechanical Engineering. Kaunas: Technologija, 2012, pp. 351-356. ISSN 1822-2951. [Conference Proceedings Citation Index (unused)] [Contribution: 0.334]

[Contribution in the publications group: 0.334]

Articles in other peer reviewed research publications
Articles published in conference proceedings

1. **ZUBAUSKIENĖ, Donata**; STRAZDIENĖ, Eugenija; URBELIS, Virginijus. (2012). The Investigation of Creep and Relaxation Deformation of Flexible Polymer Materials. In: *AUTEX 2012: Innovative Textile for High Future Demands: 12th World Textile Conference AUTEX 2012, 13–15 June 2012, Zadar, Croatia: book of proceedings. Vol. 1*. Zagreb: University of Zagreb, 2012, pp. 1067–1072. ISBN 9789537105471. [Contribution: 0.334]
2. **ZUBAUSKIENĖ, Donata**; STRAZDIENĖ, Eugenija; URBELIS, Virginijus. (2013). The Effect of Fusing Materials Structure upon the Variations of Flexible Multilayer Systems Spatial Shape. In: *AUTEX 2013 [e-resource]: proceedings of the 13th AUTEX World Textile Conference, 22–24 May, 2013, Dresden, Germany*. Institute of Textile Machinery and High Performance Material Technology, Technische Universität Dresden. Dresden: ITM, 2013, pp. 1-5. ISBN 9783867803434. [Contribution: 0.334]
3. **ZUBAUSKIENĖ, Donata**; STRAZDIENĖ, Eugenija; URBELIS, Virginijus. (2013). The Investigation of Soft Furniture Upholsteries Exploitational Behaviour. In: *Proceedings of the 1st International Conference on Natural Fibers – Sustainable Materials for Advanced Applications [e-resource] : 9–11 June 2013*. Braga: Universidade do Minho, 2013, pp. 401–402. ISBN 9789892038728. [Contribution: 0.334]
4. STRAZDIENĖ, Eugenija; ZUMARIENĖ, Jolita; **ZUBAUSKIENĖ, Donata**. (2016). Textile / Foam Strength Properties under Punch Loading. In: *AUTEX 2016 [e-resource]: proceedings of the 16th world textile conference, 8–10 June 2016, Ljubljana, Slovenia*. University of Ljubljana. Faculty of Natural Sciences and Engineering. Ljubljana: University of Ljubljana, 2016, pp. 1–6. ISBN 9789616900171. [Contribution: 0.333]

[Contribution in publications group: 1.335]

Book sections
Published by other international and national publishing offices

1. STRAZDIENĖ, Eugenija; **ZUBAUSKIENĖ, Donata**; LEIŠIS, Vitalis; SACEVIČIENĖ, Virginija; SCHACHER, Laurence. (2017). The Characterization of Upholstery Materials Performance Properties by KES-F Parameters. In: *Innovations in clothing 3D design, products, fashion, technologies and testing of clothing materials: [monograph]*. Edited by Iwona Frydrych, Gražyna Bartkowiak & Maria Pawlowa. Lodz: Lodz University of Technology, 2017, pp. 250-263. ISBN 9788372838544. [Author's sheet: 0.200]

[Author's sheets: 0.200]

Presentations in International Conferences

1. International conference "Mechanika 2012," Kaunas, Lithuania. Oral presentation: **D. Zubauskienė** "The Investigation of Relaxation Behaviour of Flexible Polymer Materials"; 2012, April 12–13.
2. 12th world textile conference "AUTEX 2012," Zadar, Croatia. Oral presentation: V. Urbelis "The Investigation of Creep and Relaxation Deformation of Flexible Polymer Materials"; 2012, June 13–15.
3. 14th international conference-school "Advanced Materials and Technologies," Palanga, Lithuania. Poster presentation: **D. Zubauskienė** "The Investigation of Upholstery Materials Performance Properties"; 2012, August 27–31.
4. 13th world textile conference "AUTEX 2013", Dresden, Germany. Oral presentation: **D. Zubauskienė** "The Effect of Fusing Materials Structure upon the Variations of Flexible Multilayer Systems Spatial Shape"; 2013, May 22–24.
5. International conference "1st International Conference on Natural Fibres – Sustainable Materials for Advanced Applications," Braga, Portugal. Poster presentation: **D. Zubauskienė** "The Investigation of Soft Furniture Upholsteries Exploitational Behaviour"; 2013, June 9–11.
6. International conference "Baltic Polymer Symposium 2013;" Trakai, Lithuania. Poster presentation: **D. Zubauskienė** "The Effect of Uniaxial Pretension upon Multi-Layer Textile Systems Biaxial Strength Parameters"; 2013, September 18–21.
7. 16th international conference-school "Advanced Materials and Technologies," Palanga, Lithuania. Poster presentation: **D. Zubauskienė** "The Effect of Friction during Punch Loading"; 2014, August 27–31.
8. 16th world textile conference "Autex 2016", Ljubljana, Slovenia. Poster presentation: E. Strazdienė "Textile/Foam Strength Properties under Punch Loading"; 2016, June 8–10.
9. 12th world textile conference "Clotech 2017," Lodz, Poland. Oral presentation: E. Strazdienė "The Characterization of Upholstery Materials Performance Properties by KES-F Parameters" 2017, October 11–14.

Publications in National Conferences

1. National conference "Medžiagų inžinerija 2012," Kaunas, Lithuania. Oral presentation: **D. Zubauskienė** "Baldinių medžiagų valkšnumo ir deformacijos relaksacijos procesų analizė"; 2012, November 16.
2. National conference "Medžiagų inžinerija 2013," Kaunas, Lithuania. Poster presentation: **D. Zubauskienė** "Pradinio deformavimo įtaka dubliuotų sistemų dviašio deformavimo procesui"; 2013, November 15.

PADĖKA

Visų pirma dėkoju savo mokslinei vadovei prof. dr. Eugenijai Strazdienei už neįkainojamą patirtį visais studijų metais, perteiktas vertingas žinias, nesuskaičiuojamas konsultacijas ir didelę įtaką mano tobulėjimui. Dėkoju doc. dr. Virginijui Urbeliui už skirtą dėmesį ir laiką, už vertingas pastabas ir suteiktas žinias rengiant mokslinius straipsnius. Taip pat noriu išreikšti padėką doc. dr. Eglei Kumpikaitei už pagalbą ir suteiktas žinias apie tiriamų objektų pynimus.

Esu dėkinga UAB įmonei „Kauno Baldai“, kuri aprūpino tyrimo objektais (baldinėmis medžiagomis) ir noriai bendradarbiavo.

Galiausiai noriu nuoširdžiai padėkoti savo vaikučiams ir vyrui už didelę kantrybę ir supratingumą dėl mažai skirto dėmesio rengiant disertaciją. Ir, žinoma, savo tėveliams už nuolatinę paramą ir palaikymą visais studijų metais.

SL344. 2017-10-27, 16 leidyb. apsk. l. Tiražas 12 egz. Užsakymas 318 .
Išleido Kauno technologijos universitetas, K. Donelaičio g. 73, 44249 Kaunas
Spausdino leidyklos „Technologija“ spaustuvė, Studentų g. 54, 51424 Kaunas

Appendices

Appendix 1

Table A1.1. Parameters of KES-F system and calculation of units from cgs (centimeter, gram, second) to SI system unit

KES-F parameter	Experiment	Parameters				
		Mark	Name	Units		Relation between systems
				cgs system units	SI system units	
KES-F-1	Tensile	*EMT*	Tensile strain	%	%	1.0
		LT	Linearity of load extension curve	-	-	1.0
		WT	Tensile energy	gf cm/cm^2	N m/m^2	0.981
		RT	Tensile resilience	%	%	-
	Shear	*G*	Coefficient of shear rigidity	gf/cm°	N/m°	0.981
		2HG	Hysteresis of shear force at 0.5°	gf/cm	N/m	0.981
		2HG5	Hysteresis of shear force at 5°	gf/cm	N/m	0.981
KES-F-2	Bending	*B*	Bending rigidity	gf cm^2/cm	N m^2/m	10^{-4} 0.981
		2HB	Hysteresis of bending moment	gf cm/cm	N m/m	10^{-2} 0.981
KES-F-3	Compression	*LC*	Linearity of compression thickness curve	-	-	1.0
		WC	Compressional energy	gf cm/cm^2	N m/m^2	0.981
		RC	Compressional resilience	%	%	1.0
		T_0	Thickness of uncompressed specimen	mm	mm	1.0
		T_m	Thickness of compressed specimen	mm	mm	1.0
KES-F-4	Surface	*MIU*	Coefficient of friction	-	-	1.0
		MMD	Mean deviation of MIU	-	-	1.0
		SMD	Geometrical roughness	μm	μm	1.0

Appendix 2

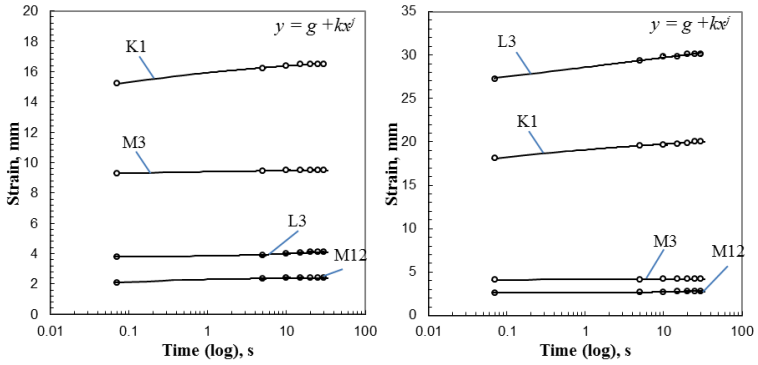

a b

Figure A2.1. The values of experiments (dots) and calculations (line) of creep deformation for upholstery materials (25 N load) in longitudinal (a) and transverse (b) directions

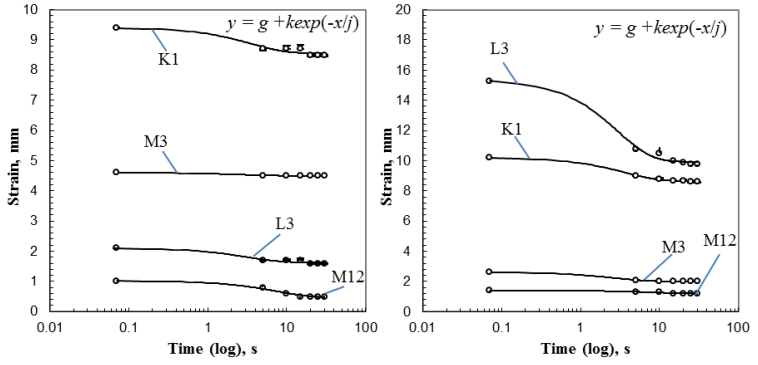

a b

Figure A2.2. The values of experiments (dots) and calculations (line) of relaxation deformation for upholstery materials (25 N load) in longitudinal (a) and transverse (b) directions

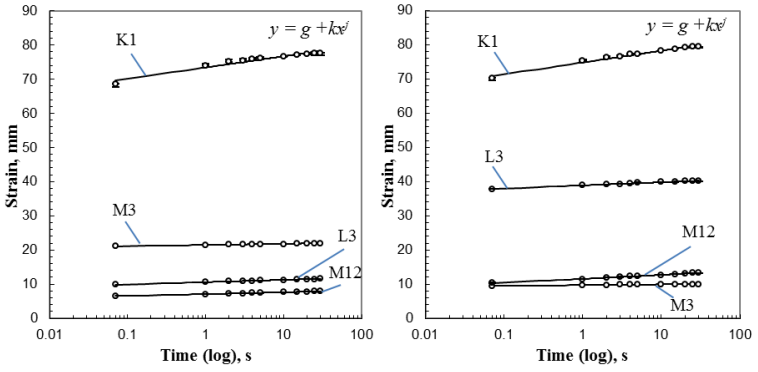

a b

Figure A2.3. The values of experiments (dots) and calculations (line) of creep deformation for upholstery materials (100 N load) in longitudinal (a) and transverse (b) directions

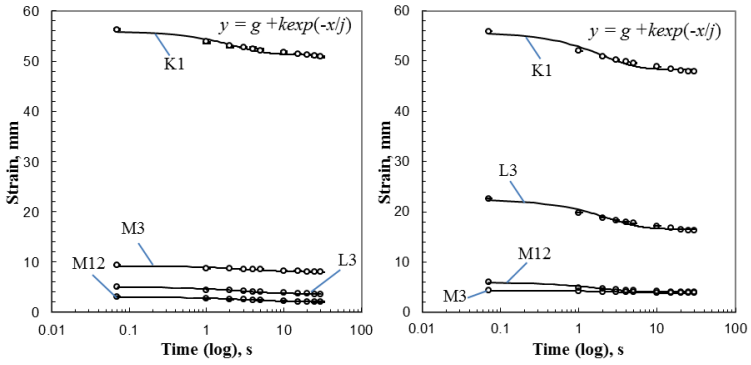

Figure A2.4. The values of experiments (dots) and calculations (line) of relaxation deformation for upholstery materials (100 N load) in longitudinal (a) and transverse (b) directions

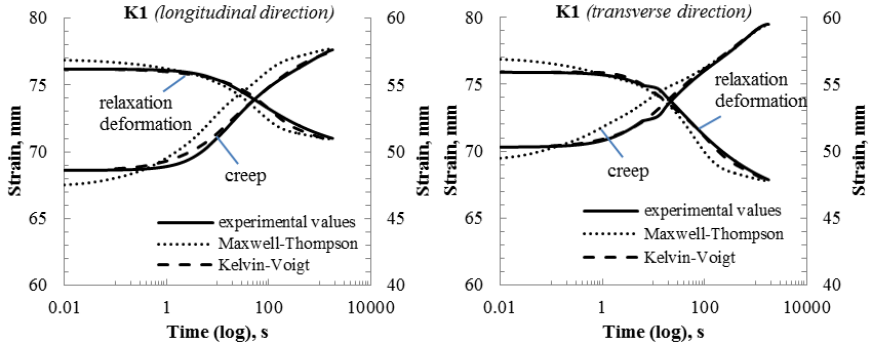

Fig. A2.5. Modeling of the creep and relaxation of deformation processes under the load of 100 N of knitted material K1 in longitudinal (a) and transverse (b) directions

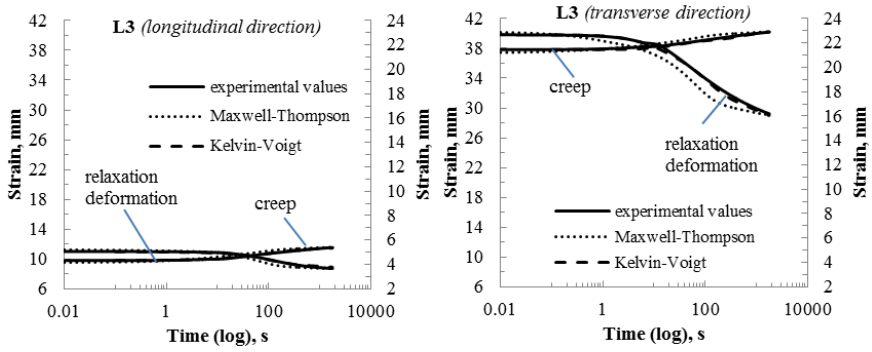

Fig. A2.6. Modeling of the creep and relaxation of deformation processes under the load of 100 N of synthetic leather L3 in longitudinal (a) and transverse (b) directions

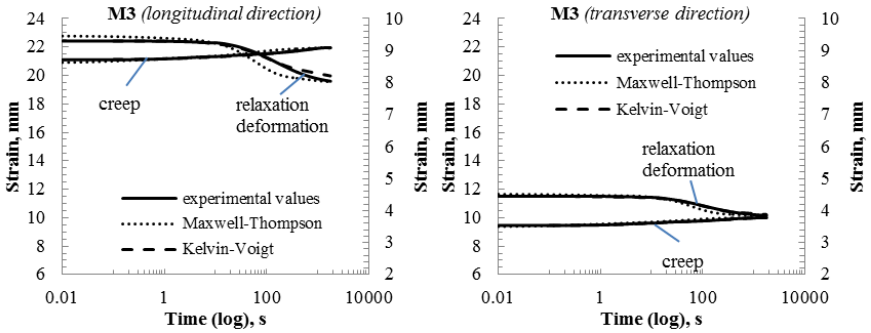

Fig. A2.7. Modeling of the creep and relaxation of deformation processes under the load of 100 N of one-layer material M3 in longitudinal (a) and transverse (b) directions

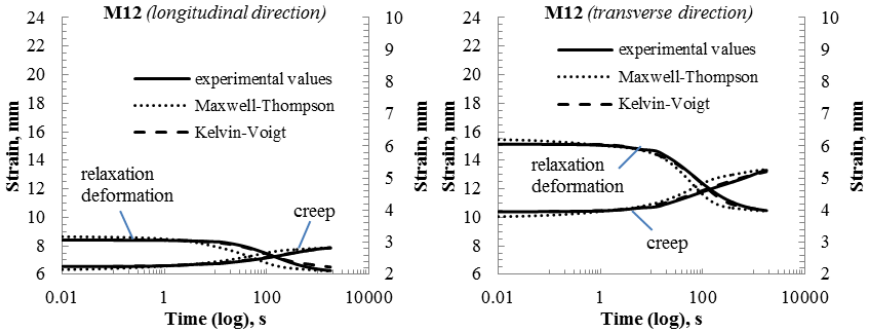

Fig. A2.8. Modeling of the creep and relaxation of deformation processes under the load of 100 N of chenille fabric M12 in longitudinal (a) and transverse (b) directions

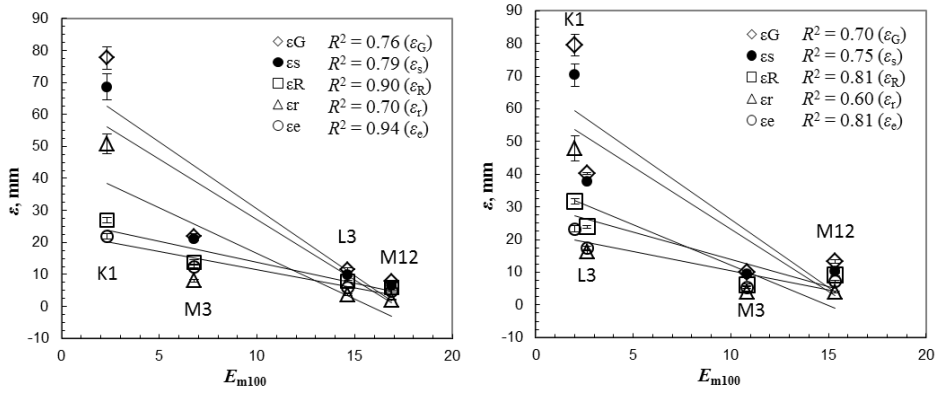

Fig. A2.9. The dependence of the coefficient of rigidity modulus (at 100 N) upon general, sudden, reversible, residual and elastic deformations in longitudinal (a) and transverse (b) directions

Appendix 3

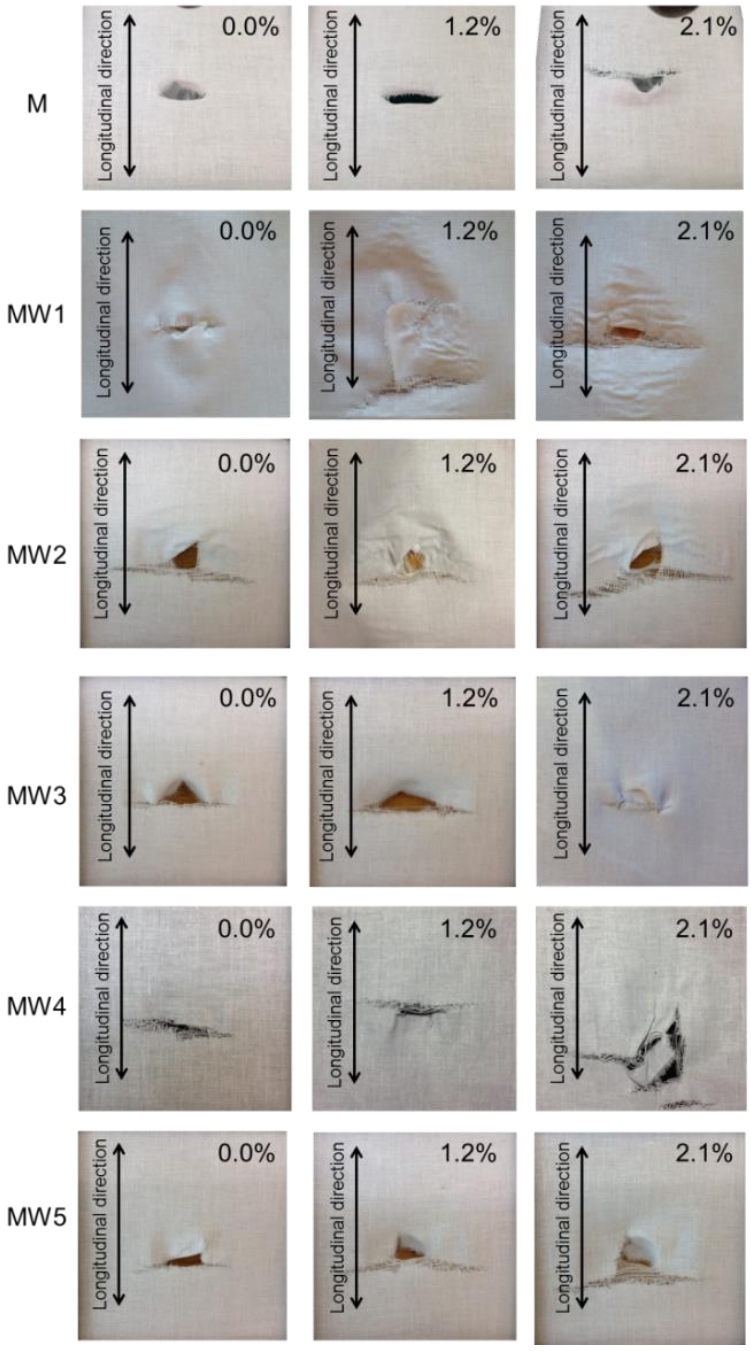

Figure A3.1. Biaxial punching photos when pre-tensioned by 0.0%, 1.2% and 2.1% for investigated base fabric M and its systems: MW1, MW2, MW3, MW4, MW5